

2018

Effect of pH, Temperature and Protein Tertiary Structure on Biomolecular Separation Engineering in Ion-Exchange Chromatography

Gorgi Pavlov
Lehigh University

Follow this and additional works at: <https://preserve.lehigh.edu/etd>

 Part of the [Chemical Engineering Commons](#)

Recommended Citation

Pavlov, Gorgi, "Effect of pH, Temperature and Protein Tertiary Structure on Biomolecular Separation Engineering in Ion-Exchange Chromatography" (2018). *Theses and Dissertations*. 4246.
<https://preserve.lehigh.edu/etd/4246>

This Dissertation is brought to you for free and open access by Lehigh Preserve. It has been accepted for inclusion in Theses and Dissertations by an authorized administrator of Lehigh Preserve. For more information, please contact preserve@lehigh.edu.

Effect of pH, Temperature and Protein Tertiary
Structure on Biomolecular Separation Engineering
in Ion-Exchange Chromatography

by

Gorgi Pavlov

Presented to the Graduate and Research Committee
of Lehigh University
in Candidacy for the Degree of
Doctor of Philosophy
in
Chemical Engineering

Lehigh University

May 2018

© Copyright by Gorgi Pavlov 2018

All Rights Reserved

Certificate of Approval

Approved and recommended for acceptance as a dissertation in partial fulfillment of the requirements for the degree of Doctor of Philosophy.

Date

Dissertation Director

Accepted Date

Committee Members:

James T. Hsu, Committee Chair

Hugo S. Caram

Mark A. Snyder

Jonas Baltrusaitis

Michael J. Behe

Acknowledgements

The completion of this thesis would not have been possible without the contribution of several individuals most of which are acknowledged here:

First and foremost, my advisor, James T. Hsu, who opened the door for me to work on this exciting research project over the last few years. His invaluable suggestions on how to improve the quality of my writing, keeping it simple yet eloquent enough to convey all important points. In addition, his training on how to think as a practicing engineer in designing my experiments and the interpretation was of great value to this work. Our discussions about the philosophy behind the work and the value derived from was a great inspiration for me to think critically about the research and chemical engineering as a field.

My thesis committee members: Hugo Caram, Mark Snyder, Jonas Baltrusaitis and Michael Behe, for their time and helpful mentorship on how to further the dissertation.

The Pennsylvania Infrastructure and Technology Alliance (PITA) and Dynalene Inc., for providing partial financial support of the work carried out in this thesis.

The Chemical Engineering Department at Lehigh University. Specifically, I would like to acknowledge Cesar Silebi for inspiring me to pursue graduate school, as well as Kemal Tuzla and Mayuresh Kothare for their encouragement. The staff at the Department, Barbara Kessler, Janine Jekels and Tracey Lopez for keeping up with their resident "drama-king". I'd also like to acknowledge Kathleen Hutnik and Amy

McCrae in the Graduate Life Office for their guidance during my leadership endeavors at Lehigh.

My closest friends since high school, Aleksandar Ilievski, Nikolche Kolev, Filip Stankovski, Stefan Kuzmanovski and Predrag Gruevski, whose unconditional support and criticism I get almost every day. All the wonderful people I met while at Lehigh: Aleksandra Dasic, Mathew Boyer, James-Evan G. Copti, JJ O'Brien, Gregory D. Potter, Victoria Caruso, Aniket Zarekar, Julia Tomassi, Nilufar Kabulova, David Dobrowski, Anshul Sharma, Melike Kurt, whose friendship kept me involved in things outside of my research endeavors. I'd also like to express my most sincere gratitude to the Krajcev family, who provided me with a home away from home and took me in as one of their own during all my years at Lehigh.

My students in the classes that I have been a teaching assistant. Thank you for providing me the opportunity to train the next generation of chemical and bioengineers. This thesis is dedicated to my family, for their constant support in the last quarter century: My father, Mitko Pavlov, who still is my inspiration in life. His unwavering commitment to support his family and his work ethic has provided me a great basis to frame my own life. My mother, Jasmina Karakabakova-Pavlova, who managed to instill ambition in me and to help me to keep things in perspective. My brother, Vasilij Pavlov, whose constant calls and messages proved to be a great source of strength during my difficult times. My aunt Dajana Pop-Ilieva and cousin Kostanda Stamadjieva for their unwavering support and for always believing in me. Last but not least, my grandparents, may God rest their souls, Vasilije Karakabakov and Desanka Karakabakova for teaching me the value of hard work and how to give back to my community.

This dissertation would not have been possible without you.

Contents

Acknowledgements	iv
List of Tables	xi
List of Figures	xiv
Abstract	1
1 Introduction to Biomolecular Separation Engineering	3
1.1 Biomolecular Chemistry and Synthesis	3
1.2 Production of Biomolecules	4
1.3 Separation Unit Operations	6
1.3.1 Membrane Filtration	6
1.3.2 Sedimentation	6
1.3.3 Extraction	7
1.3.4 Precipitation and Crystallization	7
1.3.5 Adsorption	8
1.3.6 Chromatography	8
1.4 Chromatography Types	9
1.4.1 Size-Exclusion Chromatography (SEC)	10
1.4.2 Reversed-Phase Chromatography	10
1.4.3 Hydrophobic Interaction Chromatography	11

1.4.4	Affinity Chromatography	11
1.4.5	Ion Exchange	12
1.5	Theoretical Considerations	13
1.5.1	Adsorption Principles	13
1.5.2	Chromatography Column Dynamics	17
1.6	Experimental Setup	20
1.7	Methodology and Objectives	23
2	Adsorption parameters of amino acids on DEAE Sepharose and Q Sepharose anion-exchange chromatography at different pH and temperature	30
2.1	Introduction	31
2.2	Theoretical Model	32
2.2.1	Temperature Effect on Physical Parameters	36
2.3	Materials and Methods	38
2.3.1	Equipment Used	38
2.3.2	Stationary Phase Properties	38
2.3.3	Mobile Phase Considerations	39
2.3.4	Sorbate Properties	39
2.3.5	Experimental Procedure	40
2.4	Results	41
2.4.1	Q Sepharose Adsorbent Elution Data	41
2.4.2	DEAE Sepharose Adsorbent Elution Data	42
2.5	Discussion	43
2.5.1	pH Effect	43
2.5.2	Adsorbent Considerations	43
2.5.3	Temperature Effect	44
2.6	Conclusion	47

3	The pH, Temperature and Protein Structure Effect on β-Lactoglobulin A and B Separation in Anion-Exchange Chromatography	71
3.1	Introduction	72
3.2	Theoretical Model	72
3.3	Materials and Methods	76
3.3.1	Equipment Used	76
3.3.2	Adsorbent Properties	76
3.3.3	Buffer Properties	77
3.3.4	Experimental Procedure	78
3.3.5	Computation Algorithm	78
3.4	Results	79
3.5	Discussion	80
3.6	Conclusion	83
4	Effect of pH and Temperature on Amino Acids, Immunoglobulin G and Lysozyme Separation on SP Sepharose Cation-Exchange Chromatography	104
4.1	Introduction	105
4.2	Theoretical Model	105
4.2.1	Adapting the model as a function of temperature	107
4.3	Materials and Methods	109
4.3.1	Equipment used	109
4.3.2	Stationary Phase	109
4.3.3	Sorbate Properties	109
4.3.4	Mobile Phase Properties	110
4.3.5	Experimental Procedure	110
4.3.6	Computational Algorithm	111
4.4	Results	111

4.5	Discussion	113
4.5.1	pH Effect	113
4.5.2	Temperature Effect	114
4.6	Conclusion	116
5	Modelling the Effect of Temperature on the Gel-Filtration Chromatographic Protein Separation	141
5.1	Introduction	142
5.2	Theory	144
5.2.1	Model Development	144
5.2.2	Computational Method	145
5.2.3	Adapting the model as a function of temperature	146
5.3	Parametric considerations	147
5.4	Data Analysis	149
5.5	Results	150
5.6	Discussion	151
5.7	Conclusions	153
6	Numerical Study of the Effect of pH and Temperature of Protein Separation in Anion and Cation Exchange Chromatography	168
6.1	Introduction	169
6.2	Theory	170
6.2.1	Model Development	170
6.2.2	Computational Method	172
6.2.3	Adapting the model as a function of temperature	173
6.2.4	Solution Algorithm	174
6.3	Results	175
6.3.1	pH Effect	176

6.3.2	Temperature Effect	177
6.4	Discussion	177
6.5	Conclusion	180
7	Summary of Conclusions and Future Work	203
7.1	Conclusions	203
7.1.1	pH Effect	203
7.1.2	Temperature Effect	204
7.1.3	Tertiary Structure Effect	204
7.1.4	Theoretical Studies	204
7.2	Future Work	205
	Bibliography	206
	A Curriculum Vitae	212
A.1	Publications	212
A.2	Presentations	213
A.3	Poster Presentations	213
	Biography	215

List of Tables

2.1	Values of the physical parameters estimated from correlations presented above for tryptophan as the solute and water as the solvent at 23°C	48
2.2	Tris-HCl buffer mixing table for 50mM solution[43]	49
2.3	Names of Amino Acids, their pK_a values of their ionizable groups as well as their pI values [49]	50
2.4	First moment (retention time) of each component at temperatures of 5°C, 23°C, 40°C and pH=7.8, 8.4 using Q Sepharose	51
2.5	Separation factor at pH 8.4 using Q Sepharose	52
2.6	Capacity factor at pH 8.4 using Q Sepharose	53
2.7	First moment of each component at temperatures of 5°C, 23°C, 40°C and pH=7.8, 8.4 and 8.8 using DEAE Sepharose	54
2.8	Separation factor at pH 8.4 using DEAE Sepharose	55
2.9	Capacity factor at pH 8.4 using DEAE Sepharose	56
2.10	Summary of the activation energies for each kinetic constant for Q Sepharose at pH 8.4. All values are in kJ/mol.	57
2.11	Summary of the activation energies for each kinetic constant for DEAE Sepharose at pH 8.8. All values are in kJ/mol.	58
3.1	Tris-HCl buffer mixing table for 25mM solution[43]	85

3.2	Parameters derived from the non-linear curve fitting of the experimental data for BSA, the equilibrium constant K_A with values in $[\frac{mL}{g}]$ and the adsorption rate constant k_{ads} with values in $[\frac{mL}{g \cdot sec}]$	86
3.3	Parameters derived from the non-linear curve fitting of the experimental data for LGA and LGB, the equilibrium constant K_A with values in $[\frac{mL}{g}]$ and the adsorption rate constant k_{ads} with values in $[\frac{mL}{g \cdot sec}]$	87
3.4	Activation energies of the adsorption equilibrium constants K_A for BSA in kJ/mol	88
3.5	Separation Factor as a function of pH and temperature.	89
3.6	Activation energies of the adsorption equilibrium constants K_A for both peaks in kJ/mol	90
4.1	Sodium Citrate-Citric Acid mixing tables to create 1L of buffer solution [52]	117
4.2	Data obtained by nonlinear curve fitting for the tyrosine chromatograms	118
4.3	Data obtained by nonlinear curve fitting for the tryptophan chromatograms	119
4.4	Data obtained by nonlinear curve fitting for the Immunoglobulin G chromatograms	120
4.5	Data obtained by nonlinear curve fitting for the Lysozyme chromatograms	121
4.6	Retention Factors for Tyrosine and Tryptophan for all experimental conditions studied	122
4.7	Retention Factors for Immunoglobulin G and lysozyme for all experimental conditions studied	123
4.8	Separation factor between tyrosine and tryptophan for the experimental conditions considered in this study	124
4.9	Separation factor between lysozyme and IgG for the experimental conditions considered in this study	125

4.10	Activation energies in kJ/mol of tyrosine and tryptophan for the pH conditions investigated	126
4.11	Activation energies in kJ/mol of Immunoglobulin G and lysozyme for the pH conditions investigated	127
5.1	Resolution and Selectivity values for the data at particle radius of $45\mu\text{m}$ at different superficial velocities for component 1 BSA and component 2 phenylalanine	154
5.2	Resolution and Selectivity values for the data at particle radius of $25\mu\text{m}$ at different superficial velocities for component 1 BSA and component 2 phenylalanine	155
5.3	Resolution and Selectivity values for the data at particle radius of $70\mu\text{m}$ at different superficial velocities for component 1 BSA and component 2 phenylalanine	156

List of Figures

1.1	Isotherm classification as described by Brunauer et. al.[4]	24
1.2	Packed Aqueous Chromatography Column (Copyright Spectrum, Inc.)	25
1.3	Reciprocating HPLC pump (Copyright Scientific Systems, Inc.) . . .	26
1.4	UV detector for in-line solute analysis (Copyright Spectrum, Inc.) . .	27
1.5	Process Flow Diagram of the experimental setup	28
1.6	Principle of operation of the chromatographic separation process[44] .	29
2.1	Amino Acid chromatograms at a pH of 7.8 at three different tempera- tures at a flowrate of $5ml/min$	59
2.2	Amino Acid chromatograms at a pH of 8.4 at three different tempera- tures at a flowrate of $5ml/min$	60
2.3	Amino Acid chromatograms using DEAE Sepharose at a pH of 7.8 at three different temperatures at a flowrate of $5ml/min$	61
2.4	Amino Acid chromatograms using DEAE Sepharose at a pH of 8.4 at three different temperatures at a flowrate of $5ml/min$	62
2.5	Amino Acid chromatograms using DEAE Sepharose at a pH of 8.8 at three different temperatures at a flowrate of $5ml/min$	63
2.6	Net charge of each amino acid used in this experiment as a function of pH	64
2.7	Empirical correlation between the net charge and the first moment at ambient temperature in Q Sepharose adsorbent	65

2.8	Empirical correlation between the net charge and the first moment at ambient temperature in DEAE Sepharose adsorbent	66
2.9	Titration Curve of Q Sepharose packing[40]	67
2.10	Titration Curve of DEAE Sepharose packing[40]	68
2.11	Adsorption Equilibrium Constant, Adsorption Rate Constant and Desorption Rate Constant for Phenylalanine, Tyrosine and Tryptophan as a function of temperature at a pH of 8.4 using Q Sepharose. (a) Equilibrium Constant vs. Temperature (b) Adsorption Rate Constant vs. Temperature (c) Desorption Rate Constant vs. Temperature (d) Arrhenius plot of the Equilibrium Constant (e) Arrhenius plot of the Adsorption Rate Constant (f) Arrhenius plot of the Desorption Rate Constant	69
2.12	Adsorption Equilibrium Constant, Adsorption Rate Constant and Desorption Rate Constant for Tyrosine and Tryptophan as a function of temperature at a pH of 8.8 using DEAE Sepharose. (a) Equilibrium Constant vs. Temperature (b) Adsorption Rate Constant vs. Temperature (c) Desorption Rate Constant vs. Temperature (d) Arrhenius plot of the Equilibrium Constant (e) Arrhenius plot of the Adsorption Rate Constant (f) Arrhenius plot of the Desorption Rate Constant	70
3.1	Bovine Serum Albumin chromatograms at the different pH and temperature conditions considered in this work. The vertical marker indicates column void volume.	91
3.2	β -lactoglobulin chromatograms at a pH of 7.8 at three different temperatures at a flowrate of $5ml/min$	92
3.3	β -lactoglobulin chromatograms at a pH of 8.4 at three different temperatures at a flowrate of $5ml/min$	93

3.4	β -lactoglobulin chromatograms at a pH of 8.8 at three different temperatures at a flowrate of 5ml/min	94
3.5	β -lactoglobulin chromatograms at a pH of 8.8 at room temperature at a flowrate of 5ml/min with FFT simulation for both peaks	95
3.6	Titration curves of BSA, both in the pH range of 3 - 11 and the range of interest from 7.5 - 9	96
3.7	Adsorption equilibrium constant of BSA as a function of the protein net charge.	97
3.8	Arrhenius plots for the K_A values for BSA at different pH values . . .	98
3.9	Arrhenius plots for the K_A values for both LGA and LGB at different pH values	99
3.10	Titration curves of lactoglobulin A and B, both in the pH range of 1 - 14 and the range of interest from 7.5 - 9	100
3.11	Adsorption equilibrium constant of LGB and LGA as a function of the protein net charge at 40°C.	101
3.12	β -Lactoglobulin A tertiary structure is given in both panels. On the panel on the left, aspartic acid residues are highlighted with yellow circles. The aspartic acid residue at position 64 is highlighted with a red circle. On the right panel, the valine residue at position 118 is highlighted with a blue circle and the other valine residues are highlighted with yellow circles. [22]	102
3.13	β -Lactoglobulin B tertiary structure s given in both panels. On the panel on the left, glycine residues are highlighted with yellow circles. The glycine residue at position 64 is highlighted with a red circle. On the right panel, the alanine residue at position 118 is highlighted with a blue circle and the other alanine residues are highlighted with yellow circles. [26]	103

4.1	Tyrosine and Tryptophan chromatograms at a pH of 3.0 at 5°C, 23°C and 40°C at a flow rate of 5ml/min.	128
4.2	Tyrosine and Tryptophan chromatograms at a pH of 3.6 at 5°C, 23°C and 40°C at a flow rate of 5ml/min.	129
4.3	Tyrosine and Tryptophan chromatograms at a pH of 4.2 at 5°C, 23°C and 40°C at a flow rate of 5ml/min.	130
4.4	Immunoglobulin G and Lysozyme chromatograms at a pH of 3.0 at 5°C, 23°C and 40°C at a flow rate of 5ml/min.	131
4.5	Immunoglobulin G and Lysozyme chromatograms at a pH of 3.6 at 5°C, 23°C and 40°C at a flow rate of 5ml/min.	132
4.6	Immunoglobulin G and Lysozyme chromatograms at a pH of 4.2 at 5°C, 23°C and 40°C at a flow rate of 5ml/min. In these figures both proteins eluted as a single peak.	133
4.7	Immunoglobulin G and Lysozyme chromatogram at a pH=3.0 and temperature of 23°C with their respective FFT Simulation Data	134
4.8	Titration curves of both tyrosine and tryptophan, including the pH range of interest	135
4.9	Titration curve of Lysozyme along with the pH range of interest [45] .	136
4.10	Correlation between the net charge and the equilibrium constant of tyrosine and tryptophan at 23°C	137
4.11	Adsorption Equilibrium constants correlated as a function of net charge of Lysozyme for 23°C	138
4.12	Arrhenius plots of the adsorption equilibrium constant as a function of temperature for Tyrosine and Tryptophan	139
4.13	Arrhenius plots of the adsorption equilibrium constant as a function of temperature for Immunoglobulin G and lysozyme	140

5.1	Elution curves for Bovine Serum Albumin at a fixed mass transfer coefficient ($k_f = 0.0015\text{cm}/\text{sec}$) and varying dispersion caused by temperature changes. Notice that the peak tailing increases as the temperature decreases.	157
5.2	Effect of the mass transfer coefficient at different temperatures at fixed dispersion ($D_L = 0.0015\text{cm}^2/\text{sec}$). The peak height decreases slightly at lower temperatures.	158
5.3	Chromatograms at a superficial velocity of $0.01\text{cm}/\text{s}$ and particle radius of $45\mu\text{m}$	159
5.4	Chromatograms at a superficial velocity of $0.05\text{cm}/\text{s}$ and particle radius of $45\mu\text{m}$	160
5.5	Chromatograms at a superficial velocity of $0.1\text{cm}/\text{s}$ and particle radius of $45\mu\text{m}$	161
5.6	Chromatograms at a superficial velocity of $0.01\text{cm}/\text{s}$ and particle radius of $25\mu\text{m}$	162
5.7	Chromatograms at a superficial velocity of $0.05\text{cm}/\text{s}$ and particle radius of $25\mu\text{m}$	163
5.8	Chromatograms at a superficial velocity of $0.1\text{cm}/\text{s}$ and particle radius of $25\mu\text{m}$	164
5.9	Chromatograms at a superficial velocity of $0.01\text{cm}/\text{s}$ and particle radius of $70\mu\text{m}$	165
5.10	Chromatograms at a superficial velocity of $0.05\text{cm}/\text{s}$ and particle radius of $70\mu\text{m}$	166
5.11	Chromatograms at a superficial velocity of $0.1\text{cm}/\text{s}$ and particle radius of $70\mu\text{m}$	167
6.1	Interpolated values of the net charge of BSA as a function of pH . . .	182
6.2	Interpolated values of the net charge of Lysozyme as a function of pH	183

6.3	Correlations of the adsorption equilibrium constant as a function of net charge at different experimental temperatures for BSA	184
6.4	Correlations of the adsorption equilibrium constant as a function of net charge at different experimental temperatures for Lysozyme . . .	185
6.5	Correlations of the adsorption rate constant as a function of net charge at different experimental temperatures for BSA using the regression model $y = A \exp(Bx)$	186
6.6	Arrhenius plot of the adsorption equilibrium constant as a function of temperature at different experimental pH values for BSA	187
6.7	Arrhenius plot of the adsorption equilibrium constant as a function of temperature at different experimental pH values for Lysozyme	188
6.8	Arrhenius plot of the adsorption rate constant as a function of temperature at different experimental pH values for BSA	189
6.9	Arrhenius plot of the adsorption rate constant as a function of temperature at different experimental pH values for LYS	190
6.10	Mesh plots of BSA chromatograms at a flow rate of 0.1cm/s within the pH range of 7.8 and 10 in anion-exchange chromatography	191
6.11	Mesh plots of Lysozyme chromatograms at a flow rate of 0.1cm/s within the pH range of 2.5 and 4.5 in cation-exchange chromatography	192
6.12	Mesh plots of BSA chromatograms at a flow rate of 0.1cm/s within the temperature range of 273K to 315K in anion-exchange chromatography	193
6.13	Mesh plots of Lysozyme chromatograms at a flow rate of 0.1cm/s within the temperature range of 273K to 315K in cation-exchange chromatography	194
6.14	Elution curves for BSA at pH values of 8.0, 9.0 and 10.0 for three different temperatures in anion-exchange chromatography	195

6.15	Elution curves for Lysozyme at pH values of 2.5, 3.5 and 4.5 for three different temperatures in cation-exchange chromatography	196
6.16	Elution curves for BSA at temperature values of 5°C, 20°C and 40°C for three different pH values in anion-exchange chromatography . . .	197
6.17	Elution curves for Lysozyme at 5°C, 20°C and 40°C for three different pH values in cation-exchange chromatography	198
6.18	HETP for BSA as a function of pH for three different temperatures in anion-exchange chromatography	199
6.19	HETP for Lysozyme as a function of pH for three different temperatures in cation-exchange chromatography	200
6.20	HETP for BSA as a function of temperature for three different pH values in anion-exchange chromatography	201
6.21	HETP for Lysozyme as a function of temperature for three different pH values in cation-exchange chromatography	202

Abstract

Bioseparation technology remains a key bottleneck in biomolecular manufacturing. Several important unit operations dominate the industry, with ion-exchange chromatography leading the way in providing a scalable, robust and cost-effective way to isolate a desired biomolecule. Engineering of these separation technologies remains a major hurdle, as methods that were originally developed by analytical chemistry are employed to describe the unit operations. In this thesis, the primary goal is to provide a solid engineering analysis of the ion-exchange chromatography system to aid the practicing engineer in modeling and scale-up.

The other major goal of this work is to provide sufficient explanation as to what is the effect of operating variables such as pH and temperature on the separation. When ion-exchange chromatography is used for biomolecular separation, pH is the key variable that provides the conditions for the biomolecule to have a sufficient charge to get adsorbed onto the adsorbent material. Modeling of the binding force was achieved by measuring the equilibrium constant K_A for the biomolecule, and then correlating the values to the net charges of the biomolecules at the pH conditions. In anion-exchange chromatography, more basic pH led to higher retention due to the higher negative charge of the biomolecules. More acidic pH led to more positive ionization of the biomolecules and contributed to higher retention.

For the case of temperature, industrial guidelines do not provide any direction as to how changing the temperature affects the separation. In anion-exchange, higher

retention and resolution was observed with increasing temperature, and in cation-exchange, higher retention and resolution were observed with decreasing temperature. These effects are completely opposite from one another and can provide a basis for new modes of temperature driven ion-exchange separation. Using the retention data for different temperatures, an Arrhenius plot was created to explain the trends that were observed. For the cation-exchange chromatography, a negative activation energy was observed and for anion-exchange chromatography a positive activation energy was observed.

The tertiary structure of the protein can also provide very useful information about the nature of the binding affinity of the biomolecule to the adsorbent ligand. The surface charges of the biomolecule appear to be instrumental in adsorption, providing for a higher retention when compared to a homologous biomolecule without the same surface charges.

Taking these established effects for the chemical nature of the process, a comprehensive model for the ion-exchange biomolecular separation was established. In the model, physical variables were investigated first to determine the extent by which they affect the separation. Afterwards, the correlations were coupled to the trends derived from the experimental data so that the elution chromatograms at any pH and temperature for ion-exchange chromatography can be computed in a rapid and useful fashion.

This work establishes a good theoretical basis for analysis of packed bed sorption processes to investigate the effect of physical variables such as pH, temperature and the tertiary structure. The data and models presented here provide a practicing engineer or researcher a framework for understanding the process, which can then be used in a predictive way for scale-up of the process.

Chapter 1

Introduction to Biomolecular Separation Engineering

1.1 Biomolecular Chemistry and Synthesis

Biomolecules are an important class of molecules characterized by their function in biological processes. They range in size, shape, charge and role within biological systems and have been widely produced for therapeutic and clinical purposes. This dissertation is concerned with the purification of such components while taking into consideration of their chemical and physical properties which allow for efficient and cost effective separation. Biomolecules can be separated into:

1. *Carbohydrates*: Commonly known as sugars, they range in size starting with monosaccharides which have between 3 and 6 carbon atoms to longer chains of polysaccharides, which are long polymers of monosaccharides. They provide energy to biological processes or structural support to organisms. Examples include glucose and cellulose.
2. *Lipids*: Long branched molecules where the fatty acid chains are bound to glycerol and commonly used as building blocks for cell membranes. Examples

of lipids are triglycerides and phospholipids.

3. *Proteins*: Large biomolecules comprised of amino acids. One role that they have are as enzymes which catalyze biological reactions. Common examples are pepsin and hemoglobin.
4. *Nucleic Acids*: They consist of phosphate sugar backbones which hold the nucleobases within a double-helix structure. These molecules set the hereditary basis of organisms and transmit genetic information. Examples of nucleic acids are deoxyribonucleic acid (DNA) and ribonucleic acid (RNA).

These molecules are found in all cells, which are utilized in biomolecular engineering. A typical biotechnological approach of producing any of these molecules involves manipulating the genetic material of the cell to initiate production *en masse* of the desired component. Each cell contains a copy of genetic material that carries information about a desired protein. The cellular machinery can use the genetic material as instructions to synthesize the protein. The amino acids are polymerized into proteins by structures in the cells called ribosomes which are an efficient method for protein synthesis. Other chemical methods of protein synthesis lead to errors. The proteins that are synthesized in a biological manner are of higher yield and can be used for mass production of therapeutic molecules. The separation of the biomolecule of interest from other proteins produced by the cell is a key bottleneck in biotechnological operation. A better understanding and establishing clear engineering principles of separation processes is an important step towards a better production of biomolecules.

1.2 Production of Biomolecules

A biotechnology process consists of two parts: upstream, where the cells are grown and produce the protein or biomolecule of interest, and downstream, where the molecule

of interest is separated from the cellular molecules and isolated so that it can be used for therapeutic and clinical purpose.

In the upstream part, a typical workflow involves several bioreactors, which ferment the cells that are used for production of the biomolecule of interest. They start out in a cascading fashion, from smaller batches which are fermented to saturation and then transferred to very large production bioreactors. The molecule of interest is expressed in the production bioreactor once the fermentation broth is saturated with the maximum amount of cells that it can sustain. The yield of the biomolecule of interest is usually much smaller than the overall cell concentration, making it quite challenging for the removal of the desired component.

The downstream component of biotechnological production is responsible for separating the biomolecule of interest. As discussed, the desired molecule is quite similar to the other byproduct molecules, making the recovery of the target biomolecule very challenging. The first consideration of the engineer is to know if the cells secrete the target protein outside of the cellular body, or if they store it within the cell. If the proteins are secreted, they are usually easier to separate as they are not mixed with the proteins present in the cell. The other situation is where the desired biomolecule is produced within the cell and not secreted. In this case, the cell membrane will need to be burst open, or lysed, so that the cellular contents are released, making the desired biomolecule recoverable from the rest of the cellular material.

At this point, a number of different separation techniques are used to recover the desired cellular material. Each of them has their own benefits and drawbacks, so a brief overview of the common separation strategies for biomolecules is presented in the next section.

1.3 Separation Unit Operations

This section discusses the unit operations which are involved in handling the lysate to purify the target biomolecules. There are multiple techniques that are employed in a given biotechnological process, however some of these operations may be omitted, depending on the desired biomolecule. The ones that are mentioned here are related to industrial production of biomolecules, however other techniques may also be applied to assess purity or composition of the desired biomolecule.

1.3.1 Membrane Filtration

Membrane filtration is a operation that is used to separate particulate or solute components in a fluid suspension according to their size by flowing under a pressure gradient through a porous membrane. When the product is secreted from the cells, and the cells need to be removed so that the desired product is isolated in the permeate. The fluid flows perpendicular to the membrane, which results in a cake of solids developing on the membrane surface. The other membrane filtration technique is *tangential flow filtration*, where the fluid flows parallel to the membrane to minimize buildup of solids. Membrane filtration oftentimes occurs in the early stages of bioproduct purification, when the desired biomolecule is present in a large volume of aqueous solution. Using membrane filtration the volume can be reduced so that the scale of subsequent unit operations can be minimized, thus reducing the cost of the processing. [14]

1.3.2 Sedimentation

Sedimentation represents the movement of particles in a given interial field. This unit operation has a wide-reaching application in the separation field, ranging from settling tanks to centrifuges and field-flow fractionators. Particles are separated at

a very large scale in continuous centrifuges, and analytic centrifuges such as high speed ultracentrifuges can be used for estimating molecular weights and diffusion coefficients. The most common application of sedimentation in biomolecular separation includes clarification of broths and lysates, collecting cell debris or inclusion bodies and generating density gradients for separation of fluids. [14]

1.3.3 Extraction

Extraction occurs between two phases which come into contact with the goal of transferring solute that is present in one phase into the other phase. For separation of biomolecules, the phases that are used are usually two immiscible liquids, often using an organic solvent as the extracting liquid from an aqueous solution. The biomolecules that are extracted using this method are usually stable in the organic solvent, which are usually low molecular weight antibiotics. Organic solvents are not suitable for protein extraction as they degrade in them. Proteins can be extracted using two aqueous liquid phases consisting of two immiscible or incompatible polymers. Extraction is highly advantageous due to the reduction of the processing volume to separate the desired product from the cell debris. [14]

1.3.4 Precipitation and Crystallization

Precipitation causes solutes to come out of a solution as a solid, so is used early in the purification process. The execution is inexpensive and simple, resulting in a biomolecule that is quite stable in long-term in storage. The differences between protein solubilities form the basis of precipitative separation. Fractional precipitation can be carried out to precipitate the biomolecule of interest and leave the contaminating molecules in the mother liquor.[14]

Crystallization produces solid particles from a solutions which are different than precipitates as the molecules that are crystallized are arranged in three-dimensional

arrays called space lattices. The solubility of the desired biomolecule is also much higher than in precipitation. The theoretical treatment for precipitation is quite different than the one for crystallization. Crystallization is capable of producing biomolecules at high purity, usually above 99%, where it can be applied for polishing and purification or for crystallography. For some biomolecules, for example penicillin, it is necessary to have a final crystalline form. [14]

1.3.5 Adsorption

Adsorptive processes use two phases, generally a fluid phase and a solid phase, which selectively adsorb, or bind a solute dissolved in the fluid phase onto the surface of the solid phase. Different chemistries of both the fluid and the solid have been employed to give rise to better selectivity. When the fluid comes in contact with the solid, an equilibrium is established between the solute concentration present in the fluid with the one adsorbed onto the adsorbent. [37] Adsorption is an effective way of isolating the desired biomolecule as the adsorbent surface can selectively bind the desired biomolecule. [14] This process occurs irreversibly, so when the solid phase is completely saturated with the desired biomolecule there will not be any more biomolecules adsorbed. At this point the biomolecules bound to the solid phase will be desorbed or released as pure components, by changing the fluid phase composition. Adsorptive processes are quite versatile and offer an advantage over the other processes discussed thus far due to their high selectivity for the target product. The chemistry of adsorptive processes is the basis for the chromatographic processes, which will be discussed in much greater detail in this work.

1.3.6 Chromatography

Chromatographic processes have been the gold standard and the workhorse of the biotechnological industry. Their scalability, versatility and selectivity allow them to

be efficiently used in any biomolecular manufacturing process. The engineering design and the effect of different parameters on the separation are discussed in great detail. Since the discovery of chromatography by Mikhail Tswett in 1903,[49] engineers and scientists have tried to devise a comprehensive way for theoretical analysis of the chromatography system. Chromatography is performed in a manner similar to adsorption, by using a bed of porous particles, or *stationary phase*, and a solvent, or a *mobile phase*. The column of porous particles is first equilibrated with the solvent by submerging the stationary phase with the mobile phase. After this is completed, a mixture of components is injected into the flow path of the mobile phase so it can enter the stationary phase. When the mixture of components reaches the porous particles, some of the components dissolved in the mobile phase get retained into the pores more strongly relative to other components present in the mixture. This results in some components eluting out of the column earlier, i.e. the components that are not retained as strongly, with the components that are retained more strongly elute later on. The difference in elution times enables the separation of the components present in the mixture. The types and characteristics of chromatographic processes is discussed in the next section.

1.4 Chromatography Types

The development of different types of chromatography is intrinsically related to the development of different adsorption chemistries. On the surface of the adsorbent, different ligands can be found that confer properties that are favorable for sorption of the desired biomolecule. If the solutes have very similar characteristics, the binding strength for each may be different, which will lead to retention differences of the molecules. The parameters that must be considered are the surface area available for adsorption, typically ranging from 100 to 1500 m^2/g [14] and the particle radius,

ranging from $1.8\mu\text{m}$ up to $500\mu\text{m}$ (70 mesh). The diffusion of the solute into the particle pores and the path length that the molecule will take is quite important, therefore different manufacturers have experimented with packing materials to make the surface area more accessible to the solute. The various types of packing materials and how they achieve the separation are discussed in this section.

1.4.1 Size-Exclusion Chromatography (SEC)

Oftentimes referred to as *gel-filtration*, size-exclusion chromatography separates molecules on the basis of their molecular weight, which is indicative of their molecular size. The resin itself is not bonded to any ligand, and it is not derivatized to provide any adsorption between the solutes and the packing material. The basis of the separation in this case is the molecular diffusion, where for larger molecules a small portion of the pore volume of the particle is accessible. In contrast, small molecules are able to access the majority of the intraparticle void spaces which remain inside the column longer than the larger molecules. The large molecules elute first, and the smaller molecules that were retained in the packing elute later on. This technique is useful for eliminating high or low molecular weight components from the mixture. As there is no binding, the processing capacity of size-exclusion chromatography is quite low. [14]

1.4.2 Reversed-Phase Chromatography

One of the most common materials used in reversed-phase chromatography is silica which is compatible with water or organic solvents. It is quite durable as it does not collapse under high pressure, however it is not stable at pH extremes. The silica particles can be uncoated with other ligands, which is known as *normal phase*, or they can be polymerized, or *end-capped*, which means that the uncovered silica surface is covered with an organic layer after binding with a hydrophobic chain. Reversed-

phase chromatography uses the hydrophobic phase on the surface of the resin. The naming of *reversed phase* follows the convention where hydrophobic solutes bind more strongly than they would on normal phase silica. A non-polar mobile phase gradient is applied where the solutes are first introduced in polar solvent, typically water, and then slowly applying the non-polar gradient to release the hydrophobic solutes. [14]

1.4.3 Hydrophobic Interaction Chromatography

The hydrophobic interaction chromatography is similar to reversed-phase chromatography, however the solutes adsorb to the hydrophobic surface at high salt conditions and redissolve in the mobile phase as the salt concentration is reduced. The mobile phase is kept polar throughout the elution and the salt concentration is varied to effectuate partitioning to the surface. This separation employs methods encountered in precipitation, rather than either reversed phase or ion exchange. This type of chromatography is highly sensitive to pH, the type of salt, buffer type and temperature. [14]

1.4.4 Affinity Chromatography

Affinity chromatography is a highly selective separation technology that takes advantage of native biological structural motifs. The packing is coated with antibodies, antigens or dyes (Coomassie Blue) by using cyanogen bromide to conjugate them to the packing. The attached antibody is then used to selectively capture the desired biomolecule from the mixture, while the impurities elute out of the column. A change in the pH or salt concentration can be used to recover the desired molecule after the impurities have been removed. [3]

Immobilized Metal Affinity Chromatography (IMAC)

Immobilized Metal Affinity Chromatography is a special case of affinity chromatography as it uses a metal ion chelated to the chromatography resin instead of an organic molecule. Various transition metal ions are used to recover metalloproteins or proteins with a high concentration of histidine, tryptophan or cysteine residues. Genetically engineered proteins have a high amount of poly-histidines so that they can be easily recovered using IMAC compared to other chromatographic techniques. [14]

1.4.5 Ion Exchange

This work focuses on ion-exchange chromatography. In an ion-exchange resin, the pores of the particles contain ligands that are either positively or negatively charged. In an anion-exchange resin there is a positively charged ligand such as diethylaminoethyl (DEAE) ($2C_2H_5N^+HC_2H_5$) and in an cation-exchange resin there is a negatively charged ligand such as carboxyl (COO^-). If the mixture of components injected into the anion exchange column is negatively charged, they will interact with the positively charged ligand and will get retained in the column. The components in the mixture that remain uncharged or positively charged at the mobile phase conditions would not get retained and elute out. To release the components that get retained on the ligands, a counter-ion is introduced in the form of a salt gradient, where the added ionic strength of the mobile phase causes the adsorbed proteins to desorb. The retained components elute in an order depending on their isoelectric point (pI) and the buffer pH, with the molecules that have the largest difference between the pI and the pH eluting last as they are the most ionized.

The ion-exchange unit operation first involves a binding step, where the mixture of components is loaded onto the column. The mobile phase provides conditions such that the biomolecule of interest is charged, and the rest of the components that are either uncharged or oppositely charged elute from the column. After that step is

completed, a salt gradient is applied, which causes the negatively charged molecules to desorb from the packing. This will cause the molecule of interest to elute free of any other contaminants [41], provided there is enough ionization difference from the other charged molecules.

The procedures for separating a mixture using ion-exchange chromatography are a common industry practice. Up until this point, the effect of pH and especially temperature in ion-exchange chromatography have not been fully elucidated. There have been many studies done on the effect of pH[41] but the literature on temperature is quite scarce[48]. This work aims to illustrate the effect of pH and temperature in both cation and anion exchangers, and to demonstrate how the separation is affected by changing the conditions. By utilizing a combination of theoretical models and applying them to experimental data, the effects and the trends of the separation can be understood and applied to a variety of systems. The outcome of this work will enable any researcher and engineer to computationally predict the effect of changing pH and temperature on the elution and separation.

1.5 Theoretical Considerations

A discussion about the chemistry that occurs on the surface of the adsorbent is warranted to set the theoretical basis of the separation. A short explanation about the developments of adsorption theories is presented, along with the ion-exchange mode of operation so that the subject is covered with enough detail in order to set the stage for the following chapters.

1.5.1 Adsorption Principles

Generally speaking, adsorption can be categorized as two fundamental phenomena: physical adsorption, which involves only relatively weak intermolecular forces and

chemisorption which involves the formation of a chemical bond between the sorbate molecule and the surface of the adsorbent. Despite these descriptions, there is no clear way of making a determination whether one type of adsorption falls in one category over the other. There are certain features that can be used to distinguish one type of adsorption over the other. Physical adsorption generally has low heats of adsorption with non-specific binding and can be either a monolayer or a multilayer coverage. The process reversible and quite rapid and it does not involve electron transfer. Chemisorption, on the other hand has a high heat of adsorption, highly specific sorption which only forms a monolayer. The rates are slow and irreversible and there is an electron transfer that leads to bond formation between the sorbate and the packing. [37]

In developing the adsorption theory, five isotherm types were identified and are illustrated in Figure 1.1 Type I describes a definite saturation limit, which represents complete micropore filling. This has been previously described by Langmuir[23] for monolayer adsorption. Types II and III describe adsorbents of varying pore size ranges where a progression from monolayer to multilayer adsorption is observed. Type IV suggests a formation of two surface layers due to different geometries of the packing, and the isotherm of type V is encountered due to intermolecular attraction effects.[37] To convey the mechanics of adsorption, the Langmuir isotherm will be presented and its relation to this work will be discussed

Langmuir Isotherm

Irving Langmuir[23] presented the first and simplest theoretical model for monolayer adsorption in gaseous systems, assuming that the molecules are adsorbed at a fixed number of defined states. Each site can hold one adsorbate molecule, with all sites being energetically equivalent and no interaction between molecules on neighboring

sites. The sorbate is exchanged between the adsorbed and desorbed states:

$$k_a p(1 - \Theta) \tag{1.1}$$

for the adsorption rate and

$$k_d \Theta \tag{1.2}$$

for the desorption rate. In these expressions, k_a is the adsorption rate, Θ is the fractional coverage as $\Theta = q/q_s$, with q_s being the total number of sites, q being the sorbate concentration and p is the partial pressure. At equilibrium, the rates of both adsorption and desorption are equal:

$$\frac{\Theta}{1 - \Theta} = \frac{k_a}{k_d} p = Kp \tag{1.3}$$

In expression 1.3, $K = \frac{k_a}{k_d}$ is the adsorption equilibrium constants. The fractional coverage can also be rearranged as:

$$\Theta = \frac{Kp}{1 + Kp} \tag{1.4}$$

which exhibits the behavior exactly described by the Type I isotherm. As the pressure approaches infinity, the coverage approaches 1, while at low partial pressures, Henry's law is approached.

$$\lim_{p \rightarrow 0} \left(\frac{q}{p} \right) = K \tag{1.5}$$

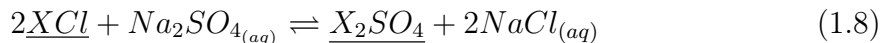
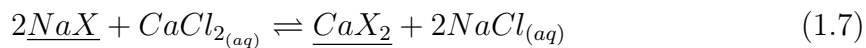
As q_s represents fixed number of surface sites, it is a temperature independent quantity. The equilibrium constant is temperature dependent, following a van't Hoff[37] or Arrhenius[11] type expression as presented in Equation 1.6.

$$K = A_0 \exp\left(\frac{-\Delta H_0}{RT}\right) \tag{1.6}$$

This model sets the basis for analysis of the temperature effects presented in latter parts of this work. One important point to note about the expression is that the ΔH_0 term should not be understood as purely the enthalpy of the process. The parameter can be understood as a phenomenological quantity without any physical significance.[27] Nevertheless, the value of the expression is quite important in interpreting the trends observed in ion-exchange chromatography.

Ion Exchange Principles

Typically, ion exchangers contain materials that release cations or anions, which can be stoichiometrically exchanged with an equivalent amount of other ions. An example of cation exchanger is given in expression 1.7 and an example for an anion exchanger is given in expression 1.8.



The underlined parameters in expressions 1.7 and 1.8 refer to the solid phase of the adsorbent. The similarities with the Langmuir isotherm presented in the previous section are not immediately apparent. For example, taking the cation process in expression 1.7, if $CaCl_2$ needs to be removed from hard water, the solid NaX will release Na^+ ions to replace the Ca^{2+} ions, shifting the reaction equilibrium to the right. As more Ca^{2+} is removed, the adsorbent material will be exhausted from its Na^+ counterion, with the bound Ca^{2+} concentration on the adsorbent resembling the Langmuir isotherm. After the bed reaches its capacity, it can be regenerated by shifting the equilibrium to the left, typically by introducing excess $NaCl$ which will strip out the bound material and replenish it with Na^+ [16].

The same principle applies to proteins in ion-exchange chromatography. The

amino acid residues that are on the surface of the protein can become charged under different pH conditions. The biomolecule is not charged if it is close to its isoelectric point (pI), and as the pH changes to more acidic, the biomolecule becomes more positively charged, and as the pH becomes more basic, the biomolecule becomes more negatively charged. Anion exchangers are suitable for adsorbing negatively charged molecules as they have a positively charged ligand, and cation exchangers are good for adsorbing positively charged biomolecules. Industry guidelines specify that the more a molecule is far from its pI value, the stronger it binds to the adsorbent.[41]

1.5.2 Chromatography Column Dynamics

In describing the dynamics of the column, a variety of models have been established in the past. The plate model, which approximates the chromatograph as a series of well-mixed tanks, has been in use since 1941. The elution curve from the chromatography can be described as a Gaussian curve, where the width of the peak w and the retention time t_R can give a broad characterization of the number of theoretical tanks, or plates that the column has. By dividing the column length by the number of plates, the height-equivalent theoretical plate (HETP) is obtained. This method is quite crude since it does not fully take into account the dispersion and film mass transfer effects inside the column, therefore it is not a good candidate for characterizing the system[29].

Another, widely used model is the van Deemeter equation, which is a simple algebraic function given in Equation 1.9 between the superficial velocity u and the HETP[46].

$$HETP = A + \frac{B}{u} + Cu \tag{1.9}$$

A number of researchers have used the expression to come up with the with the dimensionless parameters that are the coefficients A, B and C of the algebraic ex-

pression. However, the van Deemter equation does not give us a full characterization of the chromatographic peak and does not provide us with enough insight about the surface chemistry. A better model that does take into account the dispersion and the additional transport caused by solute back-mixing due to the nonuniformity of the velocity is given by Lapidus and Amundson [24]. They combine the binary diffusivity in the mobile phase with a dispersion coefficient in an algebraic fashion, but they may not always be linearly related. This makes the model inadequate for a fundamental study, since a correct accounting of all the interactions between the physical parameters is needed.

The model that is utilized in this work is based on the generalized rate model (GRM) popularized by Schneider and Smith[39]. They used several partial differential equation to fully characterize the chromatography process, using the conservation of mass and the Navier-Stokes equations to fully characterize the chromatography system. They incorporated the flow in the mobile phase, the solute transfer from the mobile phase to the pores of the particles and the surface adsorption and desorption occurring inside the pores. Unfortunately, there is no straightforward way to invert the Laplace solution that Schneider and Smith are presenting back into the time domain[33]. The model will not be introduced now as it is given adequate space in the subsequent chapters. An analysis based on this model can be done in two different ways. The first one is to use the final value theorem of the Laplace transform[47] in order to obtain the statistical moments for the experimental elution curves. The second one is to numerically invert the Laplace transform using the Fast Fourier Transform (FFT) algorithm in order to get a theoretical solution. Both methods have their own merits and drawbacks and they will be discussed in the next section.

Moments Method

The moments method uses the evaluation of the statistical moments, i.e. the absolute and central moments. Using the van der Laan theorem[47], an analytical expression can be obtained for either the breakthrough curve or the pulse response. The first moment computation is given in expression 1.10 and the second moment computation is given in expression 1.11.

$$\mu_1 = t = \frac{\int_0^\infty ct \, dt}{\int_0^\infty c \, dt} = \lim_{s \rightarrow 0} \frac{\partial c}{\partial s} \frac{1}{c_0} \quad (1.10)$$

$$\mu_2 = \sigma^2 = \frac{\int_0^\infty c(t - \mu)^2 dt}{\int_0^\infty c \, dt} = \lim_{s \rightarrow 0} \frac{\partial^2 c}{\partial s^2} \left(\frac{1}{c_0} \right) - \mu^2 \quad (1.11)$$

For example, the first absolute moment μ_1' characterizes the position of the center of gravity, representing the retention time t and the second central moment μ_2 depends on the width of the chromatographic curve which represents the variance, σ^2 . To utilize this method, the curve needs to be well defined so that the integral of the chromatogram can be accurately computed. Components that are co-eluting or eluting too close to one another cannot be analyzed using this method since the width of the chromatogram cannot be accurately measured. Despite this drawback, this method can give good results for the equilibrium constant.

Fast Fourier Transform (FFT) Method

The Fast Fourier Transform Method was first introduced for the evaluation of chromatographic and adsorption problems by Hsu [20] and Dranoff [19]. The algorithm was first popularized by Cooley and Tukey[6] and can compute the Fourier series in a relatively fast and straightforward fashion. In this work, MATLAB version R2015a was used whose IFFT subroutine was used which computes the formula given in

expression 1.12.

$$\bar{f}(t) = f(n \Delta T) = \frac{N}{2T} \left[\left(\frac{1}{N} \right) \sum_{k=1}^N F \left(\frac{i(k-1)\pi}{T} \right) \exp \left(i \frac{2\pi(n-1)(k-1)}{N} \right) \right] \quad (1.12)$$

These features makes it ideal for use in a non-linear curve fitting algorithm, to fit the theoretical model to the experimental data. One benefit here is that we can fit the theoretical model to a limited set of data, namely peaks that have co-eluted can be easily characterized. The adsorption and desorption rates will be more precise when computed by the FFT method. Regardless of which method is utilized, both should yield the same result.

Additional theoretical considerations

One important consideration to take into account is the fact that the values for dispersion, diffusion and film mass transfer will need to be characterized so that their influence is properly incorporated into the model. All of the physical parameters have correlations for packed beds that have been previously established[2, 54, 25, 5]. Each parameter was evaluated for the different temperature under which the column was run. The correlations require inputs for the viscosity and density of the mobile phase so the assumption was to take the measurements for pure water at that temperature[7] as all the buffers used in this work were aqueous.

1.6 Experimental Setup

To design the experiment used in this study, several important considerations needed to be kept in mind to gain fundamental information from the data that is collected. The experimental setup needs to withstand the conditions of the experiment, that is the equipment used needs to withstand the pressure, pH and temperature levels

that are considered in the study. Next, the stationary phase that is selected needs to remain reasonably stable and not undergo any physical or chemical changes when subjected to different variables. The adsorbent bed should not shrink or expand considerably when subjected to different temperatures, pH levels and pressures. The column was packed very carefully by first equilibrating the adsorbent material in the desired buffer, then degassing it to desorb any gases. The column was then filled with degassed buffer, in which the degassed adsorbent and buffer mixture was poured. The gel was left to sediment overnight so that the column is perfectly packed and the particles are uniformly distributed. A picture of the packed column is given in Figure 1.2. The properties of the mobile phase needs to stay constant over the course of the experiment. To avoid any variation in the composition, fresh buffer for each temperature condition was prepared so that the pH level is well maintained. This enabled our data to be directly comparable at different conditions to accurately analyze the effects of pH and temperature independently of one another.

To achieve good temperature control, a recirculating bath with a glycol-water mixture as thermal fluid was used. The column was placed in a shell, such that the combined column and shell act as a heat exchanger, where the solid phase is on the tube side and the thermal fluid is on the shell side. To reach thermal equilibrium the column was flushed with at least five column volumes (CV) of the desired buffer for the condition, while the bath temperature was set at the experimental temperature. This gave ample time for the packing to reach the desired temperature and for the column pH to equilibrate with the column packing.

The column was set up such that the packing length was held in place by syringe plungers. This prevents the bed from moving due to issues related to either pressure or temperature. To ensure uniform flow in the column, a reciprocating pump pictured in Figure 1.3 was used to ensure a precise flow rate at a constant pressure drop. The flow direction in the column was set up such that the flow was introduced from the

lowest end of the column, rather than from the top of the column. The justification behind this is that the hydrostatic pressure of the packing, along with the syringe holding it in place ensures a uniform flow throughout the column to avoid pressure that would shrink the bed.

The column effluent was analyzed in-line by a UV absorbance detector. Most common biomolecules absorb light at wavelengths below 280nm. The detector that was used in this work, pictured in Figure 1.4, has a 5mm flow cell with absorbance filters at 254nm at 280nm. In some cases, this piece of equipment limited the selection of sorbates to a few select molecules since they were detectable at those wavelengths. The signal generated by the concentration of sorbate was collected using a Data Acquisition System (DAS) and logged on a computer.

The process flow diagram for the system is given in Figure 1.5. The buffer is pumped from the storage container using the reciprocating pump, where it enters a six way sample valve. The valve has a sample loop of 1.2ml, which can be filled with a sample using a syringe. The buffer then enters the jacketed column, which is kept at the desired temperature using the thermal fluid. Upon exiting the column, the effluent passes through the UV detector, which sends solute concentration data to the computer for analysis. A schematic of the principle of operation of the column is given in Figure 1.6. Here, the components that need to be separated are labeled X, Y, Z, each of which has a different binding affinity to the column packing. As they travel along the column, the X component elutes first, followed by the Y component and the Z component. The Z component has the strongest binding as it is retained by the column the longest, and the X component has the weakest binding due to it eluting earlier than the other components. This is manifested on the chromatogram as three distinct peaks corresponding to the three components as they exit the column. With the information presented thus far, the trends and forces governing this type of separation can be quantified and explained, and subsequently implemented to design

or optimize existing separation processes.

1.7 Methodology and Objectives

Given the information presented in the previous sections, a solid foundation for our analysis of the different pH and temperature effects was established to investigate the trends emerging from these key physical parameters. For pH, the trends are well established in the literature, however they lacked an engineering parametrization to be effectively utilized in the production scale. On the other hand, temperature does not have a clear trend explained in the current literature. Therefore, the primary objective of this work is to clearly quantify and determine the trends that emerge with changing pH and temperature on the chromatographic process and the secondary objective is to use theoretical modeling to apply the data in a predictive manner for biomolecular separation engineering problems. The methodology of this investigation can be summarized as follows:

1. Establish a quantitative method based to analyze chromatographic data, which accurately accounts for physical phenomena inside the column.
2. Using adequate model systems for small and large biomolecules, collect data on the separation at different pH and temperature conditions.
3. Understand the trends when pH or temperature is varied on the process based on the data collected by applying the theoretical model to the experimental data.
4. Update the models to accurately represent the changes in pH and temperature on the separation by using the parameters derived from the experimental data.
5. Utilize the newly established model to biomolecular separation engineering problems to optimize and improve the process.

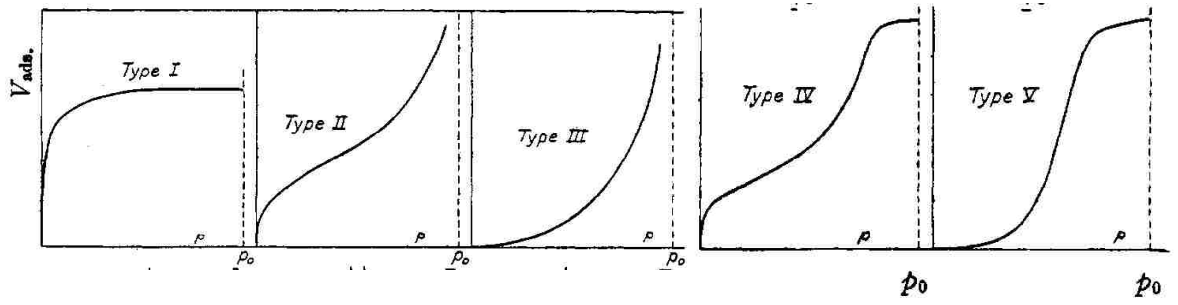


Figure 1.1: Isotherm classification as described by Brunauer et. al.[4]



Figure 1.2: Packed Aqueous Chromatography Column (Copyright Spectrum, Inc.)



Figure 1.3: Reciprocating HPLC pump (Copyright Scientific Systems, Inc.)



Figure 1.4: UV detector for in-line solute analysis (Copyright Spectrum, Inc.)

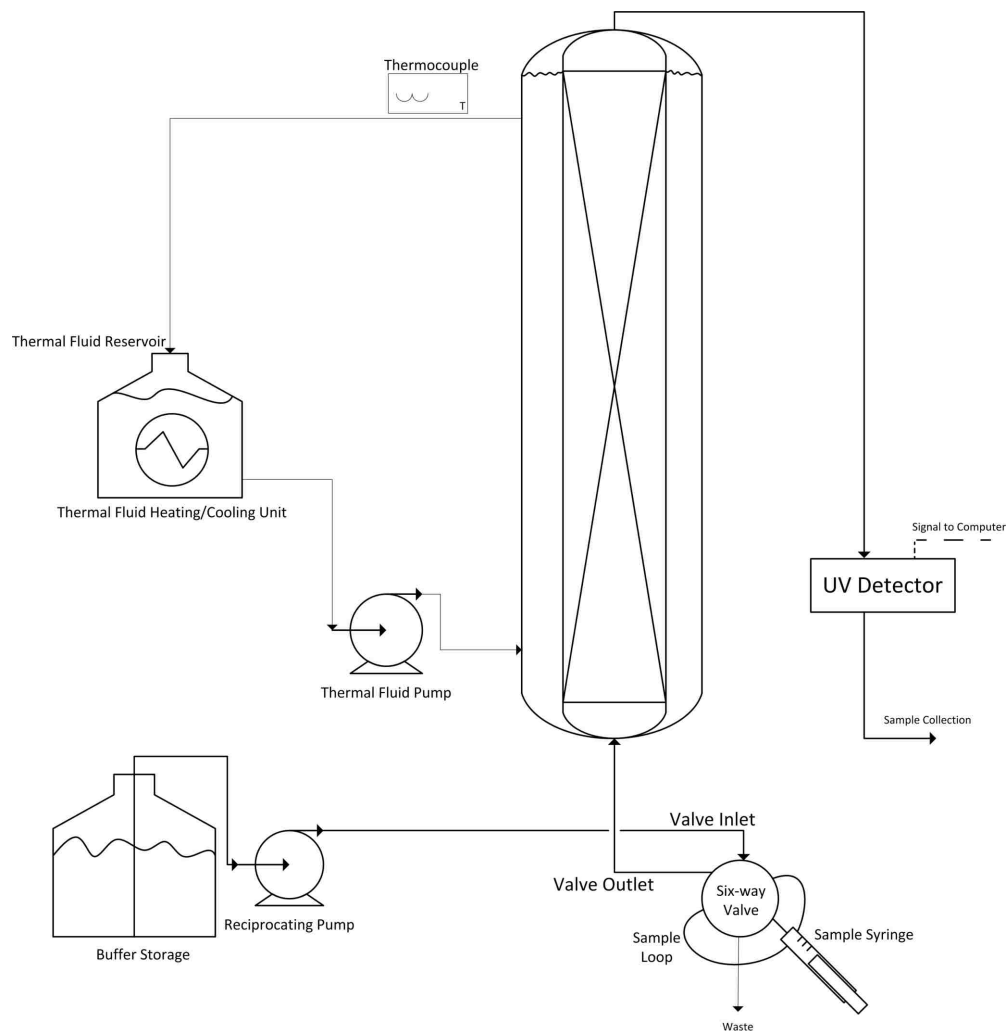


Figure 1.5: Process Flow Diagram of the experimental setup

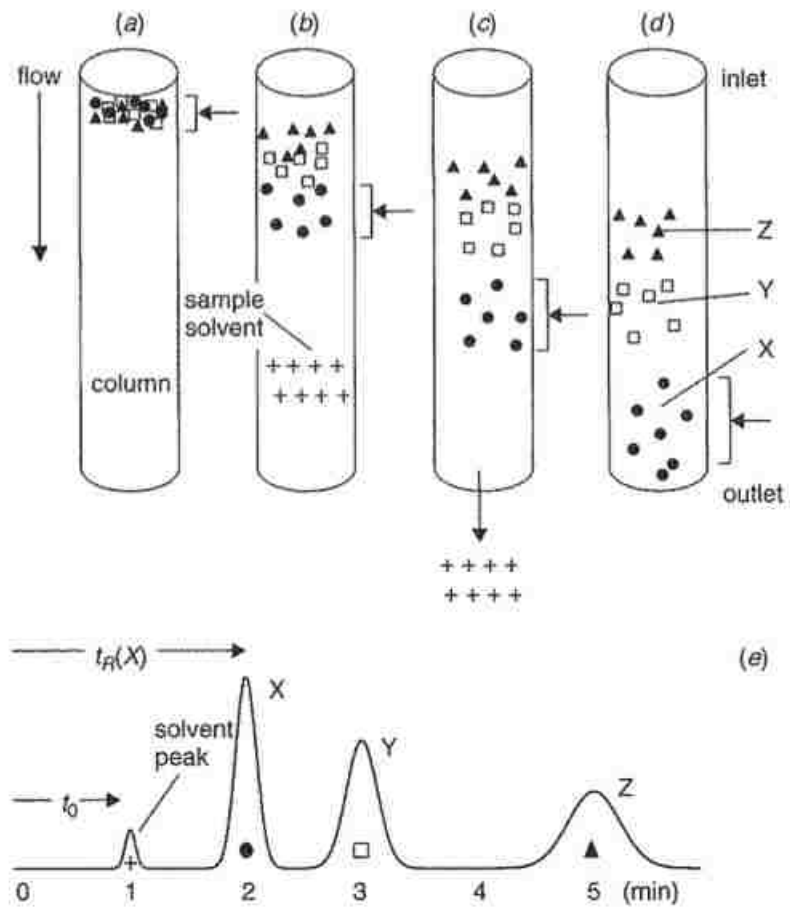


Figure 1.6: Principle of operation of the chromatographic separation process[44]

Chapter 2

Adsorption parameters of amino acids on DEAE Sepharose and Q Sepharose anion-exchange chromatography at different pH and temperature

In this chapter, the initial analysis for this work was laid out in a systematic fashion in order to understand the trends affecting anion-exchange. This analysis served as the initial guide for this work to prove that the theoretical model can adequately explain the experimental findings. The effect of temperature and pH on adsorptive processes is very important for biomolecular separation. Industrial handbooks provide some insight to the effect of pH, but they do not offer any insight into the effect of temperature on the adsorption. A comprehensive model to predict the sorption behavior of a solute at different temperature and pH is presented. The amino acids phenylalanine, tryptophan and tyrosine were selected as model compounds to see the trends of changing pH and temperature. The data for the adsorption rate constants was obtained from chromatograms by using the moments method by Schneider and

Smith[39] allowing calculation of the adsorption and desorption rates. They were fitted to an Arrhenius expression[11] to quantify the activation energy. The adsorption of the amino acids on Q Sepharose and DEAE Sepharose anion-exchange resins increases with increasing pH and temperature. Concluding, tuning the temperature and pH conditions for anion exchangers can lead to significant improvements in selectivity and resolution when separating amino acids.

2.1 Introduction

Adsorption is driven by surface affinity forces, ranging from hydrophobic interaction, to electrostatic interaction, to highly specific ligand-antibody interactions. To understand the adsorption phenomena and quantify the adsorption rate constants of the anion exchange resins a comprehensive mechanistic model is needed. This chapter presents data on a fundamental case of anion exchange and the effects of pH and temperature on the adsorption.

Several sources [15, 48, 44, 13] give some insight as to what is the effect of temperature. The importance of temperature thus far is that the viscosity of the mobile phase decreases and the diffusivity of the sorbate increases with the increase of temperature [12]. So far no model has captured enough information from temperature data which take into account all the physical phenomena. Such a model will estimate the elution behavior based on the adsorption parameters from a limited data set. This has direct implications in biomolecular separation, where the model can be used to determine if the selectivity of an adsorbent is increased under different temperature or pH conditions.

The goal of this chapter is to provide a systematic evaluation of how small biomolecules are affected by the changes in pH and temperature when adsorbed onto an anion exchange resin. A comprehensive mechanistic model to evaluate the adsorp-

tion and desorption rates, as well as the equilibrium constant is used in order to gain a fundamental understanding of the adsorption under different temperature and pH conditions. When pH is increased, the expectation is that adsorption will increase as the electrostatic forces that drive the anion-exchange adsorption are higher due to the higher net charge of the solute. For temperature, however, there is no clear trend discussed in the literature, especially in the case of biomolecular adsorption.

2.2 Theoretical Model

The theory for the model is described in the work of Schneider and Smith[39]. This mechanistic model takes into account the mass balance of the solute in the mobile phase, its behavior inside the microporous adsorbent, and the adsorption kinetics.

For the concentration, $c(z, t)$ of the adsorbable component in the mobile phase, the mass balance is presented in Equation 2.1.

$$\frac{E_a}{\alpha} \frac{\partial^2 c}{\partial z^2} - v \frac{\partial c}{\partial z} - \frac{\partial c}{\partial t} - \frac{3D_c}{R} \frac{1 - \alpha}{\alpha} \left(\frac{\partial c_i}{\partial r} \right) \Big|_{r=R} = 0 \quad (2.1)$$

The mass balance of the component inside the particle:

$$\frac{D_c}{\beta} \left(\frac{\partial^2 c_i}{\partial r^2} + \frac{2}{r} \frac{\partial c_i}{\partial r} \right) - \frac{\partial c_i}{\partial t} - \frac{\rho_p}{\beta} \frac{\partial c_{ads}}{\partial t} = 0 \quad (2.2)$$

Based on a linear adsorption rate:

$$\frac{\partial c_{ads}}{\partial t} = k_{ads} c_i - k_{des} c_{ads} \quad (2.3)$$

with an diffusion boundary condition

$$D_c \left(\frac{\partial c_i}{\partial r} \right) \Big|_{r=R} = k_f (c - c_i) \quad (2.4)$$

The internal diffusion boundary condition is

$$\frac{\partial c_i}{\partial r} = 0 \quad \text{at } r = 0 \quad \text{for } t > 0 \quad (2.5)$$

The initial conditions are

$$c = 0, \quad \text{at } z > 0 \quad \text{for } t = 0 \quad (2.6)$$

$$c_i = 0, \quad \text{at } r \geq 0 \quad \text{for } t = 0 \quad (2.7)$$

At the bed inlet, the pulse input is represented as a square function

$$c = c_0, \quad \text{at } z = 0 \quad \text{for } 0 \leq t \leq t_{0A}; \quad (2.8)$$

$$c = 0, \quad \text{at } z = 0 \quad \text{for } t > t_{0A}$$

so taking the Laplace transform of Equations 2.1 to 2.8, results in the following equations when converting function $c(z, t)$ to $\hat{c}(z, s)$, where s is the Laplace domain:

$$\hat{c}(z, s) = c_0[1 - \exp(-st_{0A})] \exp(-\gamma z) \quad (2.9)$$

where γ is

$$\gamma = -\frac{v\alpha}{2E_a} + \sqrt{\left(\frac{v\alpha}{2E_a}\right)^2 + \frac{s\alpha}{E_a}[1 + h(s)]} \quad (2.10)$$

and

$$h(s) = \frac{3k_f}{R} \frac{1 - \alpha}{\alpha} \left\{ \frac{1}{s} - \frac{\sinh(R\sqrt{\lambda})}{(sD_c/k_f)\sqrt{\lambda} \cosh(R\sqrt{\lambda}) + s[1 - (D_c/Rk_f)] \sinh(R\sqrt{\lambda})} \right\} \quad (2.11)$$

also the λ term

$$\lambda = \frac{s\beta}{D_c} \left[1 + \frac{(\rho_p/\beta)K_A k_{ads}}{K_A s + k_{ads}} \right] \quad (2.12)$$

Equation 2.3 is related to the adsorption rate and desorption rate with first order

kinetics, where the k_{ads} is the adsorption rate constant and desorption rate constant k_{des} . Defining the equilibrium constant $K_A = \frac{k_{ads}}{k_{des}}$ makes K_A a function of k_{ads} . Equation 2.3 becomes:

$$\frac{\partial c_{ads}}{\partial t} = k_{ads} \left(c_i - \frac{c_{ads}}{K_A} \right) \quad (2.13)$$

Taking the Laplace transform of Equations 2.1, 2.2 and 2.4 - 2.13, by the final value theorem[47], the statistical moments from these Laplace transforms are computed using the following formula for the n th moment:

$$m_n = (-1)^n \lim_{s \rightarrow 0} \frac{d^n}{ds^n} \left[\frac{\hat{c}(z, s)}{s} \right] \quad (2.14)$$

The n th absolute moment of $c(z, t)$ is defined as:

$$\mu'_n = \frac{m_n}{m_0} \quad (2.15)$$

where

$$m_n = \int_0^\infty t^n c(z, t) dt \quad (2.16)$$

The n th central moment is defined as:

$$\mu_n = \left(\frac{1}{m_0} \right) \int_0^\infty (t - \mu'_1)^n c(z, t) dt \quad (2.17)$$

so for the first moment:

$$\mu'_1 = \left(\frac{z}{v} \right) (1 + \delta_0) + \left(\frac{t_{0A}}{2} \right) \quad (2.18)$$

and the second central moment is:

$$\mu_2 = \left(\frac{2z}{v} \right) \left[\delta_1 + \left(\frac{E_A}{\alpha} \right) (1 + \delta_0)^2 \left(\frac{1}{v^2} \right) \right] + \left(\frac{t_{0A}^2}{12} \right) \quad (2.19)$$

where

$$\delta_0 = \left[\frac{(1 - \alpha)\beta}{\alpha} \right] \left[1 + \left(\frac{\rho_p}{\beta} \right) K_A \right] \quad (2.20)$$

$$\delta_1 = \left[\frac{(1 - \alpha)\beta}{\alpha} \right] \left[\frac{\rho_p K_A^2}{\beta k_{ads}} + \frac{R^2 \beta}{15} \left(1 + \frac{\rho_p}{\beta} K_A \right)^2 \left(\frac{1}{D_c} + \frac{5}{k_f R} \right) \right] \quad (2.21)$$

The values are as follows: E_a - axial dispersion, α - interparticle void fraction, v - linear velocity, D_c - intraparticle diffusion coefficient, c_i - concentration of the adsorbable molecule in the pore space, R - radius of the particle, z - column length, r - length coordinate of the particle radius, t - time, β - intraparticle void fraction, c_{ads} - concentration of adsorbed molecules, ρ_p - density of the particle bed, k_f - mass transfer coefficient, t_{0A} - injection time, c_0 - initial concentration.

Computing the first and second moment from the experimental data of the elution peak provide useful information. The first moment, as presented in Equations 2.18 and 2.20, is a function of physical parameters of the column: the length of the column z , the flow velocity v , the injection time t_{0A} and the bed void fraction α and particle porosity β and density ρ_p . The one parameter that is calculated from the first moment is the equilibrium constant K_A . The first moment is the retention time of the sorbate, making the equilibrium constant and its physical representation imperative in understanding the driving forces behind the adsorption.

In the second moment most parameters can be easily estimated from correlations[54, 2, 25, 5], and the adsorption specific parameter is k_{ads} , the adsorption rate constant. Knowing both K_A and k_{ads} can determine k_{des} , the desorption rate constant to quantify the rate of dissociation of the molecules. Quantifying k_{des} is important to understand the phenomena taking place on the surface of the adsorbent.

In adsorptive systems, the molecules are physisorbed onto the surface and inside the pores of the adsorbent particle, resulting in heat release. Ruthven [37] states that for physisorption, the heat released is less than 2 to 3 times than the latent heat of evaporation. The other mechanism of adsorption, chemisorption, is where the

molecules bind to a very selective active site on the surface of the adsorbent particle. There is a higher release of heat, typically more than 2 or 3 times the latent heat of evaporation of the adsorbed molecules. The other key differences in these two modes of adsorption involve the role of temperature, where physisorption is only significant at lower temperature, and chemisorption is possible over a wide temperature range. This information provides some understanding of the adsorbent surface interaction in anion-exchange chromatography.

2.2.1 Temperature Effect on Physical Parameters

The model had to be modified to account for the physical parameters at different temperatures. The chemical parameters, such as the adsorption and desorption rate constants as well as the equilibrium constant are calculated from elution data. For the physical parameters such as the film mass transfer coefficient, intraparticle diffusion and dispersion, the Liapis[25], Boyer and Hsu[2] and Chung and Wen[5] correlations were utilized as follows: Axial dispersion is estimated by a correlation by Chung and Wen [5]:

$$E_a = \frac{2\alpha Rv}{0.2 + 0.011Re_P^{0.48}} \quad (2.22)$$

the particle Reynolds number is

$$Re_P = \frac{2R\alpha v\rho}{\mu} \quad (2.23)$$

where μ - viscosity and ρ - density

For the protein solution diffusivity, the correlation by Young [54] was considered:

$$D_0 = 8.34 \times 10^{-10} \left(\frac{T}{\mu M_W^{\frac{1}{3}}} \right) \quad (2.24)$$

where M_W is the molecular weight and T - temperature and can be introduced in

the Boyer and Hsu [2] correlation for intraparticle diffusivity:

$$D_e = 8.34 \times 10^{-10} \left(\frac{T}{\mu M_W^{\frac{1}{3}}} \right) \exp \left[-0.1307 \left(M_W^{\frac{1}{3}} + 12.45 \right) c_f^{\frac{1}{2}} \right] \quad (2.25)$$

where c_f – concentration of the gel.

The mass transfer coefficient given by Liapis [25] for protein mass transfer coefficient is:

$$\frac{2k_f R}{D_0} = 2 + 0.51 \left(\frac{E^{\frac{1}{3}} (2R)^{\frac{4}{3}} \rho}{\mu} \right)^{0.60} Sc^{\frac{1}{3}} \quad (2.26)$$

E is the energy dissipation rate

$$E = \frac{25(1 - \alpha) \alpha^2 C_{D0} v^3}{R} \quad (2.27)$$

C_{D0} is the drag coefficient for a particle which is given by Stokes Law as $C_{D0} = 24/Re$ and the Schmidt number as $Sc = \mu/\rho D_0$. For the value of the void fraction of the interparticle space α a standard value of 0.33 was taken. For the density of the packing, it was estimated to be $0.625g/cm^3$ as well as a particle radius of $90\mu m$. As for the intraparticle void fraction β an estimate was made using a correlation presented in Boyer and Hsu[2], originally derived by GE and reproduced below.

$$\beta = -0.1 \log(M_W) + 1.6835 \quad (2.28)$$

The values for viscosity and density for the temperatures that were considered were taken from NIST[7]. The values obtained from the correlations were used in Equation 2.18, 2.19, 2.20 and 2.21 in order to compute the k_{ads} , k_{des} and K_A .

The computation of the rate constants using this method is indirect considering that only the effluent concentration of the sorbate is taken into account to extract the adsorption parameters. The film mass transfer coefficient k_f and the intraparticle

diffusion D_e dominate the chromatographic process, so the correlations presented in this section can be used as reasonable estimates of their values. The values for the physical parameters are adequate in order to compute the adsorption rate constant k_{ads} . As an illustration of the magnitude of these parameters, Table 2.1 displays results for a temperature of 23°C, while taking tryptophan as a solute with water as solvent.

2.3 Materials and Methods

2.3.1 Equipment Used

The experimental setup has a jacketed glass column (Spectrum Labs, Houston, TX) with a length of 30cm and an I.D. of 1.5cm. A six-way sample valve with a 1.2 ml sample loop is used to inject a sample. The buffer is pumped into the column using a HPLC reciprocating metering pump (Scientific Systems Incorporated, State College, PA) at a constant flow rate of $5ml/min$. The column effluent is analyzed using a UV detector (Spectrum Labs, Houston, TX) at a fixed wavelength of 254nm and the output voltage is recorded using a data acquisition system (Measurement Computing, Norton, MA). The column temperature is controlled using a ethylene glycol-water mixture from a circulating bath (Endocal, Newington, NH). The coolant fluid is set on the shell side of the column, while the packed column is used in the tube side.

2.3.2 Stationary Phase Properties

The column is packed with Q Sepharose Fast Flow(Sigma-Aldrich, St. Louis, MO) which is a strong anion exchanger with the functional group $-CH_2N^+(CH_3)_3$ and a counterion of SO_4^{2-} . It is a beaded cross-linked agarose gel. The molecular formula shows that the Q Sepharose anion exchanger has some alkane chains covalently bonded

to the nitrogen active site. The working temperature range of the gel that is specified by the manufacturer is 4°C to 40°C, so it limits the temperature range at which the experiment is ran.

The analysis is also repeated with the column packed with DEAE-Sepharose Fast Flow(Sigma-Aldrich, St. Louis, MO) which is a weak ion exchanger. The functional group for DEAE is $-OCH_2CH_2N^+H(CH_2CH_3)_2$ with a counterion of Cl^- . Since the charge on DEAE changes with pH, as it is the case with weak ion exchangers, a reduced retention time is expected in comparison to Q Sepharose. DEAE-Sepharose shares the same cross-linked agarose matrix with Q Sepharose, so the experiments were performed at the same temperature for both adsorbents.

2.3.3 Mobile Phase Considerations

Tris-HCl is used as the standard buffer, however the buffer pH changes with temperature, so to achieve the exact same pH value at different temperatures, the mixing table displayed in Table 2.2 is used. The buffer is prepared by mixing the appropriate weight of Trizma HCl and Trizma base in 1.0 liter of deionized water to reach the desired pH at the experimental temperature. The buffer is equilibrated at the experimental temperature before being introduced to the column to avoid temperature gradients.

2.3.4 Sorbate Properties

The molecules that were investigated were amino acids; L-tryptophan, L-tyrosine and L-phenylalanine. The concentrations of each were 0.001 mg/mL for L-tryptophan, L-tyrosine is introduced at its solubility limit and 0.1 mg/mL for L-phenylalanine. As L-tyrosine is not readily soluble, 0.1 mg were added to 10mL of deionized water and before injecting the L-tyrosine solution in the sample loop, the solution is clarified using a $0.22\mu m$ filter. The pKa values and structures of the amino acids are displayed

in Table 2.3. The pI values for L-phenylalanine, L-tryptophan and L-tyrosine are 5.48, 5.89 and 5.66 respectively. Their isoelectric range is similar, however L-tyrosine has an additional phenol group with a pKa 10.46 which would cause it to bind more strongly at higher pH values.

2.3.5 Experimental Procedure

The experimental procedure is adapted to allow the column to equilibrate to both the selected pH and temperature. The column is packed by degassing the gel slurry and then using a packing reservoir to load on the gel. The column is filled with degassed buffer prior to pouring the gel. The gel is poured and left overnight to sediment onto the column, after which the excess buffer is allowed to flow and pack the gel. Five column volumes were used to flush the column in order to ensure that the gel bed is properly packed, after which a syringe plunger is used to cap off and fix the length of the bed. The buffer is introduced in the column by feeding it from the bottom going upward, opposing gravity. This is done to maintain the integrity of the packing such that the hydrostatic pressure keeps the gel firmly in place.

The column is equilibrated to the operating pH by running 3 column volumes of the selected buffer. Three operating temperatures were selected: 5°C, 23°C and 40°C, to cover both the cold and the hot extremes of the manufacturer's recommended temperature range. Each component is added individually into the column, and all chromatograms were run at the same flowrate of 5ml/min, making the three amino acids directly comparable. This setup should give sufficient data in order to obtain a trend for both changes in pH and temperature.

2.4 Results

2.4.1 Q Sepharose Adsorbent Elution Data

The chromatograms for Q Sepharose are presented in Figures 2.1 and 2.2. They are grouped by pH, where Figure 2.1 is at a pH of 7.8, Figure 2.2 is at a pH of 8.4. Figures 2.1 and 2.2 include three different temperatures, namely chromatograms at 5°C, 23°C and 40°C.

At a pH 7.8, phenylalanine, tyrosine and tryptophan elute quite close to each other. As the temperature increased, the retention time of the components starts to increase. This variance in retention time highlights a change in the adsorption and desorption rate constants. One trend emerged between tyrosine and tryptophan, where the elution time difference between tyrosine and tryptophan increased with temperature.

The data at pH of 8.4 is shown in Figure 2.2. At 5°C, the separation is not as significant, however as temperature is increased, the resolution improved. At the temperature of 40°C, where the elution order is reversed between tryptophan and tyrosine. The retention time for all components increased dramatically. For the pH of 8.8, the experiment is ran at room temperature due to the very strong column retention which resulted in a very long analysis time, with tyrosine eluting far after tryptophan.

The first moment of each chromatographic peak for Figure 2.1 and 2.2 are summarized and shown in Table 2.4. Table 2.5 contains values for the separation factor between tryptophan and tyrosine and tryptophan and phenylalanine for Figure 2.2. The separation factor is calculated by using the following formula for separation factor between A and B components:

$$S_{B/A} = \frac{t_B - t_0}{t_A - t_0} \quad (2.29)$$

The retention time is taken as the first moment for each peak, t_A or t_B , and the residence time t_0 is the hold up time, determined to be 330s. To scale the retention of the components and make it independent of column size, the capacity factor (i.e. retention factor) k' is taken, which is the ratio between the adjusted retention time t'_A of the component and the hold up time [30].

$$k' = \frac{t'_A}{t_0} \quad (2.30)$$

The results for the capacity factor at pH of 8.4 are displayed in Table 2.6. The capacity factor is a crude approximation based on experimental data. On the other hand, the equilibrium constant from the first moment given in Equations 2.18 and 2.20 accounts for the column geometry and packing in a direct fashion.

2.4.2 DEAE Sepharose Adsorbent Elution Data

In the DEAE Sepharose case, only tryptophan and tyrosine were considered to simplify our analysis. The trends observed in Q Sepharose are mirrored in the DEAE Sepharose case. The elution chromatogram data for pH of 7.8 are given in Figure 2.3, for pH of 8.4 in Figure 2.4 and for pH of 8.8 in Figure 2.5. First moment data from those chromatograms is given in Table 2.7. The selectivity and capacity factor data for the DEAE-Sepharose adsorbent at pH of 8.4 are given in Table 2.8 and 2.9. The selectivity and capacity factors for DEAE Sepharose were lower than Q Sepharose. The packing structure is similar to Q Sepharose, so the hold up time is determined to be same, 330s.

2.5 Discussion

2.5.1 pH Effect

The common industry practice is to elute the mixture at a pH that is 0.5-1.5 higher than the pI of the molecule of interest. These heuristic guidelines are not sufficient for a fundamental understanding. An important sorbate property that changes with pH is the net charge of the molecule. In Figure 2.6, the net charge at ambient temperature of the three amino acids as a function of the pH is displayed. In the range between pH 4 and 8, the sorbate have close to zero charge, which leads to no adsorption. In the elution curves at a pH of 7.8 high selectivity is not observed. As the pH increased above 8, the amino acids gained a stronger negative net charge, causing them to adsorb more strongly onto the anion exchange packing, which is observed in the case of pH 8.4 and 8.8.

To connect adsorption and the net charge of the molecule, the first moment is presented as a function of the molecule's net charge at ambient temperature in Figure 2.7 and 2.8. The dotted lines represent the exponential curve fit for that specie. The data correlates well, and the retention increases with a higher net negative charge. Figures 2.7 and 2.8 demonstrate the magnitude of the adsorption relative to the ionization of the molecule. The pH of the elution buffer needs to be carefully calibrated in order to allow a net charge difference of the molecules that are separated to get a higher selectivity. These findings are quite important in biological macromolecules such as proteins or DNA, which carry large charges. This trend is observed in both Q Sepharose and DEAE Sepharose anion-exchangers.

2.5.2 Adsorbent Considerations

The adsorption system is not only a function of the properties of the adsorbable components. The charge of the packing must also be considered, as it retains the

charged molecules. In Figure 2.9, the titration curve for the strong anion-exchanger Q Sepharose is presented as a function of pH. The curve takes a sharp increase to a basic pH, demonstrating that even at small ionic concentrations, the packing is positively charged. For the range of pH utilized in this study, the packing has a net positive charge, enabling the electrostatic interaction between the negatively charged amino acid and positively charged anion exchange adsorbent. On the other hand for the weak anion-exchanger DEAE Sepharose, with a titration curve given in Figure 2.10, the packing is not completely charged even in the pH range of interest. This does not afford complete adsorption of the sorbate onto the surface and is an adequate explanation to the reduced retention and selectivity in this type of packing.

Considering Figures 2.9, 2.10 and 2.7, 2.8, to adsorb the molecule the system needs to be within the range where both the packing and the adsorbable component have an opposite charge. The elution pH is fundamentally important as it establishes a separation basis based on the net charge of the molecule. In line with these findings, the industry guidelines of 0.5-1.5 pH units above the pI of a molecule may not be enough to provide enough insight for the adsorption process. For this system, notice that even in the case of two different adsorbents with varying degrees of ionization, the trends that were obtained point to the fact that pH and temperature are key in finding the adequate selectivity for the biomolecule separation.

2.5.3 Temperature Effect

The adsorption equilibrium constant K_A is a function of not only the pH, but also the temperature. An Arrhenius expression[11] is proposed between the equilibrium constant and temperature:

$$\ln K_A = -\frac{\Delta E_{K_A}}{RT} + \ln A_0 \quad (2.31)$$

where ΔE represents the activation energy and A_0 is a preexponential factor associated with the process. Further derivation shows:

$$\ln\left(\frac{k_{ads}}{k_{des}}\right) = \left[-\frac{\Delta E_{ads}}{RT} + \frac{\Delta E_{des}}{RT}\right] + [\ln A_{0_{ads}} - \ln A_{0_{des}}] \quad (2.32)$$

To calculate for the heats associated for the changes in the equilibrium constant, the data from the moments method for K_A and k_{ads} is used. The data for pH of 8.4 is taken from the Q Sepharose and the data for pH 8.8 is taken from the DEAE Sepharose runs. In Figure 2.11 and 2.12, the data lies quite linearly within the proposed relation in Equations 2.31 and 2.32 for the adsorption equilibrium constant. The activation energy and pre-exponential factor associated for both the adsorption and desorption rate constants and the equilibrium rate constant are computed from the slope of the curves in the Arrhenius plots. The activation energy data for each kinetic parameter is displayed in Table 2.10 and 2.11.

Table 2.10 and 2.11 show that the combined effect of the adsorption rate and the desorption rate make up the adsorption equilibrium constant. Going back to the definition of the adsorption equilibrium constant $K_A = \frac{k_{ads}}{k_{des}}$, a relation is derived:

$$\Delta E_{K_A} = \Delta E_{k_{ads}} - \Delta E_{k_{des}} \quad (2.33)$$

Note that the Arrhenius expression has the activation energy as a fitting parameter which can be understood as an empirical or phenomenological quantity rather than a parameter with physical significance.[27] As such, no claims are made on the basis of the thermodynamic nature of the reaction. Instead, the data presented here is to provide insight to the fact that as temperature was increased, the retention time increased. These findings are consistent with published data for protein separation on the Q Sepharose resin[32]. From both Figure 2.11 and 2.12 and Table 2.10 and 2.11, the difference of the activation energies demonstrates that there are two

thermodynamically opposing processes. The energy associated with arresting the molecule onto the adsorbent surface is where they are losing all the diffusive energy when adsorbing onto the surface. The sorbate is at a lower energy state compared to when it entered the column. Energy needs to be invested to break the electrostatic force to desorb the molecule. The sorbate then returns back to its original energy state, same as when it entered in the column. Equation 2.33 combines both energies into an expression for K_A , representing the net energy path that the molecule will take when it adsorbs and desorbs onto the anion-exchange packing.

As the temperature is increased, stronger adsorption is observed. This also increases molecular diffusion. Thus, it is easier for the molecule to adsorb onto an active site since the added translational energy leads to a higher interaction with the active sites. In that way, the sorbate is more retained, giving rise to the increase in adsorption as the temperature increases.

In Table 2.10, phenylalanine has a much smaller desorption activation energy. Limited retention of phenylalanine when compared to tyrosine or tryptophan is observed. In Table 2.11, tyrosine had the highest negative desorption activation energy and the highest equilibrium constant activation energy. For the case of tyrosine, the highest negative activation energy for desorption is observed, which can be explained by the increased ionization of the molecule as its side chain contributes to the negative net charge, and this effect is observed in both anion-exchange packing materials. This explains why desorption is more difficult at elevated temperature, as the added ionization of the molecule does not allow for the electrostatic bond due to adsorption to be broken easily. Note that the Arrhenius expression has the activation energy as a fitting parameter which can be understood as an empirical or phenomenological quantity rather than a parameter with physical significance.[27]

The molecules used in this experiment are quite small relative to the pore opening of the packing, so the diffusion of the molecules is similar inside the packing and

the bulk phase. The energy required for the increase in diffusion over the given temperature range is calculated by an Arrhenius plot for the diffusion where the activation energy is calculated to be 18.48 kJ/mol. This is in close agreement with the values reported in Table 2.10 and 2.11 for the activation energy of adsorption, which confirmed our hypothesis that the pore adsorption is a diffusive phenomenon.

2.6 Conclusion

A fundamental model about the adsorption that occur on the surface of the anion-exchange adsorbent and the charged adsorbable component is presented. Following the moments method, several key rates that govern the adsorption are extracted. The pH and temperature of the elution buffer were given careful consideration as to how they change the adsorptive properties of the anion-exchange packing. The activation energy of the adsorption rate and desorption rate were quantified. In the case of amino acids adsorbing onto an anion exchange column packed with Q Sepharose Fast Flow and DEAE Sepharose Fast Flow, increasing the temperature and pH resulted in significant adsorption for anion exchange adsorbent. Concluding, temperature and pH have an important role in anion-exchange adsorption. The methods and model presented in this chapter are a good starting point for investigation of other chromatographic processes.

$\mu(g/cm \cdot s)$	0.0068
$\rho(g/cm^2)$	1.01
$D_0(cm^2/s)$	6.19×10^{-6}
$D_e(cm^2/s)$	3.45×10^{-6}
$k_f(cm/s)$	6.88×10^{-4}
$E_a(cm^2/s)$	4.95×10^{-17}

Table 2.1: Values of the physical parameters estimated from correlations presented above for tryptophan as the solute and water as the solvent at 23°C

pH	Temperature	Tris HCl (g/L)	Tris Base (g/L)
7.8	5°C	7.02	0.67
	23°C	5.32	1.97
	40°C	4.02	2.97
8.4	5°C	5.32	1.97
	23°C	2.64	4.03
	40°C	1.50	4.90
8.8	5°C	3.54	3.34
	23°C	1.23	5.13
	40°C	0.76	5.47

Table 2.2: Tris-HCl buffer mixing table for 50mM solution[43]

Name	Mass (D)	pK_1	pK_2	pK_R	pI
Phenylalanine	147.2	2.20	9.31		5.48
Tryptophan	186.2	2.46	9.41		5.89
Tyrosine	163.2	2.20	9.21	10.46	5.66

Table 2.3: Names of Amino Acids, their pK_a values of their ionizable groups as well as their pI values [49]

		Molecule retention time, sec		
Temperature	pH	Phenylalanine	Tyrosine	Tryptophan
5°C	7.8	819.2	876.2	640.5
23°C	7.8	856.2	897.8	1015.3
40°C	7.8	942.5	977.7	1168.1
5°C	8.4	856.7	904.1	1052.6
23°C	8.4	1197.1	1661.6	1803.2
40°C	8.4	1883.6	4190.0	3459.4

Table 2.4: First moment (retention time) of each component at temperatures of 5°C, 23°C, 40°C and pH=7.8, 8.4 using Q Sepharose

Temperature	$S_{\frac{Trp}{Phe}}$	$S_{\frac{Tyr}{Phe}}$
5°C	1.37	1.09
23°C	1.71	1.54
40°C	2.01	2.48

Table 2.5: Separation factor at pH 8.4 using Q Sepharose

Temperature	k'_{phe}	k'_{tyr}	k'_{trp}
5°C	1.60	1.74	2.19
23°C	2.63	4.04	4.46
40°C	4.71	11.70	9.48

Table 2.6: Capacity factor at pH 8.4 using Q Sepharose

Temperature	pH	Retention Time, sec	
		Tryptophan	Tyrosine
5°C	7.8	872.4	801.8
23°C	7.8	907.2	853.7
40°C	7.8	995.9	912.6
5°C	8.4	902.3	833.1
23°C	8.4	1207	1078
40°C	8.4	2035	2592
5°C	8.8	1055	950.5
23°C	8.8	2269	2458
40°C	8.8	3865	4986

Table 2.7: First moment of each component at temperatures of 5°C, 23°C, 40°C and pH=7.8, 8.4 and 8.8 using DEAE Sepharose

Temperature	$S_{\frac{T_{rp}}{T_{yr}}}$
5°C	1.14
23°C	1.17
40°C	1.33

Table 2.8: Separation factor at pH 8.4 using DEAE Sepharose

Temperature	k'_{trp}	k'_{tyr}
5°C	2.73	2.52
23°C	3.66	3.26
40°C	6.17	7.85

Table 2.9: Capacity factor at pH 8.4 using DEAE Sepharose

Molecule	$\Delta E_{k_{ads}}$	$\Delta E_{k_{des}}$	ΔE_{K_A}
Phenylalanine	17.92	-0.01	17.93
Tyrosine	18.46	-13.68	32.14
Tryptophan	18.40	-6.59	24.99

Table 2.10: Summary of the activation energies for each kinetic constant for Q Sepharose at pH 8.4. All values are in kJ/mol.

Molecule	$\Delta E_{k_{ads}}$	$\Delta E_{k_{des}}$	ΔE_{K_A}
Tyrosine	19.10	-15.80	34.91
Tryptophan	18.09	-9.30	27.39

Table 2.11: Summary of the activation energies for each kinetic constant for DEAE Sepharose at pH 8.8. All values are in kJ/mol.

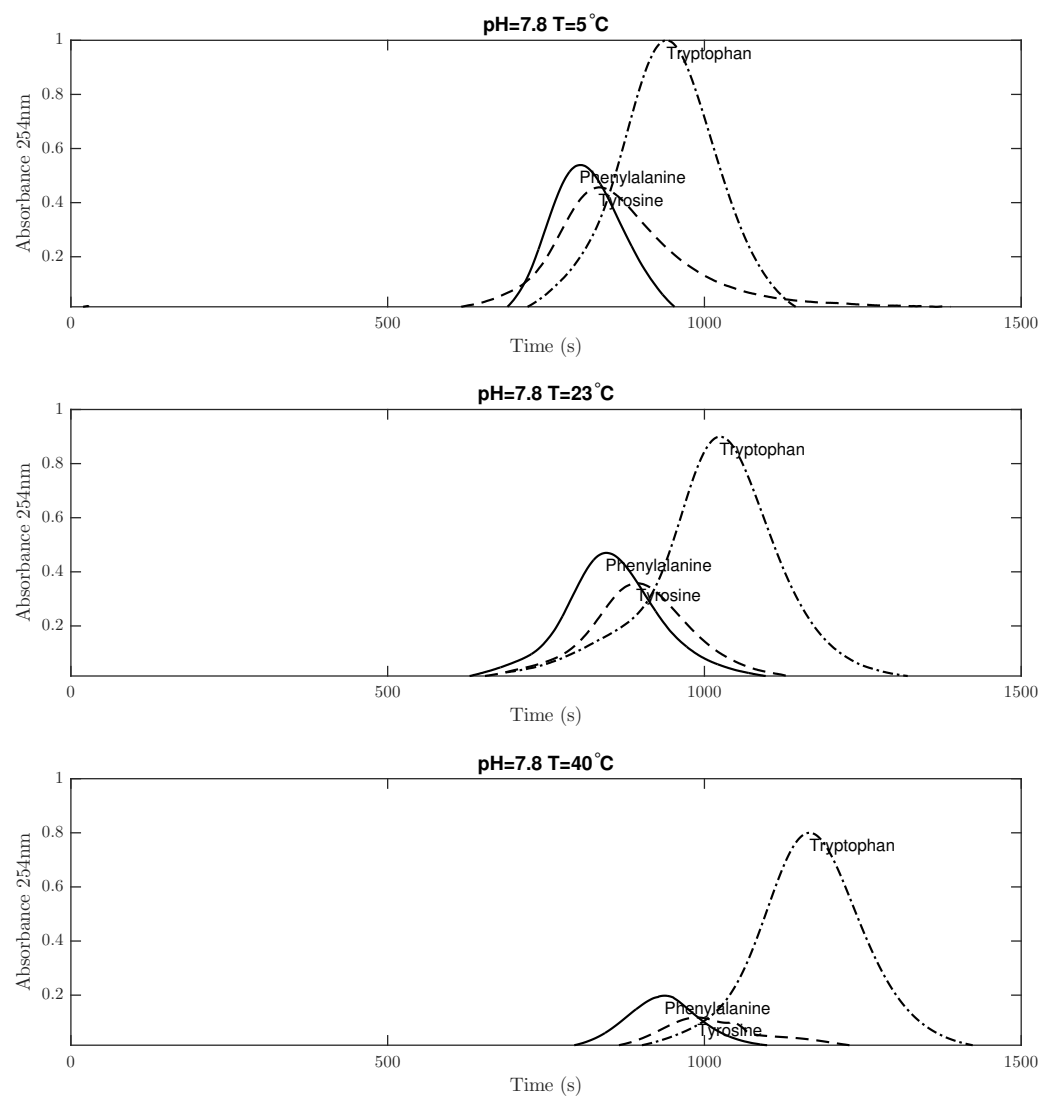


Figure 2.1: Amino Acid chromatograms at a pH of 7.8 at three different temperatures at a flowrate of $5\text{ml}/\text{min}$

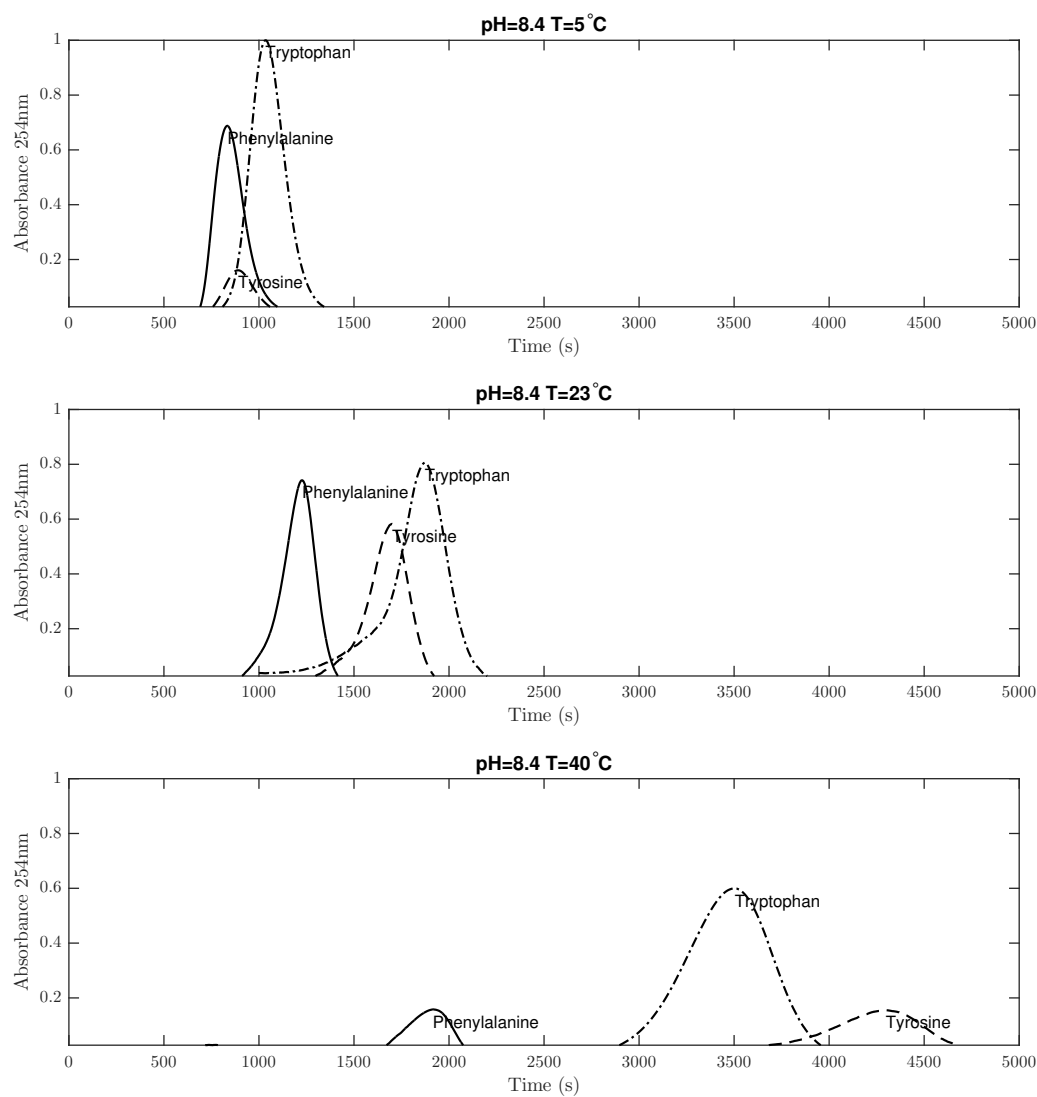


Figure 2.2: Amino Acid chromatograms at a pH of 8.4 at three different temperatures at a flowrate of $5\text{ml}/\text{min}$

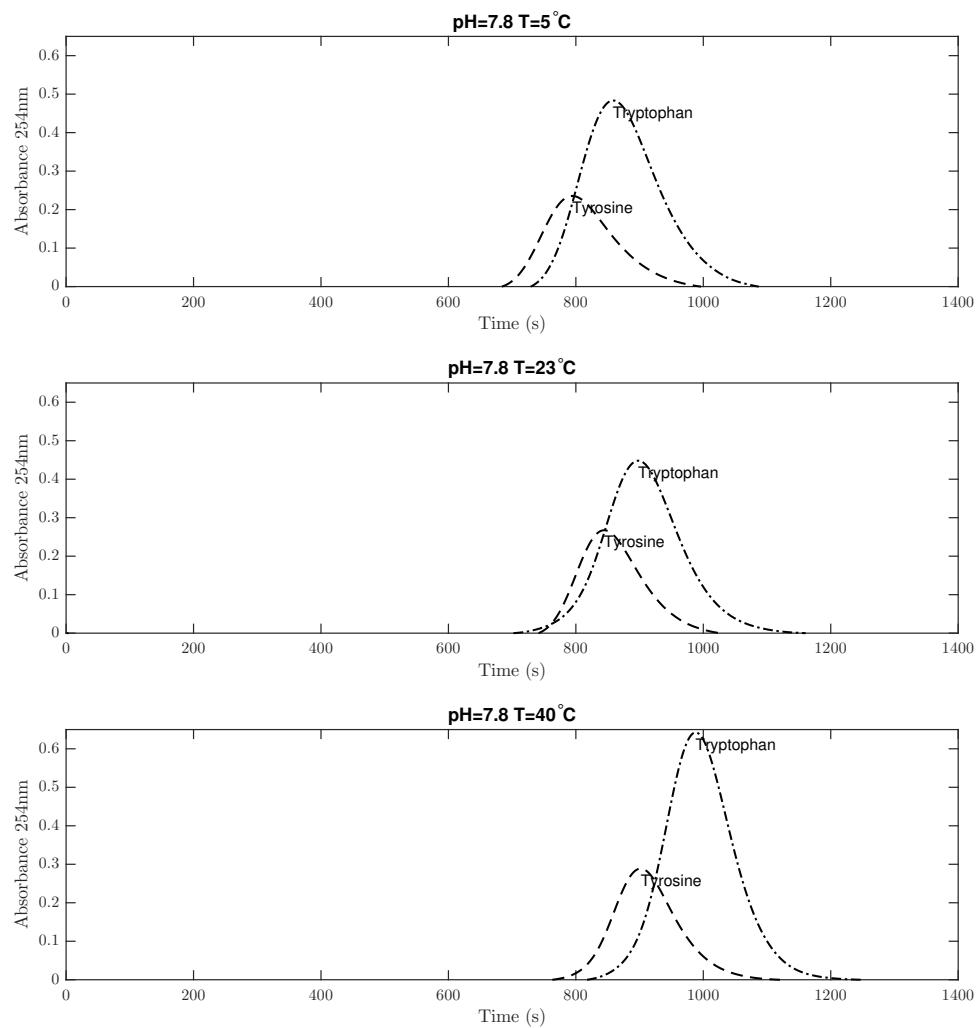


Figure 2.3: Amino Acid chromatograms using DEAE Sepharose at a pH of 7.8 at three different temperatures at a flowrate of $5\text{ml}/\text{min}$

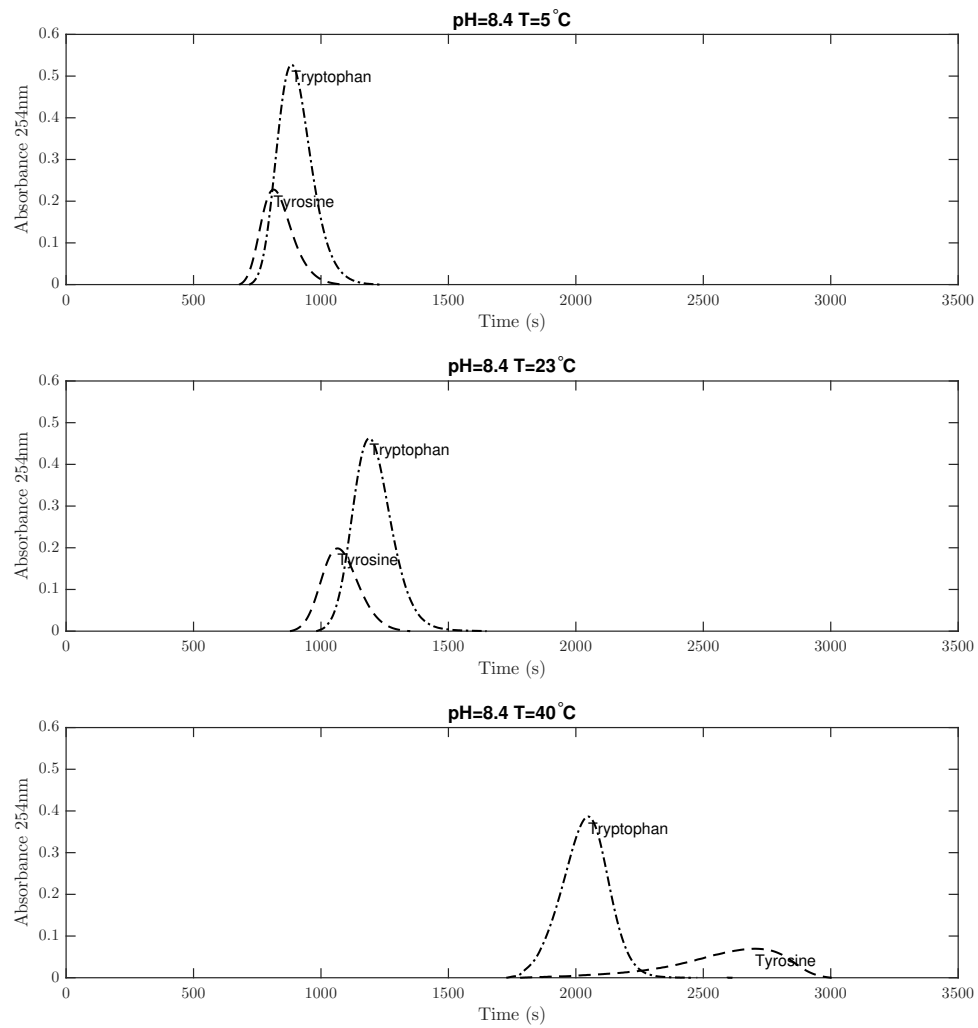


Figure 2.4: Amino Acid chromatograms using DEAE Sepharose at a pH of 8.4 at three different temperatures at a flowrate of $5\text{ml}/\text{min}$

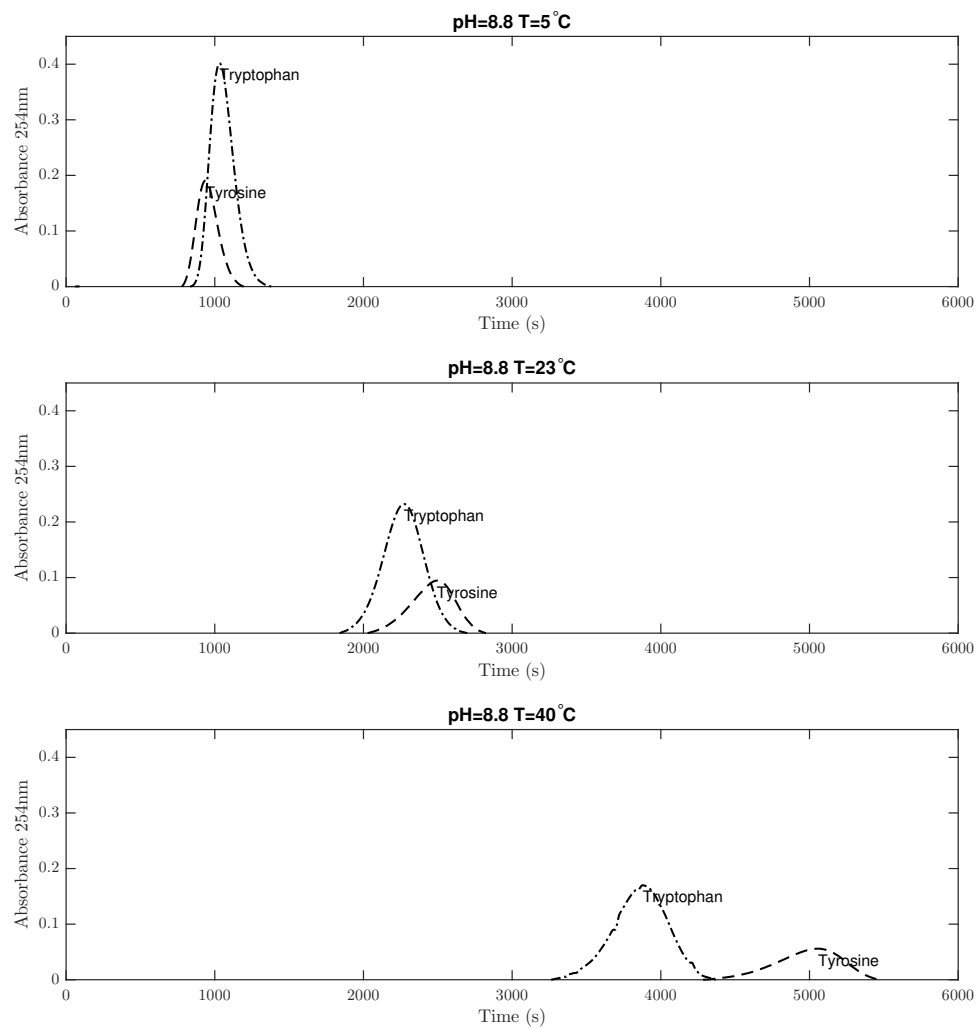


Figure 2.5: Amino Acid chromatograms using DEAE Sepharose at a pH of 8.8 at three different temperatures at a flowrate of $5\text{ml}/\text{min}$

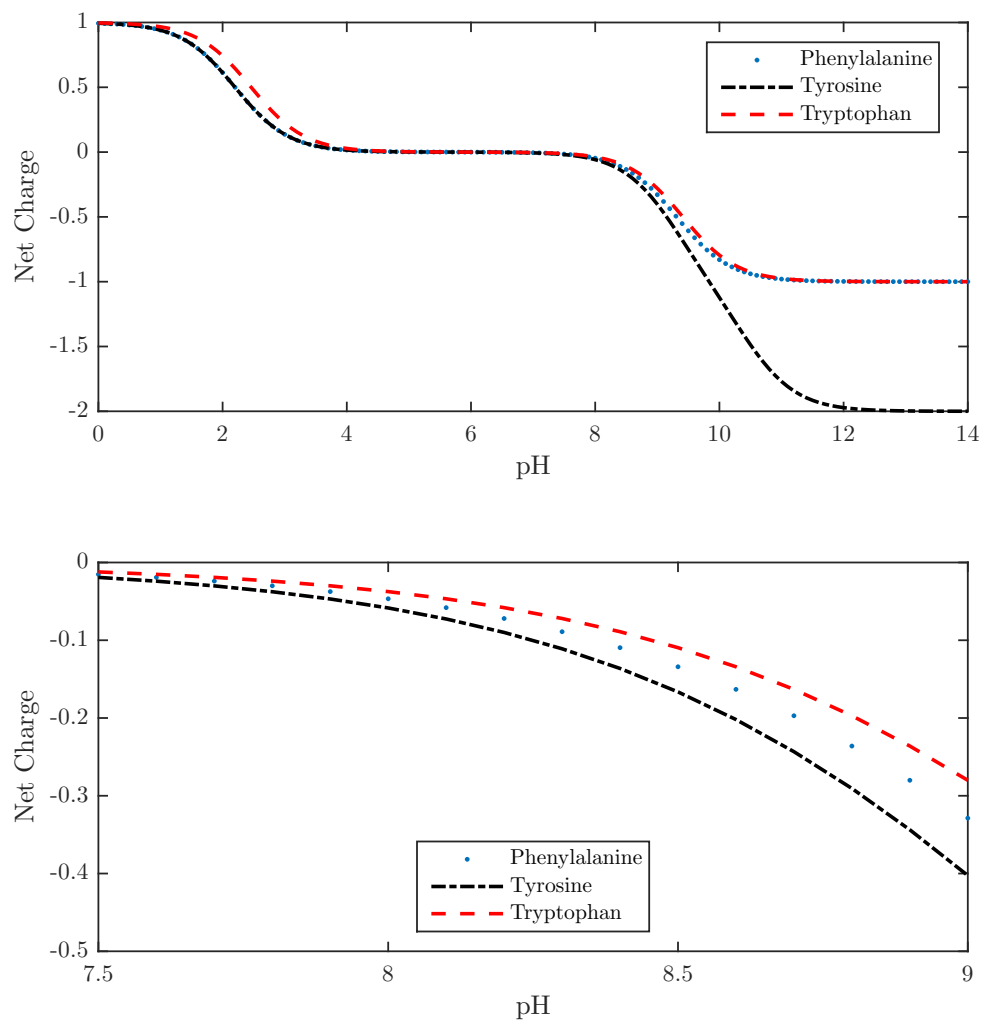


Figure 2.6: Net charge of each amino acid used in this experiment as a function of pH

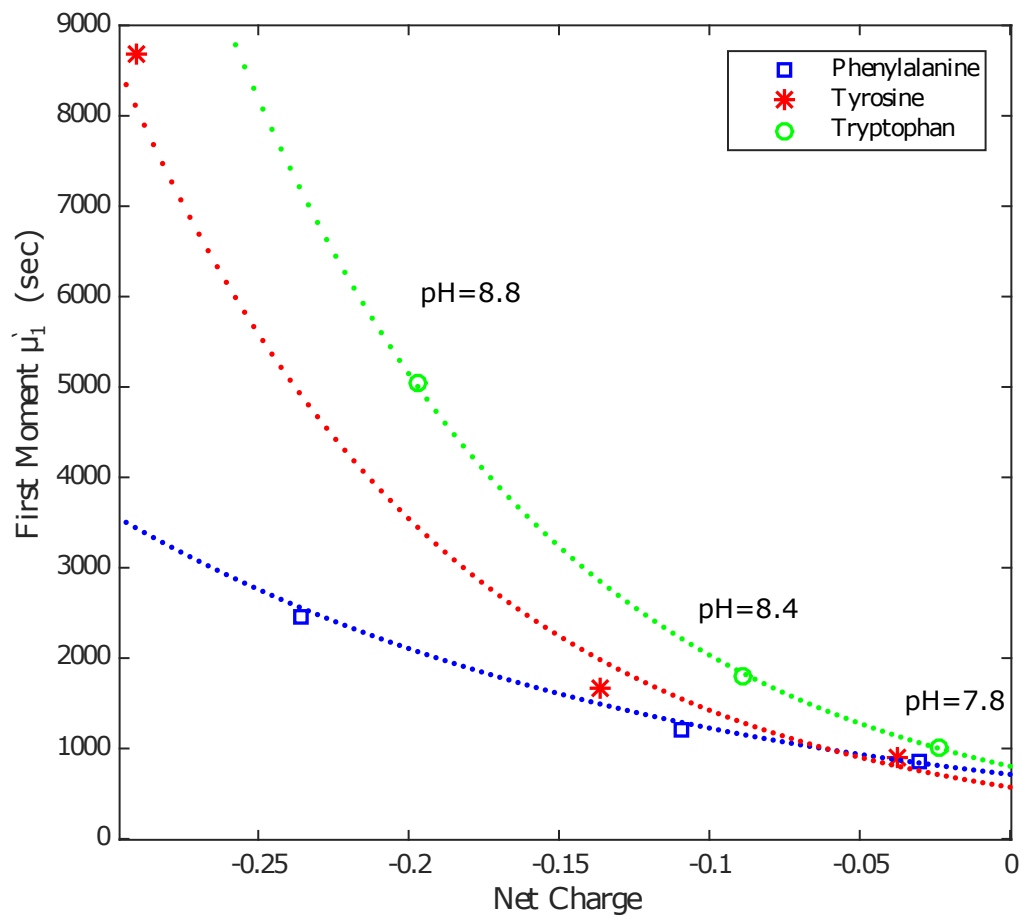


Figure 2.7: Empirical correlation between the net charge and the first moment at ambient temperature in Q Sepharose adsorbent

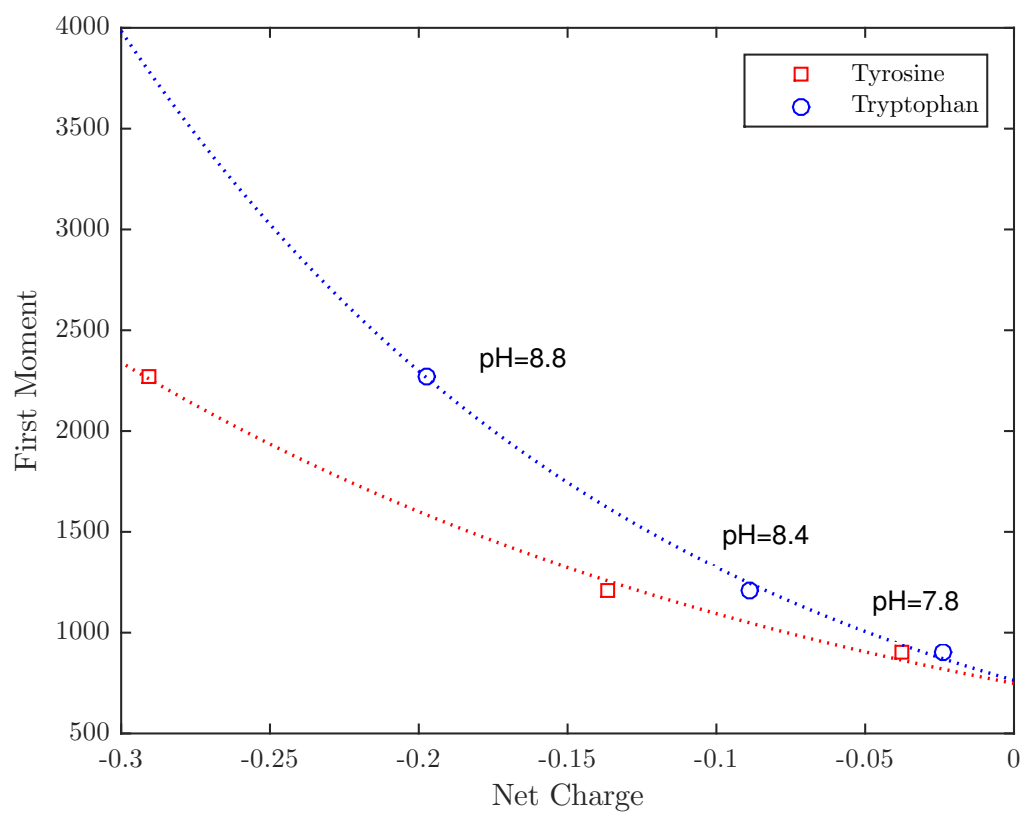


Figure 2.8: Empirical correlation between the net charge and the first moment at ambient temperature in DEAE Sepharose adsorbent

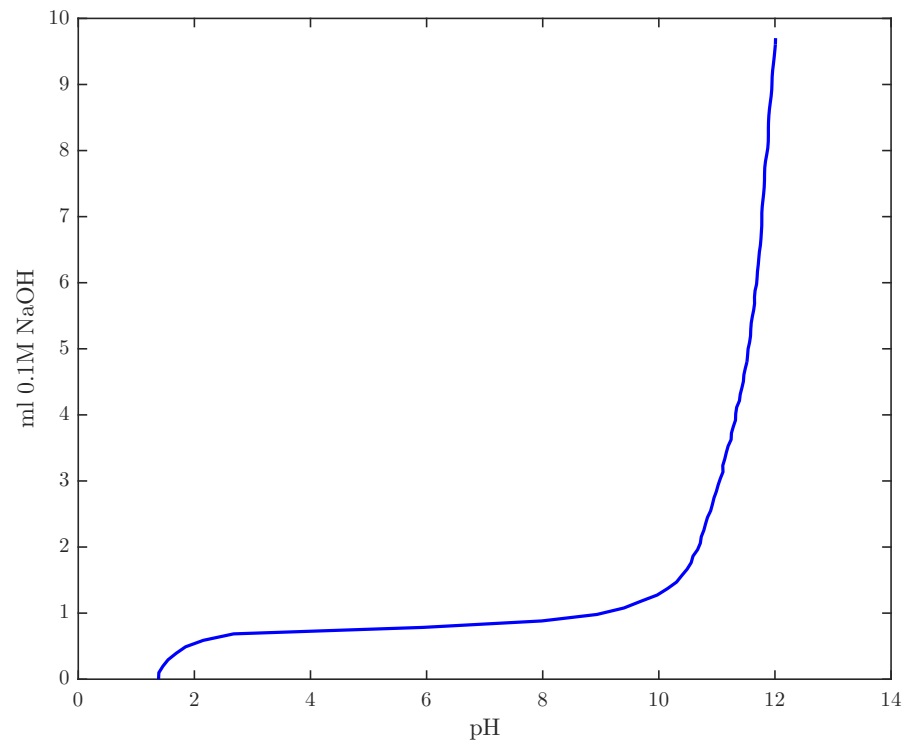


Figure 2.9: Titration Curve of Q Sepharose packing[40]

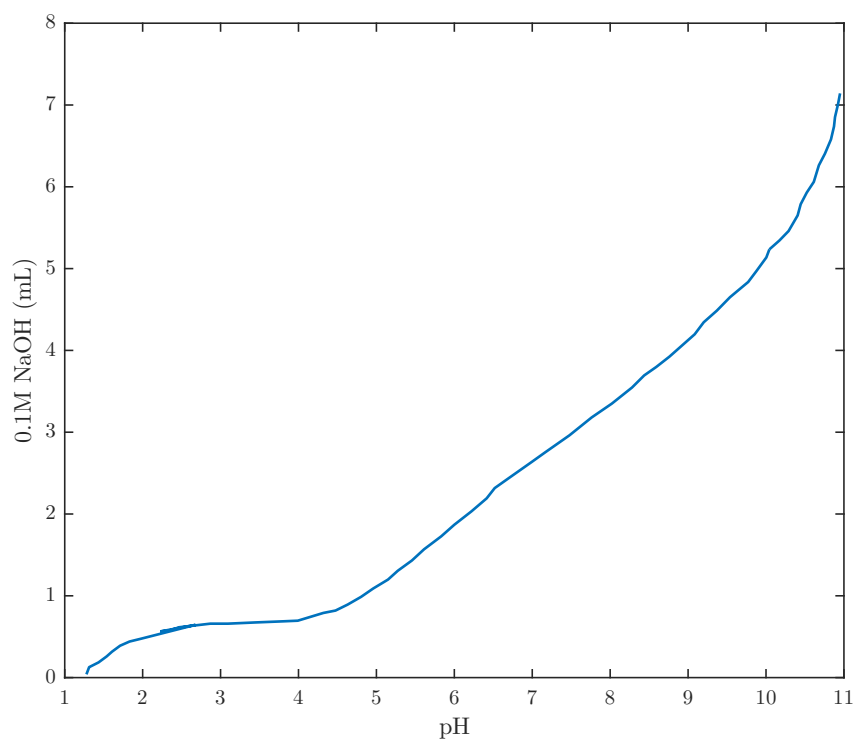


Figure 2.10: Titration Curve of DEAE Sepharose packing[40]

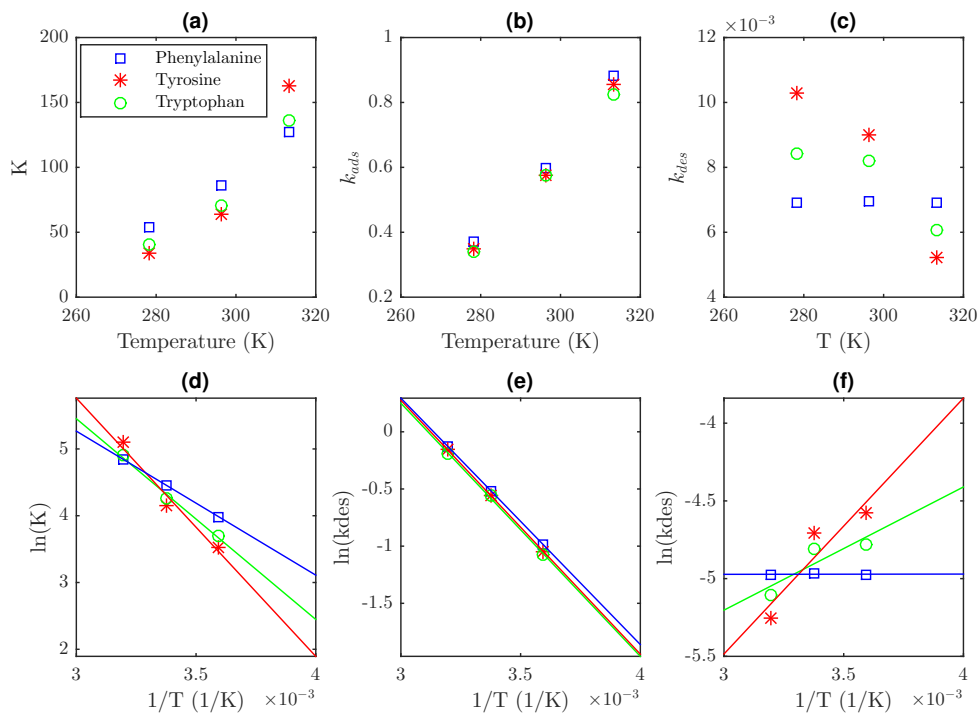


Figure 2.11: Adsorption Equilibrium Constant, Adsorption Rate Constant and Desorption Rate Constant for Phenylalanine, Tyrosine and Tryptophan as a function of temperature at a pH of 8.4 using Q Sepharose. (a) Equilibrium Constant vs. Temperature (b) Adsorption Rate Constant vs. Temperature (c) Desorption Rate Constant vs. Temperature (d) Arrhenius plot of the Equilibrium Constant (e) Arrhenius plot of the Adsorption Rate Constant (f) Arrhenius plot of the Desorption Rate Constant

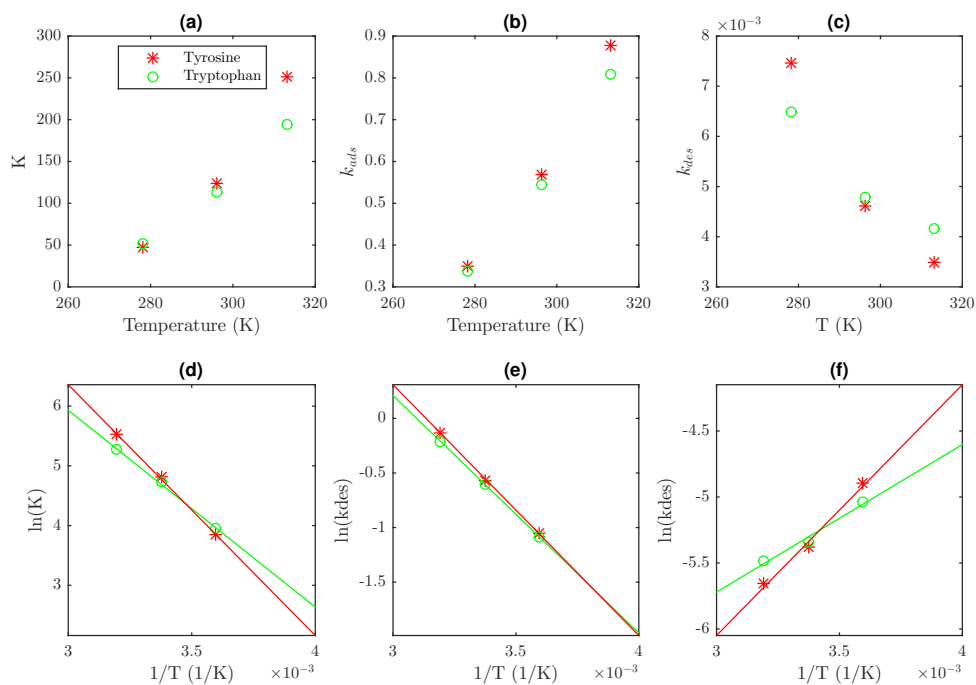


Figure 2.12: Adsorption Equilibrium Constant, Adsorption Rate Constant and Desorption Rate Constant for Tyrosine and Tryptophan as a function of temperature at a pH of 8.8 using DEAE Sepharose. (a) Equilibrium Constant vs. Temperature (b) Adsorption Rate Constant vs. Temperature (c) Desorption Rate Constant vs. Temperature (d) Arrhenius plot of the Equilibrium Constant (e) Arrhenius plot of the Adsorption Rate Constant (f) Arrhenius plot of the Desorption Rate Constant

Chapter 3

The pH, Temperature and Protein Structure Effect on β -Lactoglobulin A and B Separation in Anion-Exchange Chromatography

The effect of pH and temperature on separating a mixture of similar proteins, namely β -lactoglobulin A (LGA) and β -lactoglobulin B (LGB) in anion-exchange chromatography is explored. The proteins carry a slight difference in negative charge at basic pH, providing a separation basis on an Q Sepharose Fast Flow anion-exchange resin. They were separated at different temperatures and pH values, and the separation factor was evaluated. The experimental results were matched to a theoretical model to compute the equilibrium constant K_A . The data shows that an increase in temperature and pH leads to an increase in the retention time of the proteins. The results were correlated with the net charge of the molecule for the separation so that the elution can be simulated for any condition that was studied. The tertiary structures of LGA and LGB are analyzed to illustrate the structure effect on the separation.

3.1 Introduction

Protein purification using ion exchange is a common industry practice with clearly defined separation optimization parameters such as flow rate, column size and protein loading. As a physical variable the effect of temperature on the separation properties of proteins is oftentimes neglected as an optimization parameter. On the other hand, the effect of pH is carefully investigated as it directly affects the ionization of the protein and the packing material. This chapter presents data on the temperature and pH when separating a mixture of β -lactoglobulin A (LGA) and β -lactoglobulin B (LGB) using Q Sepharose Fast Flow, a strong anion exchanger. To get the general trend of the protein behavior at different temperature and pH, bovine serum albumin (BSA) was used as model species to understand the behavior of an individual protein without interactions with another protein. This study shows that as temperature or pH increased the retention of the proteins increased. The separation factors of the proteins increase with increasing temperature and pH. To provide an explanation why LGA and LGB can be separated in anion-exchange chromatography, the protein tertiary structures are analyzed and presented. The main focus of this work is to give a comprehensive mechanistic model that is applicable for analyzing chromatography data at different temperatures to use it in a predictive manner to determine the optimal separation conditions.

3.2 Theoretical Model

Hsu and Chen [18] used a model derived by Horvath and Lin [17] to do a theoretical analysis for chromatographic separations. They describe an isothermal chromatographic column packed with spherical particles, accounting for transport processes such as external film diffusion, intraparticle diffusion and adsorption on the pore surface. The flow pattern was assumed axial-dispersed plug flow with a linear adsorption

equilibrium.

For the flowing phase

$$\frac{\partial C}{\partial t} + V \frac{\partial C}{\partial z} - D_L \frac{\partial^2 C}{\partial z^2} = -\frac{1}{m} \frac{\partial q}{\partial t} \quad (3.1)$$

Intraparticle mass balance

$$\epsilon_p \frac{\partial C_p}{\partial t} + \frac{\partial C_s}{\partial t} = \epsilon_p D_p \left(\frac{\partial^2 C_p}{\partial r^2} + \frac{2}{r} \frac{\partial C_p}{\partial r} \right) \quad (3.2)$$

Adsorption term

$$\frac{\partial C_s}{\partial t} = k_{ads} \left(C_p - \frac{C_s}{K_A} \right) \quad (3.3)$$

The initial and boundary conditions

$$C = C_p = C_s = 0 \text{ at } z > 0, t = 0 \quad (3.4)$$

$$C = C_0 \delta(t) \text{ at } z = 0 \quad (3.5)$$

$$C = 0 \text{ at } z = \infty \quad (3.6)$$

The last boundary condition leads to a simpler solution than using $\frac{\partial C}{\partial z} = 0$ at $z = L$ however this will only affect the solution if the axial Peclet number and column length are both small.

The other boundary conditions are:

$$\frac{\partial C_p}{\partial r} = 0 \text{ at } r = 0 \quad (3.7)$$

$$\frac{\partial q}{\partial t} = \frac{3k_f}{b}(C - C_p) = \frac{3}{b}\epsilon_p D_p \frac{\partial C_p}{\partial r} = 0 \text{ at } r = b \quad (3.8)$$

The variables introduced are as follows: C – solute concentration in mobile phase, C_p – solute concentration in the pores, C_s – solute concentration on solid, C_0 – initial pulse concentration, V – mobile phase velocity, D_L – axial dispersion coefficient, $m = \epsilon/(1 - \epsilon)$, ϵ – column void fraction, ϵ_p – particle porosity, q – concentration in particles, D_p – intraparticle diffusivity, k_{ads} – adsorption rate constant, K_A – adsorption equilibrium constant, k_f – external mass transfer coefficient, t – time, z – axial position, r – intraparticle radial position, b – radius of the bead.

A solution can be obtained by taking the Laplace transform, resulting in:

$$\bar{C}(z, s) = C_0 \exp \left[\left(\frac{V}{2D_L} - \sqrt{\frac{V^2}{4D_L^2} + \frac{s}{D_L} + \frac{3k_f\varphi_2}{bmD_L}} \right) z \right] \quad (3.9)$$

$$\varphi_2(s) = \frac{\epsilon_p D_p \varphi_1 b \cosh \varphi_1 b - \sinh \varphi_1 b}{\epsilon_p D_p \varphi_1 b \cosh \varphi_1 b - \epsilon_p D_p \sinh \varphi_1 b + k_f b \sinh \varphi_1 b} \quad (3.10)$$

$$\varphi_1(s) = \left[\frac{1}{\epsilon_p D_p} \left(\epsilon_p s + \frac{k_{ads}s}{s + \frac{k_{ads}}{K_A}} \right) \right]^{1/2} \quad (3.11)$$

Adapting the model as a function of temperature

Several correlations were used to characterize all of the physical parameters associated with the mass transfer occurring inside the column, and fundamental properties such as solute diffusivity. The viscosity and density of the buffer were taken from NIST [7] using the physical properties for water between the range of 273K and 350K.

Axial dispersion was calculated by a correlation by Chung and Wen [5].

$$D_L = \frac{2\epsilon b V}{0.2 + 0.011 Re_p^{0.48}} \quad (3.12)$$

where Re_P is the particle Reynolds Number:

$$Re_P = \frac{2b\epsilon V\rho}{\mu} \quad (3.13)$$

For the solute diffusivity, Young [54] gave the following expression for proteins:

$$D_0 = 8.34 \times 10^{-10} \left(\frac{T}{\mu M_W^{\frac{1}{3}}} \right) \quad (3.14)$$

It can then be introduced in the Boyer and Hsu [2] correlation for intraparticle diffusivity:

$$D_e = 8.34 \times 10^{-10} \left(\frac{T}{\mu M_W^{\frac{1}{3}}} \right) \exp \left[-0.1307 \left(M_W^{\frac{1}{3}} + 12.45 \right) c_f^{\frac{1}{2}} \right] \quad (3.15)$$

For the intraparticle void fraction, data from GE Life Sciences [42] gives the following approximation:

$$\epsilon_p = -0.1 \ln(M_W) + 1.6835 \quad (3.16)$$

The mass transfer coefficient given by Liapis [9] for protein mass transfer coefficient is:

$$\frac{2k_f b}{D_0} = 2 + 0.51 \left(\frac{E^{\frac{1}{3}} (2b)^{\frac{4}{3}} \rho}{\mu} \right)^{0.60} Sc^{\frac{1}{3}} \quad (3.17)$$

E is the energy dissipation rate

$$E = \frac{25(1 - \epsilon) \epsilon^2 C_{D0} V^3}{b} \quad (3.18)$$

C_{D0} is the drag coefficient for a particle which is given by Stokes Law as $C_{D0} = 24/Re$ with the Reynolds number $Re = \rho V d / \mu$ and the Schmidt number as $Sc = \mu / \rho D_0$. Other variables that were not previously defined include: M_W – molecular

weight, d – column diameter, c_f – concentration of the gel, μ – viscosity, ρ – density, T – temperature.

3.3 Materials and Methods

3.3.1 Equipment Used

The system used to perform these investigations was a jacketed glass column (Spectrum Labs, Houston, TX) with a length of 30cm and I.D. of 1.5cm and a top plunger attachment. A six-way sample valve with a 1.2 ml sample loop was taken to inject a sample into the column. The buffer was pumped into the column using a HPLC reciprocating metering pump (Scientific Systems Incorporated, State College, PA). The column effluent was analysed using a UV detector (Spectrum Labs, Houston, TX) at a fixed wavelength of 280nm and the output voltage was recorded using a data acquisition board (Measurement Computing, Norton, MA). The column temperature was controlled using a ethylene glycol-water mixture from a circulating bath (Endocal, Newington, NH). The coolant fluid was set on the shell side of the column, while the column was used in the tube side.

3.3.2 Adsorbent Properties

The column was packed with Q Sepharose Fast Flow (Sigma-Aldrich, St. Louis, MO) which is a strong ion exchanger that utilizes the functional group $-CH_2N^+(CH_3)_3$ with a counterion of SO_4^{-2} . The molecular formula shows that the Q Sepharose ion exchanger has some alkane chains covalently bonded to the nitrogen active site. It is a beaded cross-linked agarose gel, with a working temperature between 4°C and 40°C, limiting the selection of experimental temperature to within this range.

Protein Characteristics

The analyte that was used was β -lactoglobulin from bovine milk (Sigma-Aldrich, St. Louis, MO), which is lyophilized powder of >90% purity, and a mixture of β -lactoglobulin A (LGA) and β -lactoglobulin B (LGB). LGA and LGB differ in their primary structure at two amino acid residues, at position 64 and 118, where LGA has aspartic acid at 64 and valine at 118, and LGB has glycine at 64 and alanine at 118, with a total of 162 residues each. They both have a pI in the range of 4.9-5.1.[28] The other protein that is analyzed in this work is bovine serum albumin (BSA)(Sigma-Aldrich, St. Louis, MO), which has a similar pI between 4.7-5.3. [35] The concentration of the β -lactoglobulin mixture was 0.001 g/mL, and the mass of the β -lactoglobulin is 18.4kDa, which makes it a relatively small protein. For BSA, the concentration was 0.01g/ml with a molecular weight of 66kDa, which makes it a medium-sized protein.

3.3.3 Buffer Properties

The recommended buffer [42] for the packing has a pH of at least 1 above the pI of the molecule of interest. That is a loose criterion, so a range of pH values was used at the same ionic concentration in order to investigate the binding affinity. Tris-HCl which is a standard buffer used in most biotechnology applications was used. Using pure Tris-HCl of 50mM to achieve the desired separation resulted in very long retention times due to the low ionic strength of the buffer. A guideline was taken from Luo and Hsu [28] where they used a 50:50 mixture of Tris-HCl 50mM and NaCl 0.5M solution. Therefore, 29.22g/L of NaCl were dissolved along with the salt values presented in Table 3.1. Tris-HCl 25mM and NaCl 0.25M in one liter of deionized water were prepared.

3.3.4 Experimental Procedure

The experimental procedure was adapted to allow the column to equilibrate to both the selected pH and temperature. The column was packed by degassing the gel slurry and then used a packing reservoir to load the gel. The column was filled with buffer prior to pouring the gel, which was left overnight to sediment onto the column, after which the excess buffer was allowed to flow and pack the gel. Five column volumes of buffer were used to flush the column in order to ensure that the gel bed is properly packed, after which a syringe plunger was used to cap off the top of the column. The buffer was introduced in the column by feeding it from the bottom going upward, opposing gravity. This maintained the integrity of the packing and the hydrostatic pressure kept the gel firmly in place.

Before each run, the column was equilibrated to the operating pH by running 3 column volumes of the buffer at the desired temperature. The buffer was first degassed by utilizing a vacuum Erlenmeyer flask and heated up so that it releases all the absorbed gases. The buffer itself is also equilibrated at the column temperature to avoid temperature gradients within the column. As the column is flushed, the recirculating bath is keeping the column at the desired temperature. Three operating temperatures were selected: 5°C, 23°C and 40°C. With this selection both the cold and the hot extremes of the manufacturer's recommended temperature range as well as the room temperature range are covered.

3.3.5 Computation Algorithm

To analyze the data with the model that is presented, the Fast Fourier Transfer (FFT) method was implemented. This enables us to directly simulate the elution data in the time domain. Chromatogram data was analyzed by inverting the Laplace domain to the time domain using the FFT method. The adsorption rate constant and the adsorption equilibrium constant were used to fit the experimental data to the

theoretical model. Chromatogram data was matched to the digital numbers returned by the FFT algorithm by least squares curve fitting, which was taken from MATLAB `lsqcurvefit` function. This method of computing the elution curve was introduced by Hsu and Dranoff [19] and has proven to be quite robust and effective in estimating the elution parameters. The parameters used in computing the elution curve for LGA and LGB for a temperature of 23°C are given as follows: $V = 0.0475\text{cm/s}$, $b = 0.009\text{cm}$, $\epsilon = 0.34$, $M_W = 18400\text{Da}$, $\epsilon_p = 0.701$, $\rho = 1.011\text{g/cm}^3$, $\mu = 0.0067\text{cP}$, $D_0 = 1.38 \times 10^{-6}\text{cm}^2/\text{s}$, $D_e = 4.00 \times 10^{-7}\text{cm}^2/\text{s}$, $D_L = 0.0014\text{cm}^2/\text{s}$, $k_f = 9.81 \times 10^{-4}\text{cm/s}$.

The inversion of the transfer function is computed using MATLAB and the built-in `IFFT` function. As the frequency spectrum of this function is symmetrical, it was specified in the function which aids the algorithm and decreases computation time. Inverting the transfer function was accomplished on a Dell Optiplex 790 with an Intel i7-2600 CPU with 8.00 GB of RAM using MATLAB version R2015a. Simulating one elution curve with the FFT method required 0.1019 seconds with 1024 digital numbers. Other inversion methods [8] required 21.7594 seconds. The computation performance makes the FFT method quite useful in obtaining rapid and precise results.

3.4 Results

For the BSA case, the results are displayed in Table 3.2. The chromatograms have a void volume marker, t_0 , and display how the pH and temperature affect the separation, where the peak gets retained much stronger in the column when pH and temperature are increased. The chromatograms are given in Figure 3.1 where the effect is very prominent.

For the β -lactoglobulin case, the column was run with the protein mixture at the experimental temperature and pH conditions. The chromatograms are presented in

Figures 3.2, 3.3 and 3.4, grouped by pH and with subplots at each temperature. Each figure has two peaks, with LGB eluting first and LGA eluting second. The elution order was determined based on previous experimental data [28] for this resin.

In Figure 3.2 to 3.4, at a temperature of 5°C, the two components elute very close to each other, so in a more acidic pH they even elute as a single peak. As the temperature is increased, the resolution between the two peaks increases very significantly, as well as the retention time increases. An example of fitting the model to the chromatograms is given in Figure 3.5. The chromatogram data set was reduced so that the FFT method can be implemented with the least squares fitting method directly. The resulting K_A and k_{ads} values are presented in Table 3.3.

The data has k_{ads} values that are quite small for the first peak, LGB, and the values for the second peak that are much larger. This is due to the fact that the adsorption for the first peak is much weaker in comparison to the second peak as evidenced by the higher K_A values. The second peak, LGA, has an aspartic acid on the surface, which causes higher adsorption rate on the adsorbent surface, thus showing higher k_{ads} values. k_{ads} was not considered as a critical parameter, as the primary parameter behind the separation is the adsorption equilibrium constant K_A .

3.5 Discussion

The theoretical model presented in this work gave us a clear direction as to how to perform our study. The protein concentration used in this study was low enough to assume a linear isotherm as given in the model and the salt concentration stayed constant during the elution.

Looking at the BSA data, there is a clear trend where the protein gets quite strongly retained as both pH and temperature are increased. The BSA becomes more negatively charged with increasing pH, which correlates well to the equilibrium

constant. To understand the degree of negative ionization of BSA, the experimental titration curve of BSA is given in Figure 3.6[38]. Looking at how the equilibrium constant changes with increasing negative charge of the solute, the K_A values with the net charge of the protein were correlated and displayed in Figure 3.7.

For the activation energies for the equilibrium constant of BSA, the Arrhenius plot is given in Figure 3.8 and data for the activation energies given in Table 3.4. There is good correlation between the inverse temperature, and the activation energies are quite different for all cases which is in line with the retention trends.

To gain an understanding behind the separation, the following formula for the separation factor was utilized:

$$S_{B/A} = \frac{K_{AB}}{K_{AA}} \quad (3.19)$$

This formula is given as the ratio between the retention times of the two peaks, however from the statistical moments of Schneider and Smith [39] they show that retention time is most directly affected by the adsorption equilibrium constant. Substituting the first moment, presented in Equations 3.20 to 3.22, as a ratio of the retention times yields Equation 3.19 which is used to calculate the separation factor. K_{AB} is the equilibrium constant of the more retained component, divided by K_{AA} the equilibrium constant of the less retained component. The separation factor results are tabulated in Table 2.5.

$$\mu'_n = \frac{m_n}{m_0} \quad (3.20)$$

where

$$m_n = \int_0^\infty t^n c(z, t) dt \quad (3.21)$$

which for the model yields

$$\mu'_1 = \left(\frac{z}{v}\right)[1 + m(1 + K_A)] \quad (3.22)$$

The separation factor is significantly improved by increasing temperature. By increasing pH there is slight improvement in the separation factor. This can be attributed to the increased adsorption of both proteins as they get more strongly ionized. In the temperature range between 5°C and 40°C the protein tertiary structure will not change significantly, thus it will not affect the result.

The thermodynamics of the process was key to understand the effect of temperature. The values for K_A were plotted on an Arrhenius plot, and their slopes were used to compute the activation energy of the adsorption equilibrium constant. This value is the net energy change of the molecule due to adsorbing and desorbing onto the packing. The plots are shown in Figure 3.9 and the values of the activation energies (in kJ/mol) are displayed in Table 3.6.

To better understand the charges on the proteins, a computational software, In-Charge, [10] was employed to calculate the titration curves of each protein. This data gives an estimate of the overall charge of the molecule to understand what gives rise to the separation of the two proteins. Given this data, the adsorption equilibrium constant was correlated to the net charge. The data for 23°C is taken and displayed in Figure 3.10. The increase in pH contributes to a more negative charge, leading to increase the retention which was experimentally observed.

In Figure 3.10, the difference in charge between the two proteins is only one negative charge unit. This is due to the aspartic acid in LGA which is the only residue that would contribute to the charge difference. As the molecules got more negative, the difference between equilibrium constants of the two molecules increased very significantly, and the results for 40°C are presented in Figure 3.11.

Along with these findings, looking at the tertiary structure of the protein for the position of the amino acid residue in the chain provides important insight as to what gives rise to the separation. The Protein Data Bank[1] has the β -lactoglobulin A [22], and β -lactoglobulin B [26], the tertiary structure of the proteins was observed.

Position 64 is on a turn in on the outside and position 118 is on a beta strand inside the core of the protein. Locating whether they are on the outside of the protein or inside the protein structure is instrumental to understanding the interaction of the protein with the anion-exchange packing. In Figure 3.12 and 3.13, position 64 is on the furthestmost bend from the center of the protein, and it is highlighted with a red circle in both figures. At position 64 in LGA there is aspartic acid and in LGB there is glycine. The aspartic acid residue is negatively charged under basic pH conditions, making it ideal for anion-exchange chromatographic separation. The amino acid residues at position 118 are found in the center of the protein in both LGA with valine and LGB with alanine so they will not affect the ion-exchange separation as they are uncharged. They are displayed in Figure 3.12 and 3.13 and highlighted with a blue circle. This highlights the fact that the charges on the surface of the protein are key to adsorption of the proteins onto the resin, whereas the residues that are inside the protein do not affect the separation significantly. These structural differences can improve the separation in anion-exchange chromatography.

Using the correlations that are derived from the experimental data and the theoretical model, the elution peaks at different temperatures and pH for the given system can be simulated. From protein properties the researcher can use the model and solve it by FFT algorithm to predict the elution curves for any pH and temperature condition within the experimental range.

3.6 Conclusion

The protein tertiary structure provides the information of charges on the protein external surface, thus it will be helpful for biochemical engineers to explore the optimal strategy for separation. The retention time of the proteins increased with temperature and pH, leading to better separation of the two components. Using the data and the

model provided for the elution of anion-exchange chromatography under different pH and temperature conditions can be predicted. This will allow to use temperature and pH as important variables to optimize and improve chromatographic biomolecule separations. Also, the tertiary structure of proteins will be helpful to visualize the interaction between protein and anion-exchange adsorbent.

pH	Temperature	Trizma HCl (g/L)	Trizma Base (g/L)
7.8	5°C	3.51	0.335
	23°C	2.66	0.99
	40°C	2.01	1.49
8.4	5°C	2.66	0.99
	23°C	1.32	2.02
	40°C	0.75	2.45
8.8	5°C	1.77	1.67
	23°C	0.62	2.57
	40°C	0.38	2.74

Table 3.1: Tris-HCl buffer mixing table for 25mM solution[43]

Temperature	pH	K_A	k_{ads}
5°C	7.8	0.0175	20.1
23°C	7.8	0.288	341.3
40°C	7.8	1.327	880.9
5°C	8.4	0.253	31.0
23°C	8.4	1.091	562.4
40°C	8.4	6.281	1123.8
5°C	8.8	0.461	43.0
23°C	8.8	2.317	713.1
40°C	8.8	8.244	3122.5

Table 3.2: Parameters derived from the non-linear curve fitting of the experimental data for BSA, the equilibrium constant K_A with values in $[\frac{mL}{g}]$ and the adsorption rate constant k_{ads} with values in $[\frac{mL}{g \cdot sec}]$

		Peak LGB		Peak LGA	
Temperature	pH	K_A	k_{ads}	K_A	k_{ads}
5°C	7.8	0.1381	0.0002	0.1390	13.914
23°C	7.8	0.3555	0.0021	0.9421	182.3
40°C	7.8	0.4625	0.0094	1.7508	1742.9
5°C	8.4	0.3258	0.0003	0.3740	232.05
23°C	8.4	0.4564	0.0054	1.1643	514.53
40°C	8.4	1.1148	0.1053	3.4044	1718.9
5°C	8.8	0.7224	0.0025	0.9155	369.73
23°C	8.8	1.1863	0.0143	3.0134	728.38
40°C	8.8	1.5978	0.3798	4.7851	4817.6

Table 3.3: Parameters derived from the non-linear curve fitting of the experimental data for LGA and LGB, the equilibrium constant K_A with values in $[\frac{mL}{g}]$ and the adsorption rate constant k_{ads} with values in $[\frac{mL}{g \cdot sec}]$

pH	Activation Energy of BSA
7.8	749.0
8.4	66.1
8.8	59.7

Table 3.4: Activation energies of the adsorption equilibrium constants K_A for BSA in kJ/mol

Temperature	pH	$S_{B/A}$
5°C	7.8	1.01
23°C	7.8	2.65
40°C	7.8	3.79
5°C	8.4	1.15
23°C	8.4	2.55
40°C	8.4	3.05
5°C	8.8	1.27
23°C	8.8	2.54
40°C	8.8	2.99

Table 3.5: Separation Factor as a function of pH and temperature.

pH	Activation Energy of LGB	Activation Energy of LGA
7.8	25.36	53.06
8.4	25.05	45.62
8.8	16.50	34.57

Table 3.6: Activation energies of the adsorption equilibrium constants K_A for both peaks in kJ/mol

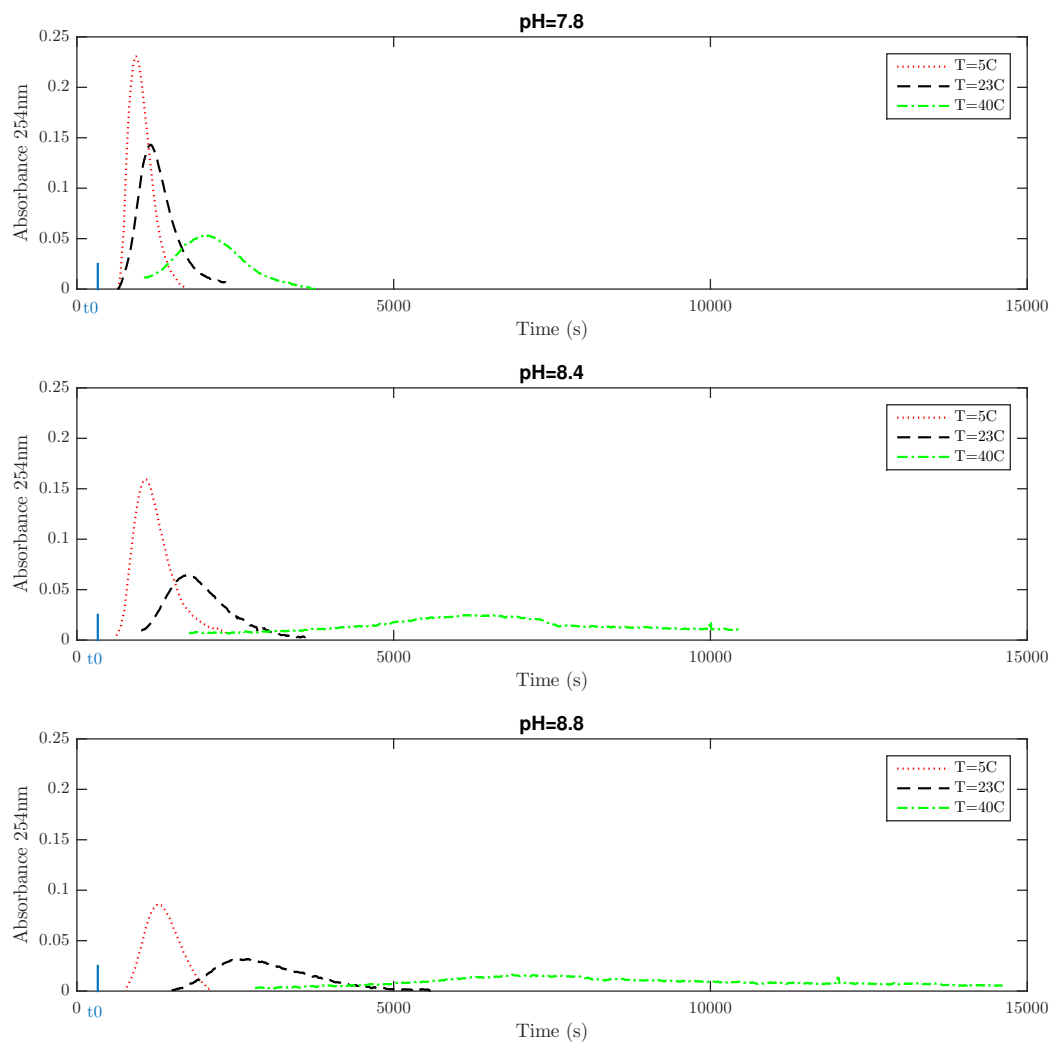


Figure 3.1: Bovine Serum Albumin chromatograms at the different pH and temperature conditions considered in this work. The vertical marker indicates column void volume.

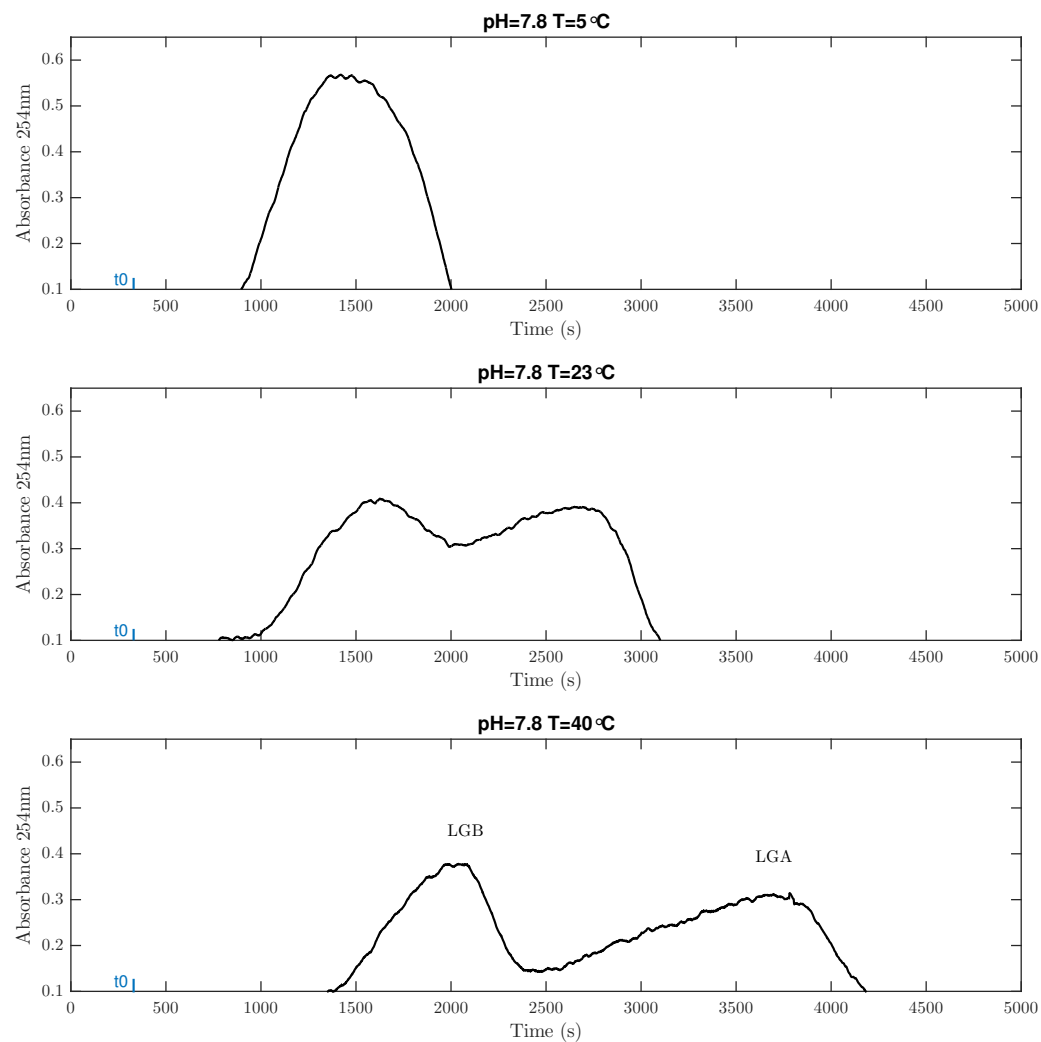


Figure 3.2: β -lactoglobulin chromatograms at a pH of 7.8 at three different temperatures at a flowrate of $5\text{ml}/\text{min}$

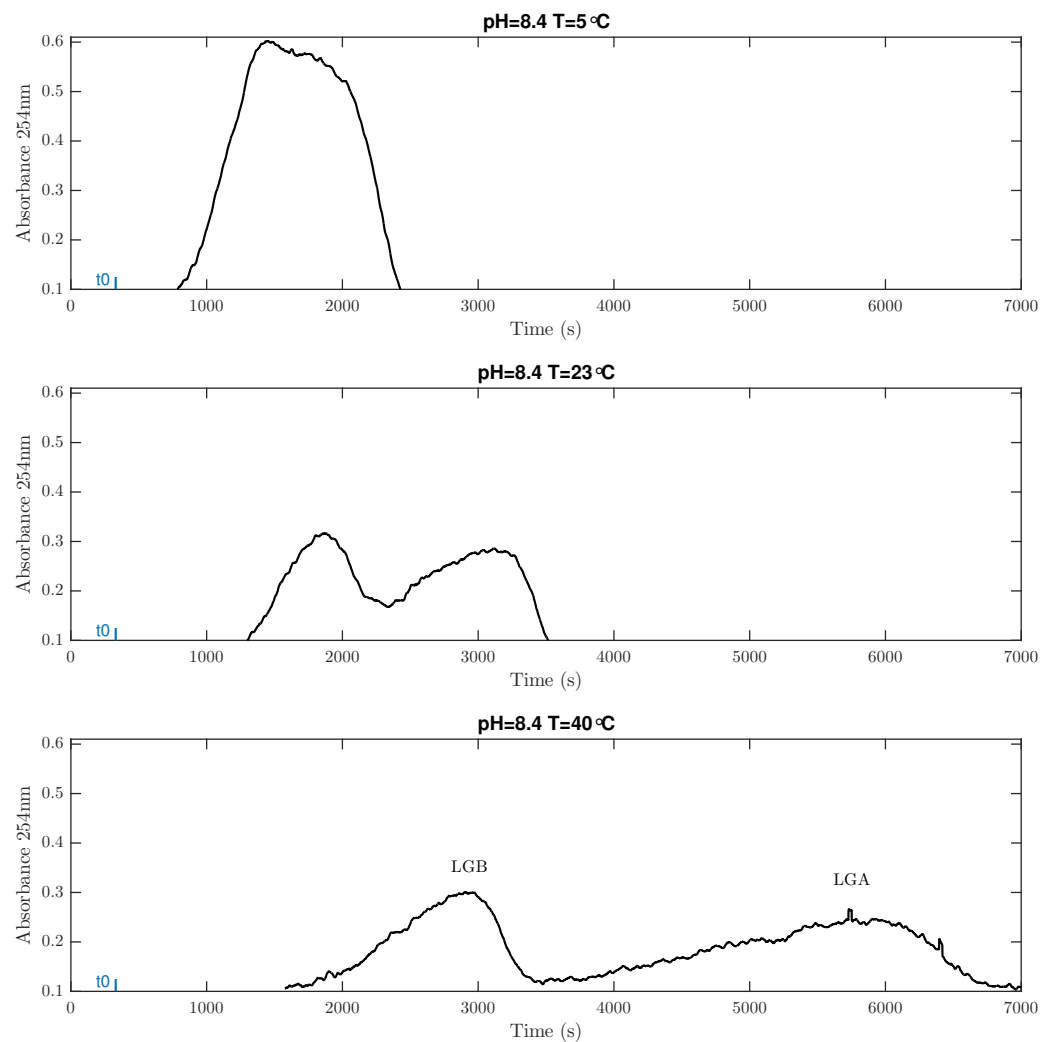


Figure 3.3: β -lactoglobulin chromatograms at a pH of 8.4 at three different temperatures at a flowrate of 5ml/min

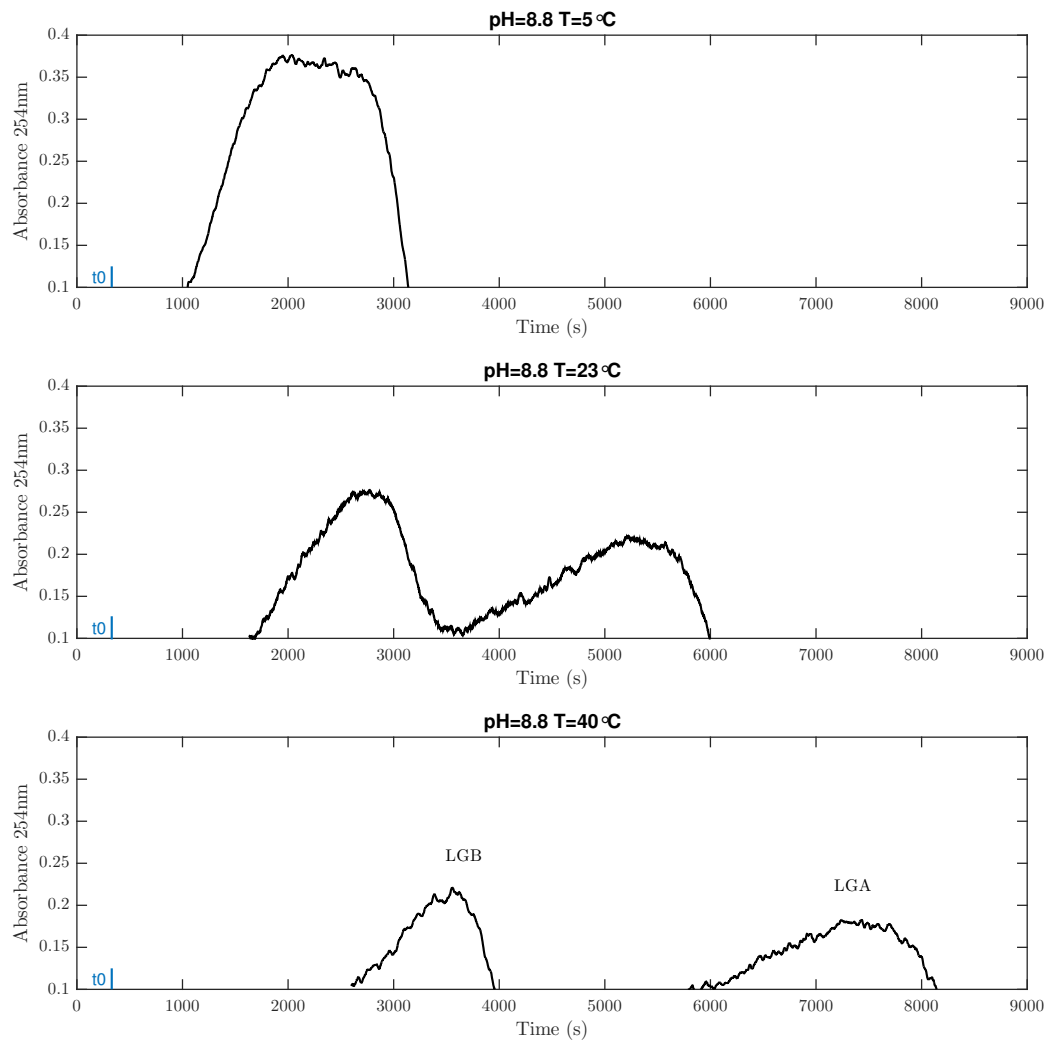


Figure 3.4: β -lactoglobulin chromatograms at a pH of 8.8 at three different temperatures at a flowrate of $5\text{ml}/\text{min}$

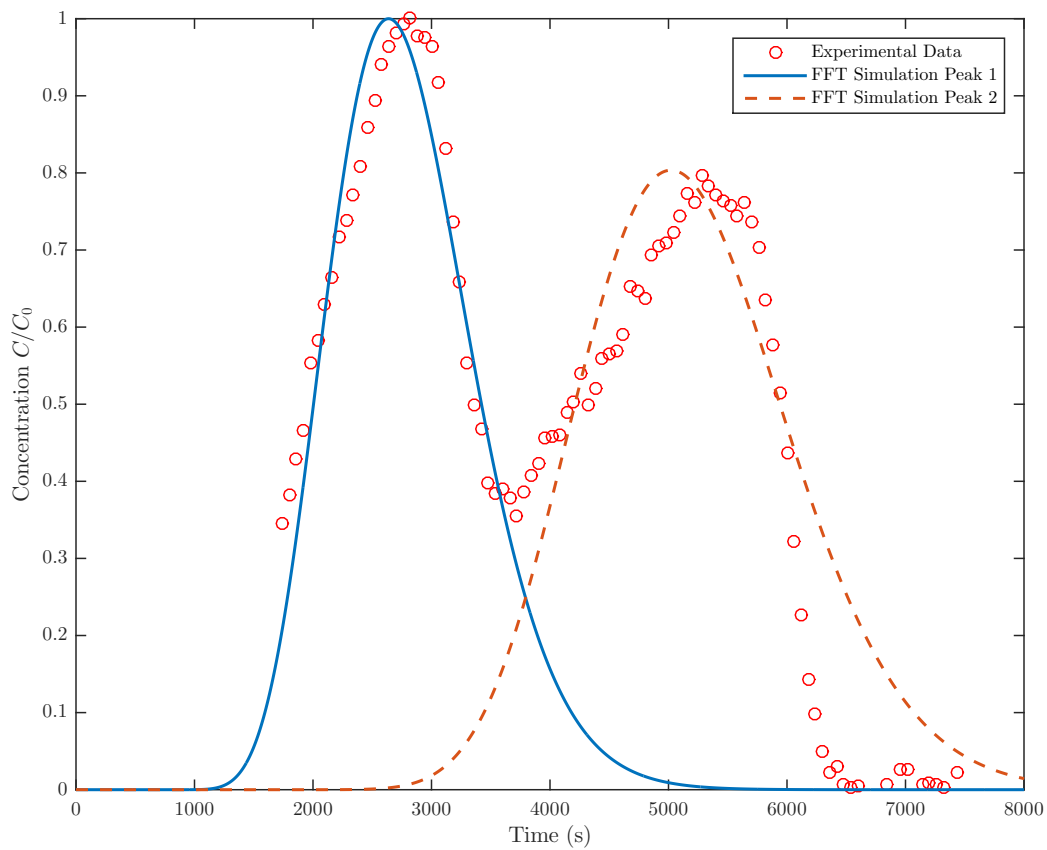


Figure 3.5: β -lactoglobulin chromatograms at a pH of 8.8 at room temperature at a flowrate of $5\text{ml}/\text{min}$ with FFT simulation for both peaks

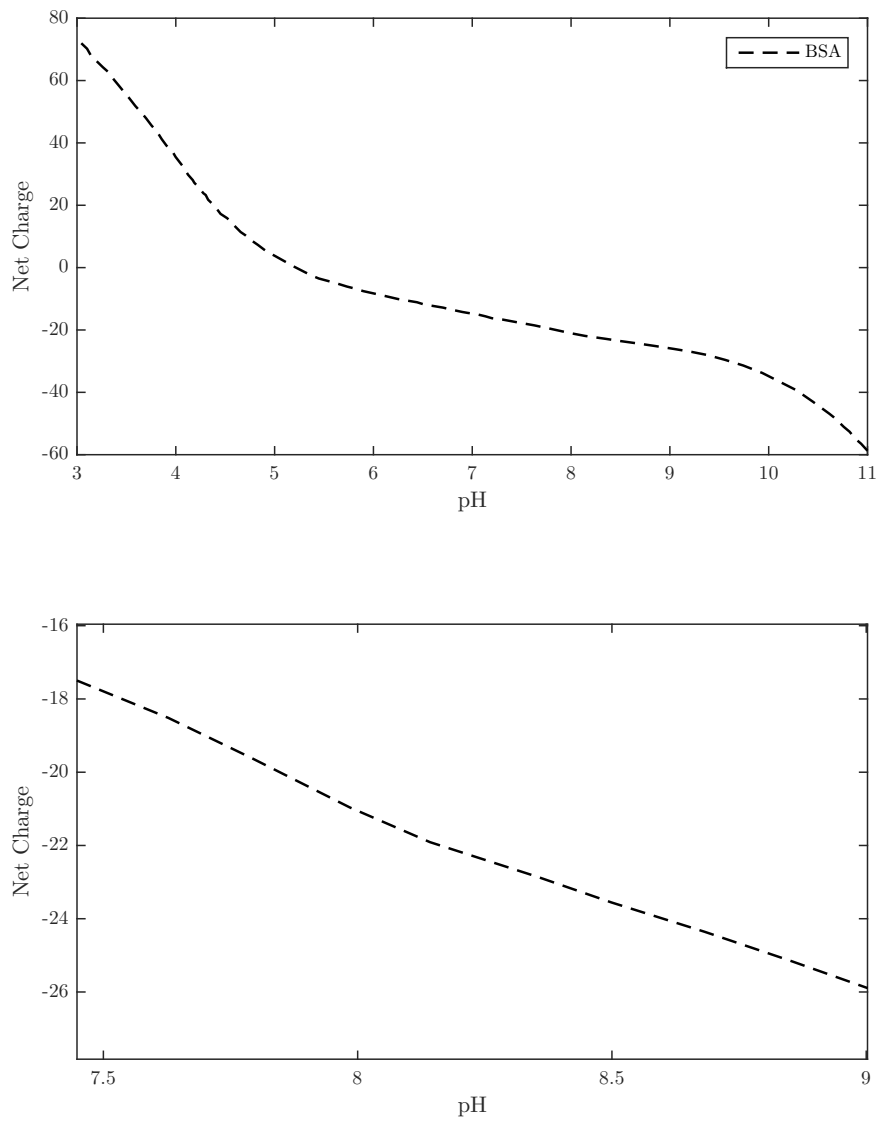


Figure 3.6: Titration curves of BSA, both in the pH range of 3 - 11 and the range of interest from 7.5 - 9

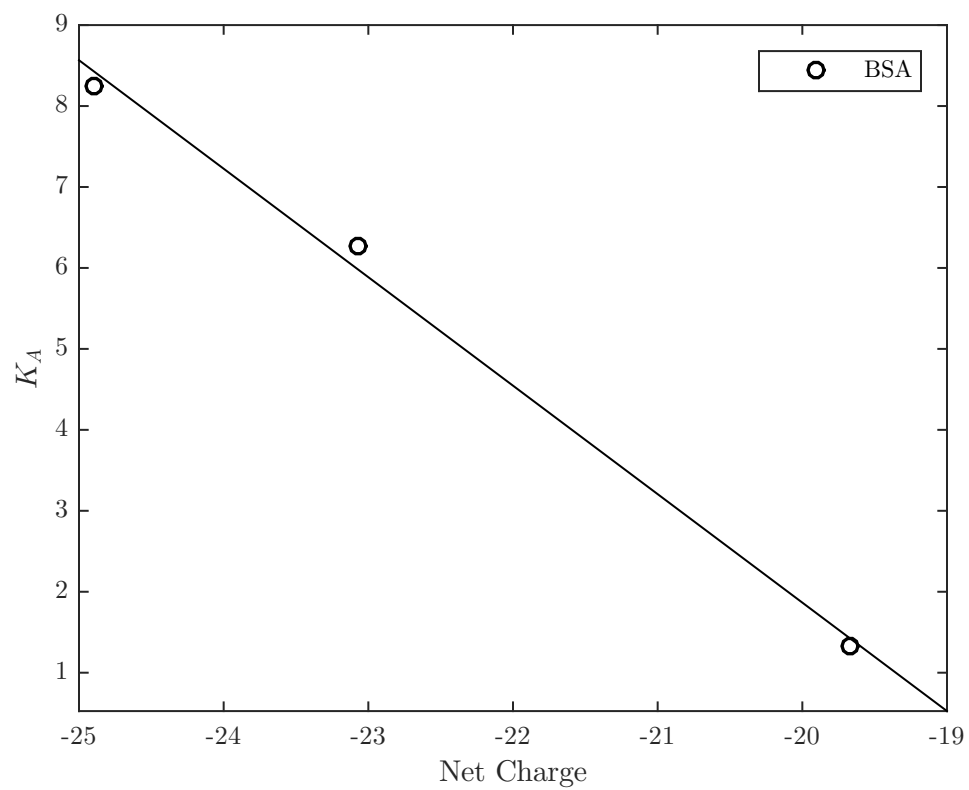


Figure 3.7: Adsorption equilibrium constant of BSA as a function of the protein net charge.

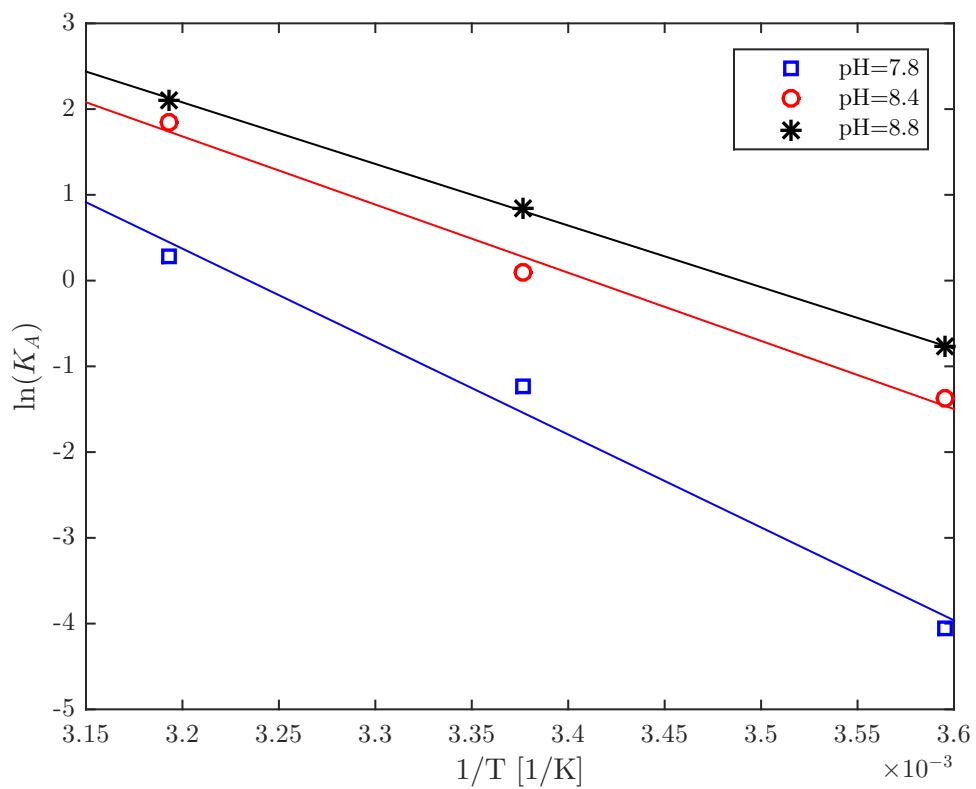


Figure 3.8: Arrhenius plots for the K_A values for BSA at different pH values

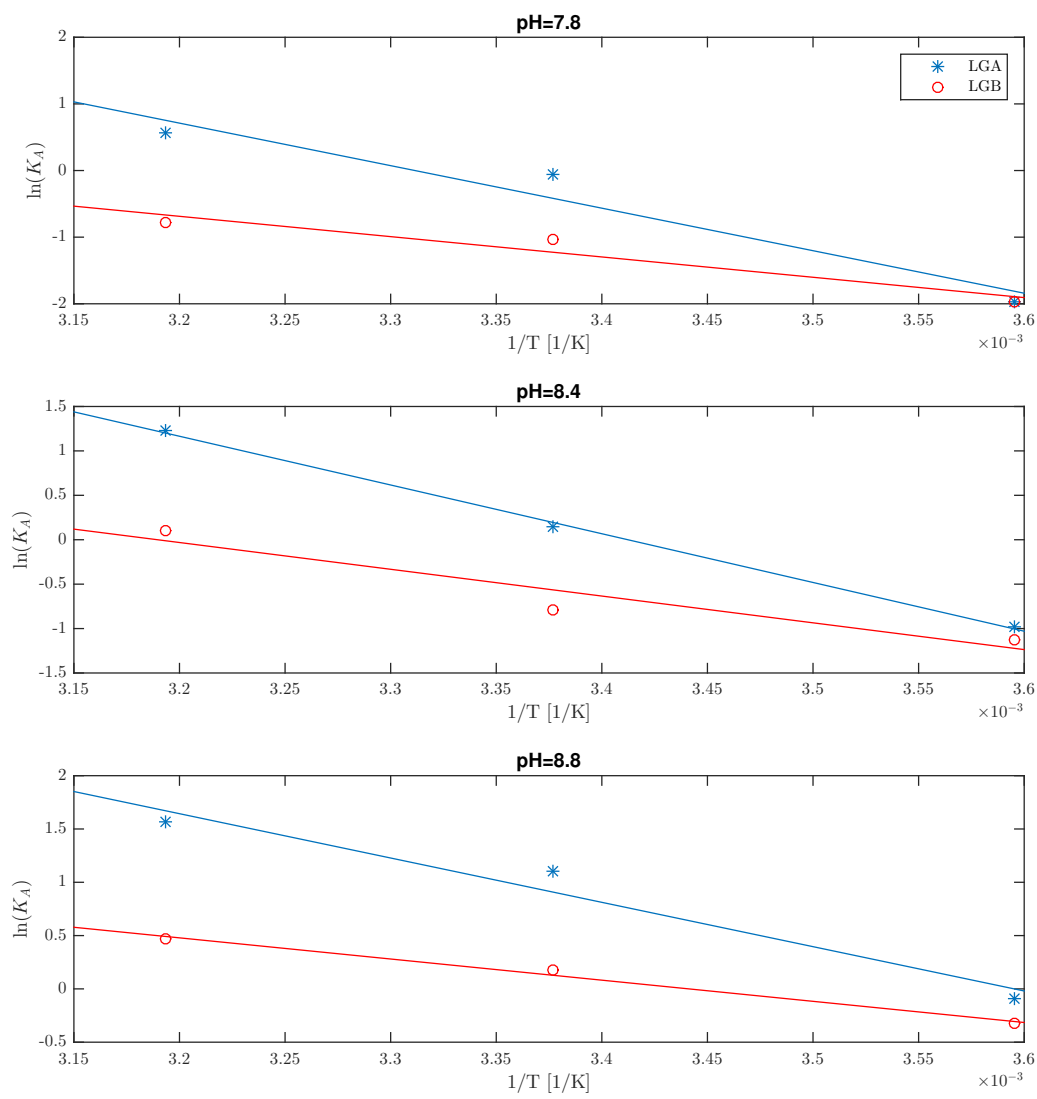


Figure 3.9: Arrhenius plots for the K_A values for both LGA and LGB at different pH values

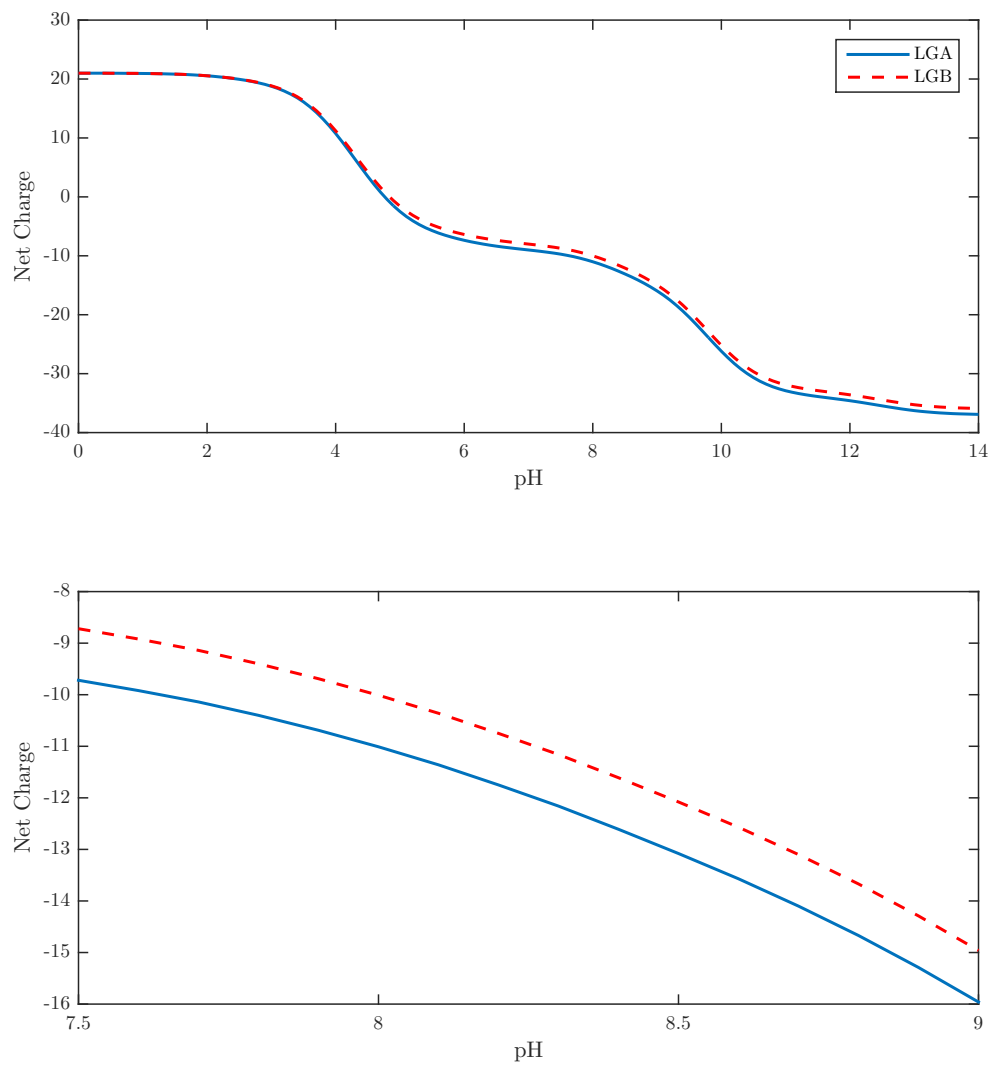


Figure 3.10: Titration curves of lactoglobulin A and B, both in the pH range of 1 - 14 and the range of interest from 7.5 - 9

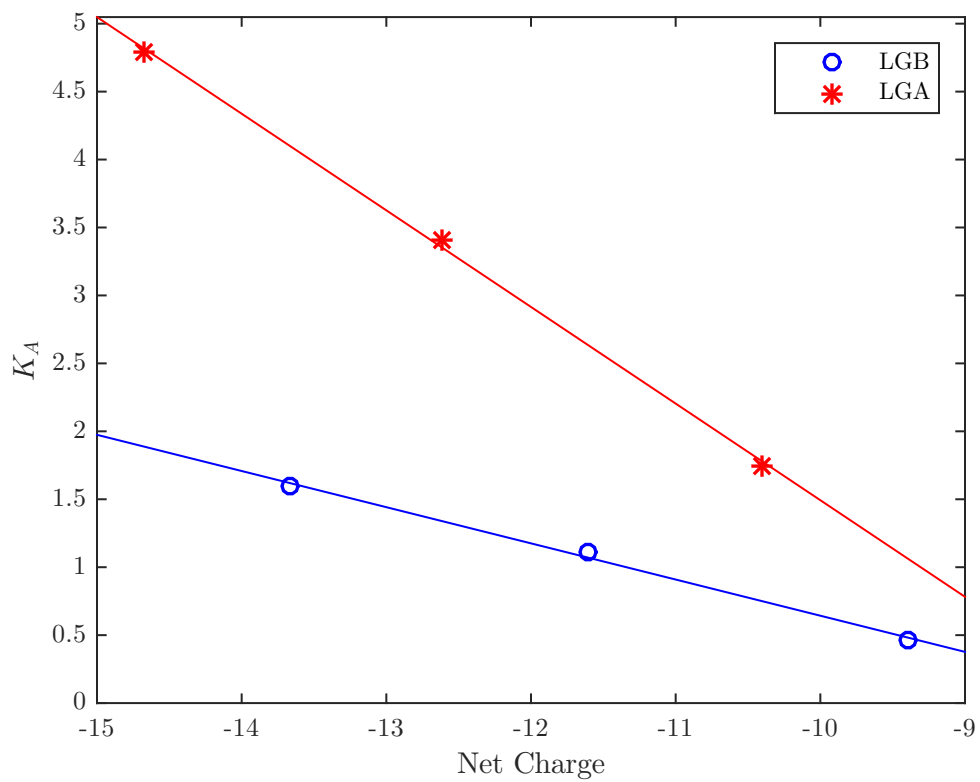


Figure 3.11: Adsorption equilibrium constant of LGB and LGA as a function of the protein net charge at 40°C.

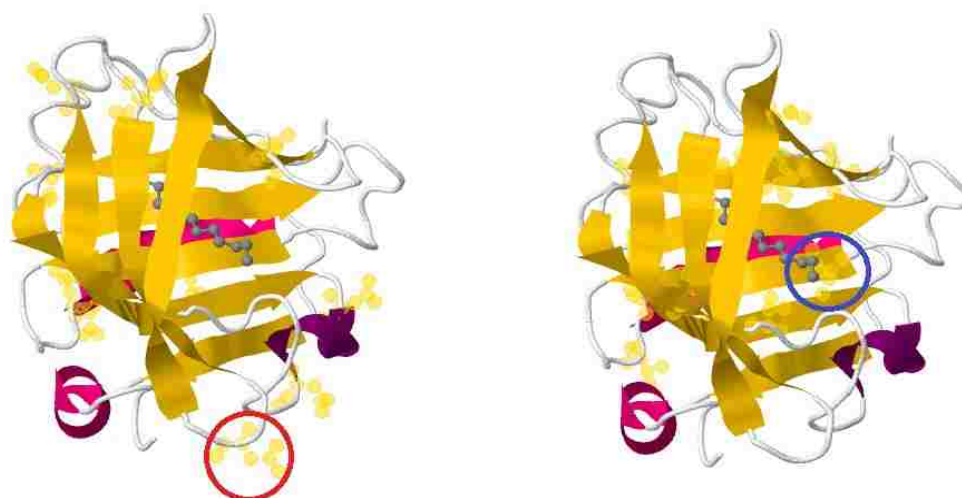


Figure 3.12: β -Lactoglobulin A tertiary structure is given in both panels. On the panel on the left, aspartic acid residues are highlighted with yellow circles. The aspartic acid residue at position 64 is highlighted with a red circle. On the right panel, the valine residue at position 118 is highlighted with a blue circle and the other valine residues are highlighted with yellow circles. [22]

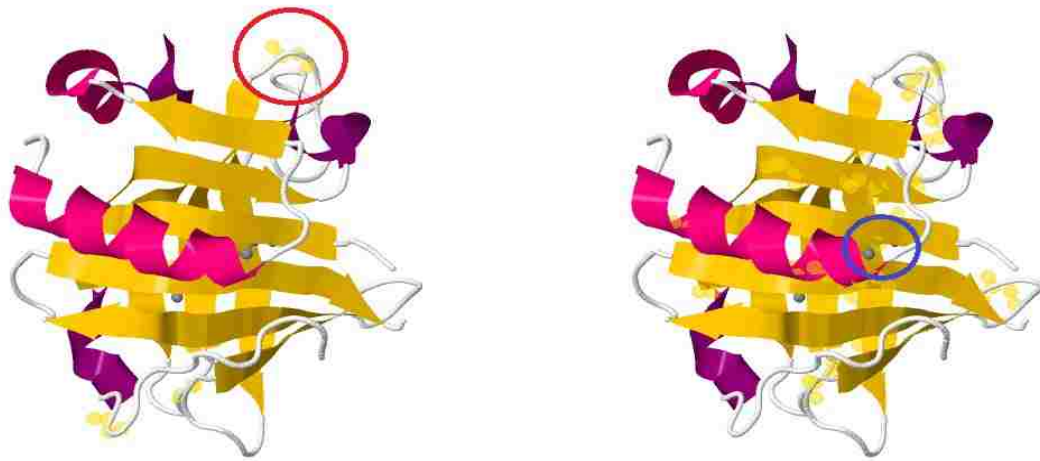


Figure 3.13: β -Lactoglobulin B tertiary structures given in both panels. On the panel on the left, glycine residues are highlighted with yellow circles. The glycine residue at position 64 is highlighted with a red circle. On the right panel, the alanine residue at position 118 is highlighted with a blue circle and the other alanine residues are highlighted with yellow circles. [26]

Chapter 4

Effect of pH and Temperature on Amino Acids, Immunoglobulin G and Lysozyme Separation on SP Sephacrose Cation-Exchange Chromatography

Retention data at different pH and temperatures was collected for the SP Sepharose cation-exchange chromatography system using a variety of small and large biomolecules. A mechanistic model for chromatography was fitted to the chromatogram which resulted in computing the equilibrium constant K_A to quantify the separation. The data shows important trends between the net charge of the proteins and the equilibrium constant. An Arrhenius plot was made to represent the relationship between the equilibrium constant and temperature. The main result from the analysis was the relation where pH and temperature decreased, the retention of the biomolecules increased. The result from cation exchange chromatography is exactly opposite from

the one observed in previous reports on anion exchange chromatography where the retention increased with increasing temperature and pH.

4.1 Introduction

Ion exchange chromatography has been an industry workhorse for any biological separation application. This process can be described by a mechanistic model [39], however these models do not represent the effect of pH and temperature on the separation. These physical parameters are essential for the selectivity and resolution of the separation and need to be accounted for so that the model can be used in a predictive manner.

For the pH effect, industry guidelines[42] indicate that as pH is decreased, the overall charge of the molecule increases and contributes to stronger retention inside the column. Previous research on Immunoglobulin G (IgG) behavior on a cation exchange columns [21] reported that the IgG is retained more when temperature is decreased. In this work, a systematic analysis of the effect on the pH and temperature is performed by taking molecules of different sizes and investigating their retention. A general case on how separations in a cation exchange chromatography are affected by changes in the pH and temperature is explored. The retention inside the column is quantified using the equilibrium constant K_A , which is directly related to the retention time of the solute. A clear trend between the pH and temperature and the separation selectivity emerged. The model that follows is the same as presented in a previous work for anion exchange chromatography [32].

4.2 Theoretical Model

Hsu and Chen [18] used a model derived by Horvath and Lin [17] for a theoretical analysis for chromatographic separations. The model considers an isothermal chro-

matographic column packed with uniform spherical particles, and includes external film diffusion, intraparticle diffusion and adsorption on the particle surface. The flow pattern was assumed axial-dispersed plug flow with a linear adsorption equilibrium.

For the mobile phase material balance

$$\frac{\partial C}{\partial t} + V \frac{\partial C}{\partial z} - D_L \frac{\partial^2 C}{\partial z^2} = -\frac{1}{m} \frac{\partial q}{\partial t} \quad (4.1)$$

Intraparticle material balance

$$\epsilon_p \frac{\partial C_p}{\partial t} + \frac{\partial C_s}{\partial t} = \epsilon_p D_p \left(\frac{\partial^2 C_p}{\partial r^2} + \frac{2}{r} \frac{\partial C_p}{\partial r} \right) \quad (4.2)$$

Adsorption term on the particle surface

$$\frac{\partial C_s}{\partial t} = k_{ads} \left(C_p - \frac{C_s}{K_A} \right) \quad (4.3)$$

The initial and boundary conditions

$$C = C_p = C_s = 0 \text{ at } z > 0, t = 0 \quad (4.4)$$

$$C = C_0 \delta(t) \text{ at } z = 0 \quad (4.5)$$

$$C = 0 \text{ at } z = \infty \quad (4.6)$$

$$\frac{\partial C_p}{\partial r} = 0 \text{ at } r = 0 \quad (4.7)$$

$$\frac{\partial q}{\partial t} = \frac{3k_f}{b} (C - C_p) = \frac{3}{b} \epsilon_p D_p \frac{\partial C_p}{\partial r} = 0 \text{ at } r = b \quad (4.8)$$

The variables introduced are: C – solute concentration in mobile phase, C_p -

solute concentration in the pores, C_s – solute concentration on solid, C_0 – initial pulse concentration, V – mobile phase velocity, D_L – axial dispersion coefficient, $m = \epsilon/(1 - \epsilon)$, ϵ – column void fraction, ϵ_p – particle porosity, q – concentration in particles, D_p – intraparticle diffusivity, k_{ads} – adsorption rate constant, K_A – adsorption equilibrium constant, k_f – external mass transfer coefficient, t – time, z – axial position, r – intraparticle radial position, b – radius of the bead.

A solution can be obtained by taking the Laplace transform:

$$\bar{C}(z, s) = C_0 \exp \left[\left(\frac{V}{2D_L} - \sqrt{\frac{V^2}{4D_L^2} + \frac{s}{D_L} + \frac{3k_f\varphi_2}{bmD_L}} \right) z \right] \quad (4.9)$$

$$\varphi_2(s) = \frac{\epsilon_p D_p \varphi_1 b \cosh \varphi_1 b - \sinh \varphi_1 b}{\epsilon_p D_p \varphi_1 b \cosh \varphi_1 b - \epsilon_p D_p \sinh \varphi_1 b + k_f b \sinh \varphi_1 b} \quad (4.10)$$

$$\varphi_1(s) = \left[\frac{1}{\epsilon_p D_p} \left(\epsilon_p s + \frac{k_{ads} s}{s + \frac{k_{ads}}{K_A}} \right) \right]^{1/2} \quad (4.11)$$

4.2.1 Adapting the model as a function of temperature

Correlations for fundamental physical parameters were used to quantify the mass transfer occurring inside the column for properties such as diffusion of the solute. The viscosity and density of the buffer were taken from NIST data [7] for properties of water.

Axial dispersion was evaluated using a correlation by Chung and Wen [5].

$$D_L = \frac{2\epsilon b V}{0.2 + 0.011 Re_P^{0.48}} \quad (4.12)$$

where

$$Re_P = \frac{2b\epsilon V \rho}{\mu} \quad (4.13)$$

The protein solution diffusivity, was estimated by correlation by Young [54]:

$$D_0 = 8.34 \times 10^{-10} \left(\frac{T}{\mu M_W^{\frac{1}{3}}} \right) \quad (4.14)$$

which is introduced in the Boyer and Hsu [2] correlation for intraparticle diffusivity:

$$D_e = 8.34 \times 10^{-10} \left(\frac{T}{\mu M_W^{\frac{1}{3}}} \right) \exp \left[-0.1307 \left(M_W^{\frac{1}{3}} + 12.45 \right) c_f^{\frac{1}{2}} \right] \quad (4.15)$$

For the intraparticle void fraction, a correlation based on data provided by GE Life Sciences [42] was used:

$$\epsilon_p = -0.1 \ln(M_W) + 1.6835 \quad (4.16)$$

The mass transfer coefficient for proteins is given by Liapis [9]:

$$\frac{2k_f b}{D_0} = 2 + 0.51 \left(\frac{E^{\frac{1}{3}} (2b)^{\frac{4}{3}} \rho}{\mu} \right)^{0.60} Sc^{\frac{1}{3}} \quad (4.17)$$

E is the energy dissipation rate

$$E = \frac{25 (1 - \epsilon) \epsilon^2 C_{D0} V^3}{b} \quad (4.18)$$

C_{D0} is the drag coefficient for a particle which is given by Stokes Law as $C_{D0} = 24/Re$ and the Schmidt number as $Sc = \mu/\rho D_0$. Other variables that were not previously defined include: M_W – molecular weight, c_f – concentration of the gel, μ – viscosity, ρ – density, T – temperature.

4.3 Materials and Methods

4.3.1 Equipment used

The equipment used in this study involved was a jacketed glass column (Spectrum Labs, Houston, TX) with a length of 30cm and a top plunger attachment. A six-way sample valve with a 1.2 ml sample loop was used for injection. The buffer was pumped into the column using a HPLC metering pump (Scientific Systems Incorporated, State College, PA). The column effluent was analyzed using a UV detector (Spectrum Labs, Houston, TX) at a fixed wavelength of 254nm and the output voltage was recorded using a data acquisition system (Measurement Computing, Norton, MA). The column temperature was regulated using a ethylene glycol-water mixture from a circulating bath (Endocal, Newington, NH). The coolant fluid was set on the shell side of the column, while the column packing was set in the tube side.

4.3.2 Stationary Phase

The column was packed with SP Sepharose Fast Flow (Sigma-Aldrich, St. Louis, MO) which is a strong cation exchanger that has a sulphopropyl group $-O-CH_2CHOHCH_2O(CH_2)_3SO_3^-$. SP Sepharose Fast Flow is beaded cross-linked agarose gel with a 6% concentration and a working temperature between 4°C and 40°C. The packing has a broad pH working range where it is highly negatively charged. The properties of the stationary phase set our experimental working temperature and pH range.

4.3.3 Sorbate Properties

The amino acids that were used as analytes are tryptophan, with a molecular weight of 186.2Da and a pI of 5.89 and tyrosine, with a molecular weight of 163.2Da and a pI of 5.66.[49]. The amino acids were individually introduced into the column, where

tryptophan was dissolved in deionized water at a concentration of 0.001 g/mL and tyrosine was introduced at its solubility limit by injecting it to the sample loop by clarifying it using a 0.22 μ m filter. Proteins that were used as analytes are Immunoglobulin G from rabbit serum and hen white lysozyme (Sigma-Aldrich, St. Louis, MO). The proteins were introduced in the column as a 1:1 volumetric mixture of 0.075 mg/mL of rabbit serum IgG and 0.001 g/mL of hen white lysozyme. The lysozyme has a pI of 11.35[50] and the rabbit IgG has a pI of 6.1-6.5[53].

4.3.4 Mobile Phase Properties

For the amino acid analysis, the buffer was 0.1M sodium citrate and 0.1M citric acid mixture.[52] The pH values that are used in this experiment are 3.0, 3.6 and 4.2. The volumes of trisodium citrate dihydrate and citric acid monohydrate that were mixed are given in Table 4.1. For the amino acid elution, no sodium chloride was added to the buffer, and for the protein elution, the sodium citrate buffer was mixed in 1:1 volumetric ratio with 0.8M sodium chloride to enable isocratic elution.

4.3.5 Experimental Procedure

The column was equilibrated to the selected pH and temperature for each experiment. The gel slurry was degassed prior to pouring in the column and then using a packing reservoir to load on the gel. The column was filled with buffer prior to pouring the gel to ensure that no bubbles were trapped. The gel was left overnight to sediment onto the column, afterwards the buffer was allowed to flow and pack the gel. Five column volumes of buffer were used to flush the column to ensure that the bed is properly packed. A syringe plunger capped off the top of the column. The buffer was introduced in the column by feeding it from the bottom going upward, opposing gravity. This was done to maintain the integrity of the packing and for the hydrostatic pressure to keep the gel firmly in place.

Before each run, the column was equilibrated to the operating pH by running 3 column volumes of the selected buffer. The buffer was first degassed by utilizing a vacuum Erlenmeyer flask and heating it up so that it releases all the absorbed gases. The buffer was brought to the column temperature before introducing it to the column to avoid temperature gradients within the column. Three operating temperatures were selected: 5°C, 23°C and 40°C which cover both the cold and the hot extremes of the manufacturer’s recommended temperature range[42] for the packing as well as the room temperature range.

4.3.6 Computational Algorithm

To analyze the data with the model, the Fast Fourier Transfer (FFT) solution method was implemented. This allowed to compute the elution curve in the time domain. This method was introduced by Hsu and Dranoff [19] and has proven to be quite robust and effective in estimating the elution parameters. As an example, the parameters used in computing the elution curve for tryptophan for a temperature of 23°C are as follows: $V = 0.121\text{cm}/s$, $b = 0.009\text{cm}$, $\epsilon = 0.34$, $M_W = 18400\text{Da}$, $\epsilon_p = 0.9$, $\rho = 1.011\text{g}/\text{cm}^3$, $\mu = 0.0067\text{cP}$, $D_0 = 3.834 \times 10^{-6}\text{cm}^2/s$, $D_e = 2.13 \times 10^{-6}\text{cm}^2/s$, $D_L = 0.0036\text{cm}^2/s$, $k_f = 2.7 \times 10^{-3}\text{cm}/s$.

4.4 Results

The chromatograms were plotted on the same graph so that the tyrosine and the tryptophan peak can be directly compared. Both amino acids were run at the same flow rate, temperature and pH. The resulting chromatograms for pH values of 4.2, 3.6 and 3.0 are displayed in Figure 4.1, 4.2 and 4.3 for 5°C, 23°C and 40°C. The same experiment was done for the Immunoglobulin G (IgG) and lysozyme, however in this case the IgG and lysozyme were injected at the same time and their chromatograms

are presented in Figure 4.4, 4.5 and 4.6.

The data was analyzed by using the model described in the previous section, by transforming the Laplace domain to the time domain using the Fast Fourier Transform (FFT) algorithm[19]. The adsorption rate constant and the adsorption equilibrium constant were used to fit the experimental data to the theoretical model. This was achieved by the MATLAB `lsqcurvefit` function by reducing the chromatogram data points to match the digital numbers returned by the FFT algorithm. A sample of the curve fitting data is given in Figure 4.7 for the cases of IgG and lysozyme. This procedure was repeated for all the chromatograms, and the data is compiled in Table 4.2 and 4.3 for Tryptophan and Tyrosine and Tables 4.4 and 4.5 for IgG and lysozyme. The emphasis of this work is on the equilibrium constant K_A rather than the adsorption equilibrium constant k_{ads} , which is used as a fitting parameter.

The chromatogram data can also be represented by calculating the retention factor k' , calculated as the ratio of the retention time t_A of the component and the hold up time, t_0 . [30] In this experiment, the hold up time was determined to be 330s. Mathematically is computed as presented in Equation 4.19, and the results of the retention factor are given in Table 4.6 and 4.7.

$$k' = \frac{t_A - t_0}{t_0} \quad (4.19)$$

As demonstrated in Tables 4.2-4.7, the equilibrium constant K_A and retention factor k' increase significantly as temperature and pH are decreased. Increased retention with decreasing pH in an cation exchanger is to be expected as the net charge of the molecule increases, therefore the ion binding forces increase. The increased retention due to the decrease in temperature was similarly observed in previous work.[21]

4.5 Discussion

The separation between the amino acid group and protein group is greatly improved as both pH and temperature are decreased. To quantify the degree of separation, the separation factor is utilized which is computed by taking the ratio of the equilibrium constants for the two components (K_{AB} and K_{AA}). The formula is given in Equation 4.20 and the results are given in Table 4.8 and 4.9.

$$S_{B/A} = \frac{K_{AB}}{K_{AA}} \quad (4.20)$$

From these results, it can be concluded that the separation is the best in more acidic condition and at lower temperatures. Both of these variables contribute to higher sorbate retention and improve the separation selectivity between the molecules. This effect is important as its quantification will allow for selecting appropriate conditions that lead to higher selectivity in cation-exchange chromatography.

4.5.1 pH Effect

In this experiment, the pH was elevated from 3.0 to 4.2, which leads to lower positive ionization of the sorbates. The chromatograms show that the sorbates will be retained longer at the most acidic pH value, as the sorbates have the highest positive charge at those conditions. The change in net charge can best be observed by the titration curves of the molecules. The titration curves for both tryptophan and tyrosine are given in Figure 4.8 and the curve for lysozyme[45] is given in Figure 4.9. The titration curves show that the molecules become more positively charged as the pH decreases.

The charge values for each molecule at the experimental pH is taken to establish a correlation to the equilibrium constant to observe the difference in retention of the two molecules. This relationship is demonstrated in Figure 4.10, where tryptophan is more retained as it becomes more positively charged. Tyrosine has the same behavior,

however it does not become more positively charged than tryptophan so it remains less retained. The same analysis was done for the lysozyme case and the correlation is presented in Figure 4.11, where it shows higher retention at increased net charges.

Note that in Figure 4.6 where the chromatograms for IgG and lysozyme are presented at a pH of 4.2, the peaks were not resolved and both components eluted as a single peak. This data set emphasizes that the pH of the elution buffer needs to be carefully calibrated to allow enough charge difference between the proteins that are being separated. This effect can be seen more clearly in Figure 4.3 where the later portion of the tyrosine peak mixes with the tryptophan peak, leading to diminished resolution.

4.5.2 Temperature Effect

For the effect of temperature, higher retention is observed as temperature is decreased. The values for the equilibrium constant were correlated with temperature on an Arrhenius plot for the three different pH values. From the slope of the data, the activation energy of tyrosine and tryptophan for their equilibrium constants was computed for the three different pH values. The Arrhenius plot is displayed in Figure 4.12 and the activation energy values are given in Table 4.10. For the protein case, the Arrhenius plot is given in Figure 4.13 and the activation energy values are presented in Table 4.11.

One important note to make here is that the values for the activation energy should be considered as purely phenomenological quantity without any physical significance[27]. The activation energies reported in this work are all negative, a result which is contrary to what was observed in the case of anion exchange[32]. In addition, for cation exchange, the resolution and the retention was increased with decreasing temperature, which was a trend that was exactly opposite from the one observed in anion exchange chromatography.

These important observations require more explanation to fully understand the meaning of the results. Exothermic processes decrease their rate as temperature is increased. The activation energy about these processes is usually negative. This phenomenon can be compared to cation exchange, as the increased temperature leads to decreased adsorption, and it has a negative activation energy as reported in Table 4.10 and 4.11. On the other hand, endothermic processes have an increased rate with increasing temperatures. In these processes the reported activation energies are usually positive. This is similar to the quantity of the activation energies reported earlier about anion exchange[32].

Ross and Subramanian[36] in their paper about the thermodynamics of protein associations report that for electrostatic interactions, the enthalpy of the process, is negative for van der Waals interactions and approximately zero for electrostatic interactions. The enthalpy is related to the activation energy reported in this work. This may imply that the adsorptive forces are van der Waals interactions between the adsorbent ligands and the sorbate, with the negative ligand polarizing the sorbate in order to adsorb it onto the surface. As polarization can be countered by molecular diffusion, at higher temperatures the diffusive forces counter the van der Waals forces, causing less adsorption. For the anion exchange case, Ross and Subramanian[36] discuss proton release as having positive enthalpy. In that case the negative sorbate releases protons to the adsorbent ligand, causing it to bind more strongly than van der Waals polarization. Even with increased molecular diffusion, at elevated temperatures more protons will be released which will contribute to even higher adsorption.

The comprehensive model for chromatography, combined with the Fast Fourier Transform (FFT) solution method proved to be a great analytical tool for investigating the temperature effects in cation-exchange chromatography. From the pH and temperature trends, significant insight into the separation behavior was obtained. This information will prove useful in designing and improving ion-exchange chro-

matographic separations, especially in selecting the operating conditions that are optimal for the separation.

As displayed in Table 4.10 and 4.11, the activation energy increases with more acidic pH. This is due to the stronger adsorptivity of the solute onto the packing as the solute is more charged. Note that the value of the activation energies is negative, meaning that the process favors lower temperatures to increase the adsorption. This is quite significant, since this means that better selectivity can be achieved at lower temperature in this system.

4.6 Conclusion

A link between the pH, temperature and the adsorption equilibrium constant of amino acids and proteins is presented. A detailed mechanistic model was used to analyze the data and take into account all the physical phenomena. The retention time of the proteins increased with decreasing temperature and pH, leading to better selectivity. The retention trends for pH and temperature in cation exchange chromatography are elucidating an important separation trend. This can be used with the mechanistic model in a predictive manner to improve chromatographic separations.

pH	0.1M citric acid monohydrate	0.1M trisodium citrate dihydrate
3.0	820mL	180mL
3.6	685mL	315mL
4.2	540mL	460mL

Table 4.1: Sodium Citrate-Citric Acid mixing tables to create 1L of buffer solution [52]

pH	Temperature	K_A	k_{ads}
3.0	5°C	1.953	150.8
	23°C	1.913	145.6
	40°C	1.757	140.2
3.6	5°C	0.5259	89.69
	23°C	0.5120	89.56
	40°C	0.4840	89.01
4.2	5°C	0.2548	32.88
	23°C	0.2417	32.78
	40°C	0.2352	31.65

Table 4.2: Data obtained by nonlinear curve fitting for the tyrosine chromatograms

pH	Temperature	K_A	k_{ads}
3.0	5°C	7.487	265100
	23°C	6.275	146010
	40°C	5.393	105050
3.6	5°C	1.798	108900
	23°C	1.550	52610
	40°C	1.322	28241
4.2	5°C	0.6473	1970
	23°C	0.5828	1833
	40°C	0.5129	1632

Table 4.3: Data obtained by nonlinear curve fitting for the tryptophan chromatograms

pH	Temperature	K_A	k_{ads}
3.0	5°C	0.829	310.7
	23°C	0.738	374.2
	40°C	0.634	481.0
3.6	5°C	0.485	48.54
	23°C	0.473	500.0
	40°C	0.466	1370.7

Table 4.4: Data obtained by nonlinear curve fitting for the Immunoglobulin G chromatograms

pH	Temperature	K_A	k_{ads}
3.0	5°C	5.654	2.928
	23°C	4.616	0.499
	40°C	3.659	0.232
3.6	5°C	1.064	0.053
	23°C	1.042	0.055
	40°C	1.023	0.045
4.2	5°C	0.302	0.0064
	23°C	0.419	0.0476
	40°C	0.432	0.0228

Table 4.5: Data obtained by nonlinear curve fitting for the Lysozyme chromatograms

pH	Temperature	k'_{Tyr}	k'_{Trp}
3.0	5°C	3.912	11.98
	23°C	3.888	10.25
	40°C	3.634	8.967
3.6	5°C	1.830	3.645
	23°C	1.803	3.300
	40°C	1.782	2.988
4.2	5°C	1.409	1.993
	23°C	1.394	1.897
	40°C	1.376	1.815

Table 4.6: Retention Factors for Tyrosine and Tryptophan for all experimental conditions studied

pH	Temperature	k'_{IgG}	k'_{Lys}
3.0	5°C	1.895	9.876
	23°C	1.752	8.238
	40°C	1.272	6.730
3.6	5°C	1.353	2.636
	23°C	1.333	2.606
	40°C	1.323	2.572

Table 4.7: Retention Factors for Immunoglobulin G and lysozyme for all experimental conditions studied

pH	Temperature	$S_{Tyr/Trp}$
3.0	5°C	3.83
	23°C	3.28
	40°C	3.07
3.6	5°C	3.42
	23°C	3.03
	40°C	2.73
4.2	5°C	2.54
	23°C	2.41
	40°C	2.18

Table 4.8: Separation factor between tyrosine and tryptophan for the experimental conditions considered in this study

pH	Temperature	$S_{Lys/IgG}$
3.0	5°C	6.82
	23°C	6.26
	40°C	5.78
3.6	5°C	2.19
	23°C	2.21
	40°C	2.19

Table 4.9: Separation factor between lysozyme and IgG for the experimental conditions considered in this study

pH	Tryptophan	Tyrosine
3.0	-2.14	-6.79
3.6	-1.70	-6.34
4.2	-1.67	-4.79

Table 4.10: Activation energies in kJ/mol of tyrosine and tryptophan for the pH conditions investigated

pH	Immunoglobulin G	Lysozyme
3.0	-5.53	-8.96
3.6	-0.81	-0.80

Table 4.11: Activation energies in kJ/mol of Immunoglobulin G and lysozyme for the pH conditions investigated

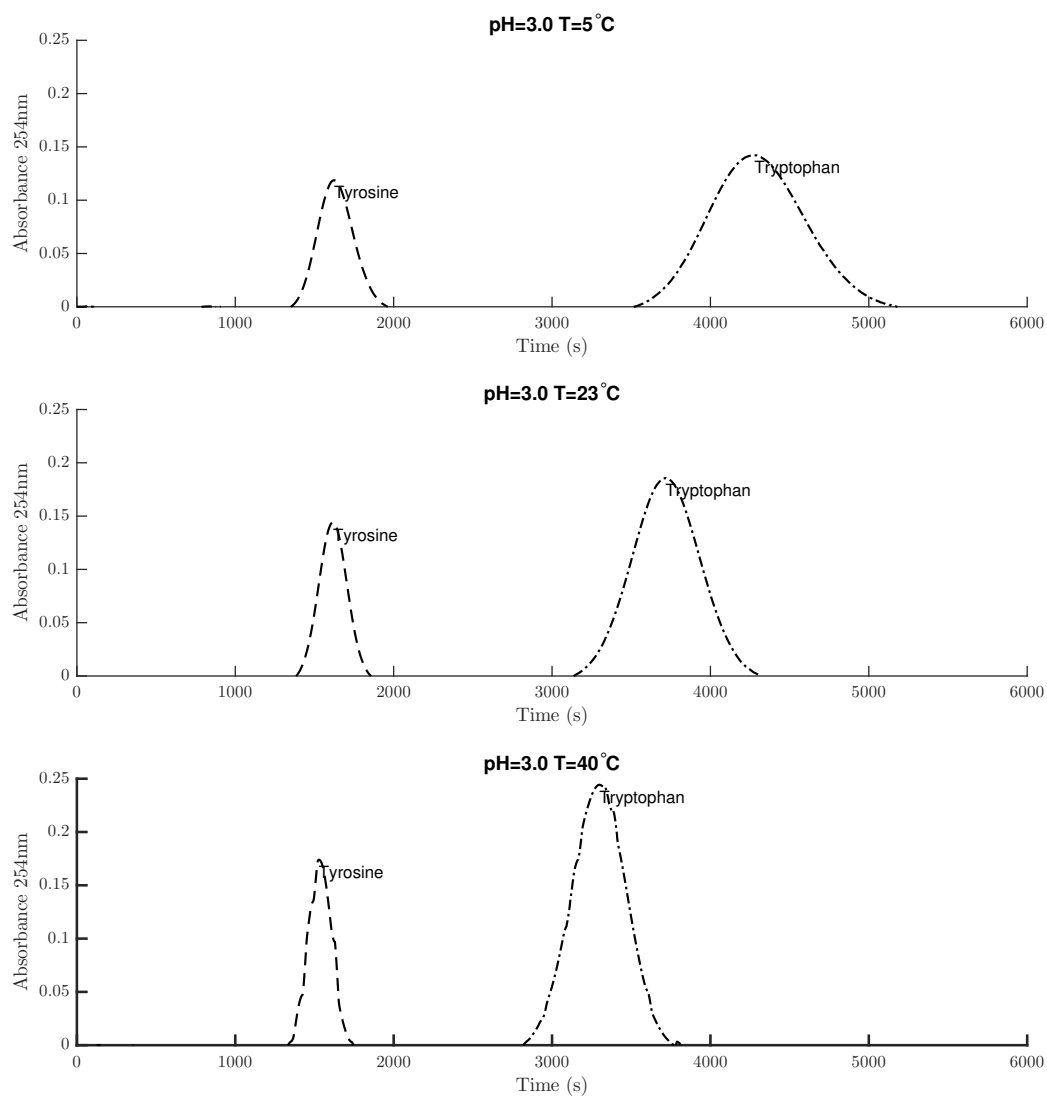


Figure 4.1: Tyrosine and Tryptophan chromatograms at a pH of 3.0 at 5°C, 23°C and 40°C at a flow rate of 5ml/min.

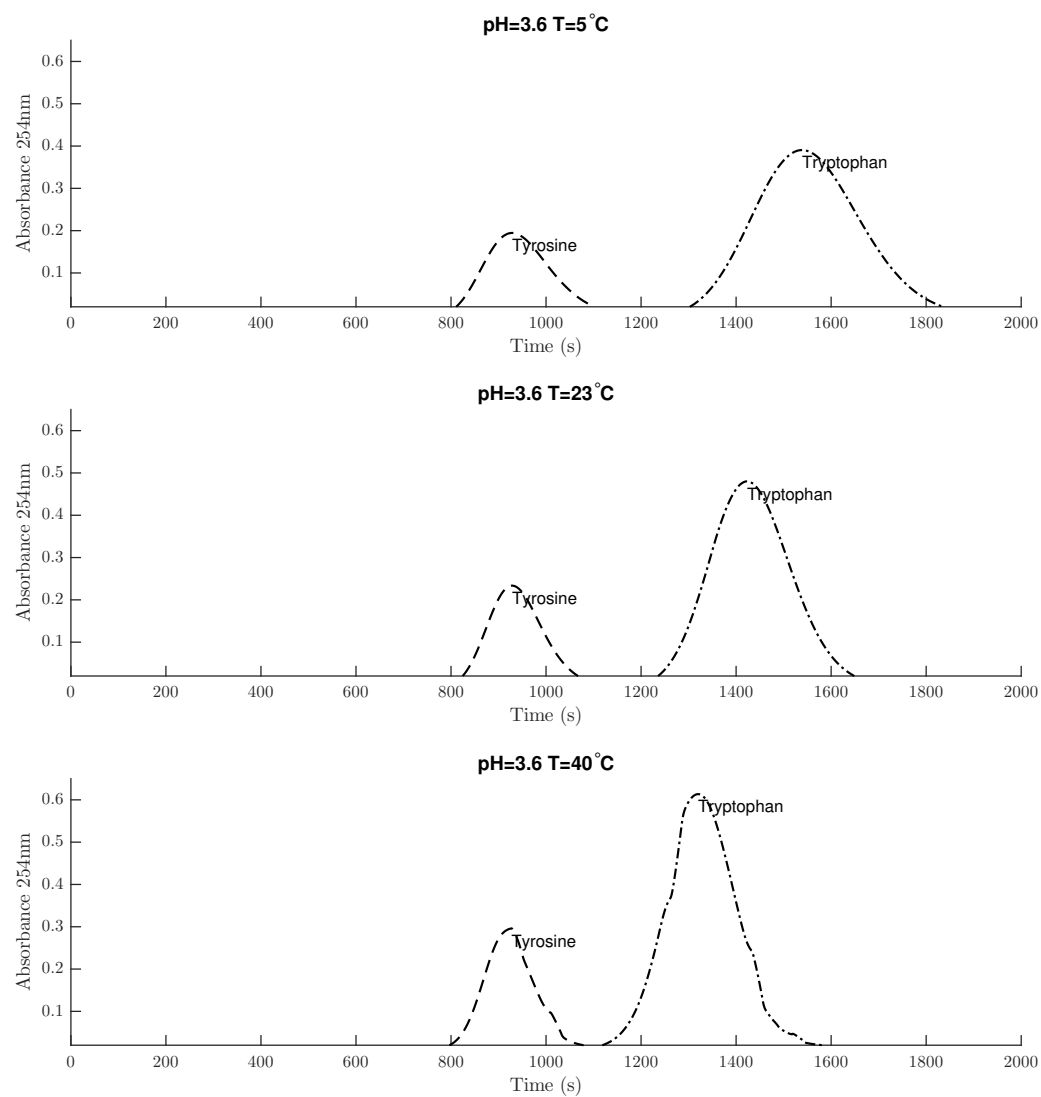


Figure 4.2: Tyrosine and Tryptophan chromatograms at a pH of 3.6 at 5°C, 23°C and 40°C at a flow rate of 5ml/min.

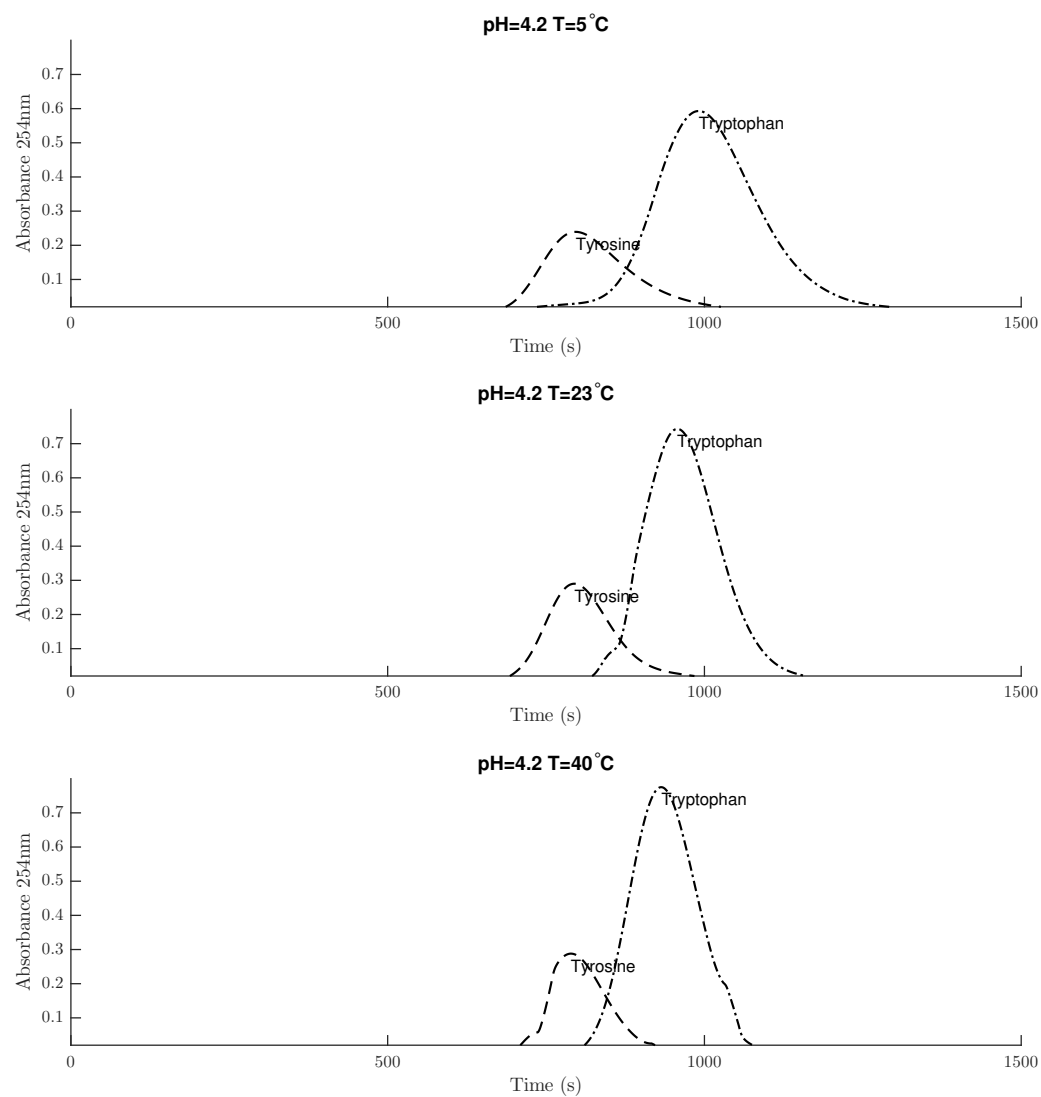


Figure 4.3: Tyrosine and Tryptophan chromatograms at a pH of 4.2 at 5°C, 23°C and 40°C at a flow rate of 5ml/min.

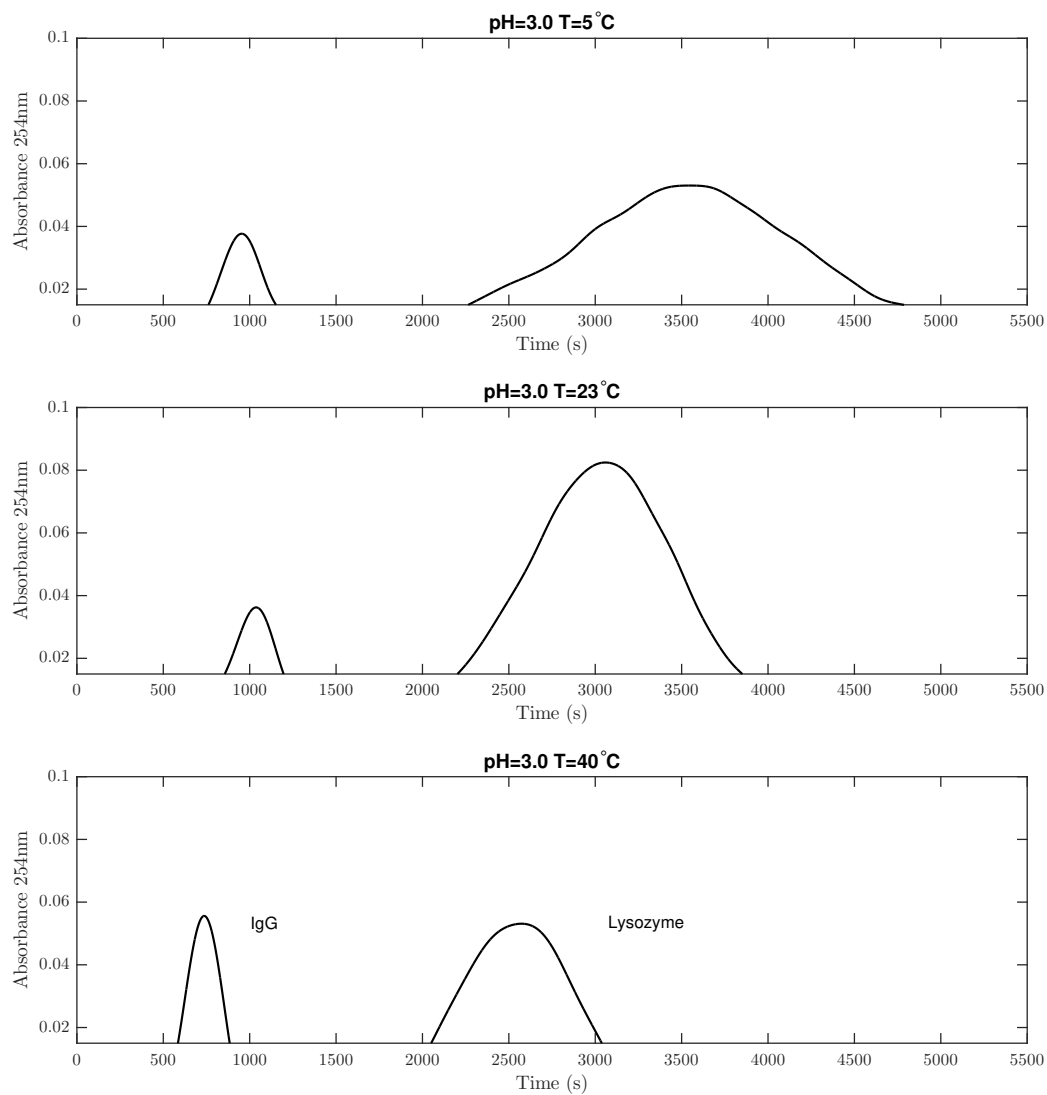


Figure 4.4: Immunoglobulin G and Lysozyme chromatograms at a pH of 3.0 at 5°C, 23°C and 40°C at a flow rate of 5ml/min.

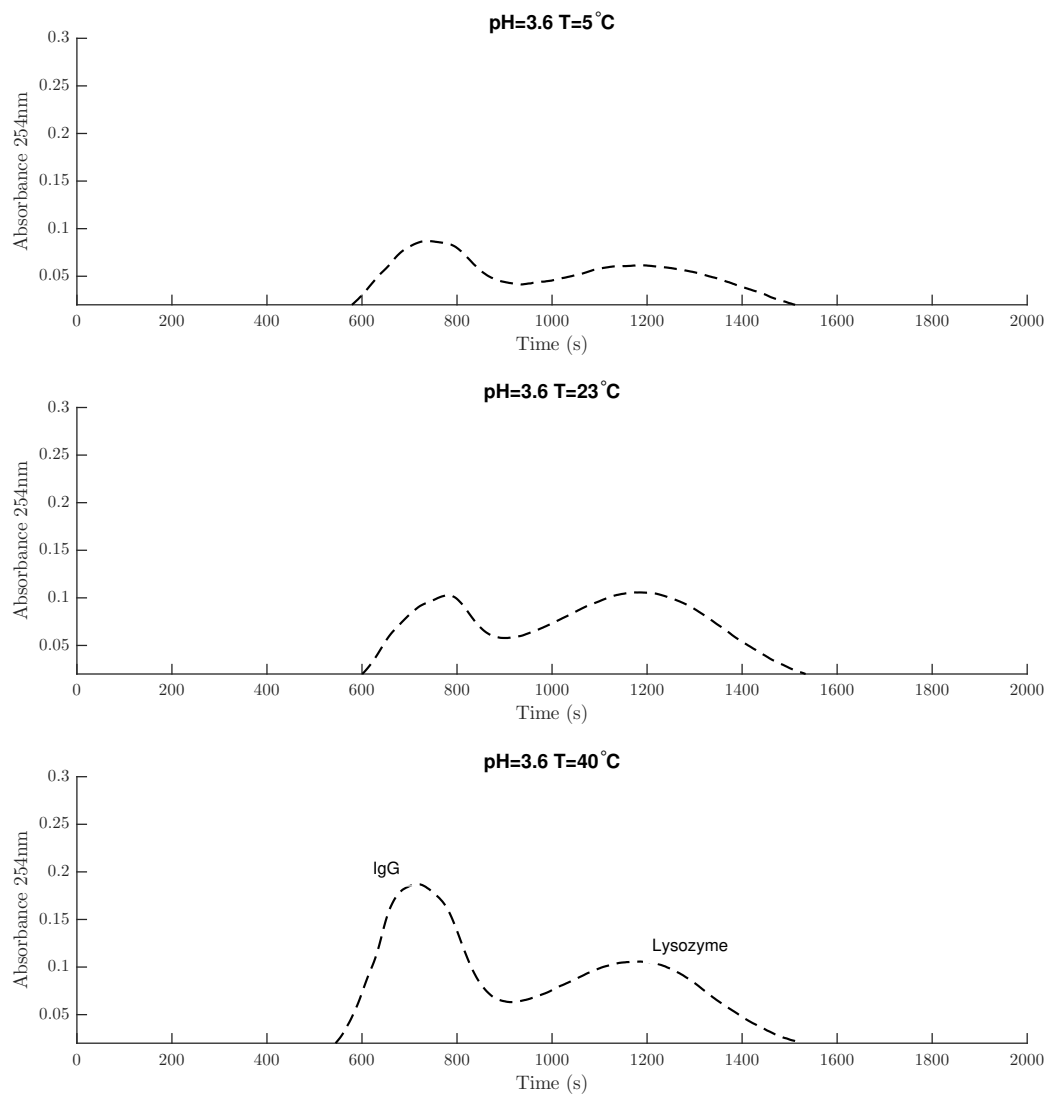


Figure 4.5: Immunoglobulin G and Lysozyme chromatograms at a pH of 3.6 at 5°C, 23°C and 40°C at a flow rate of 5ml/min.

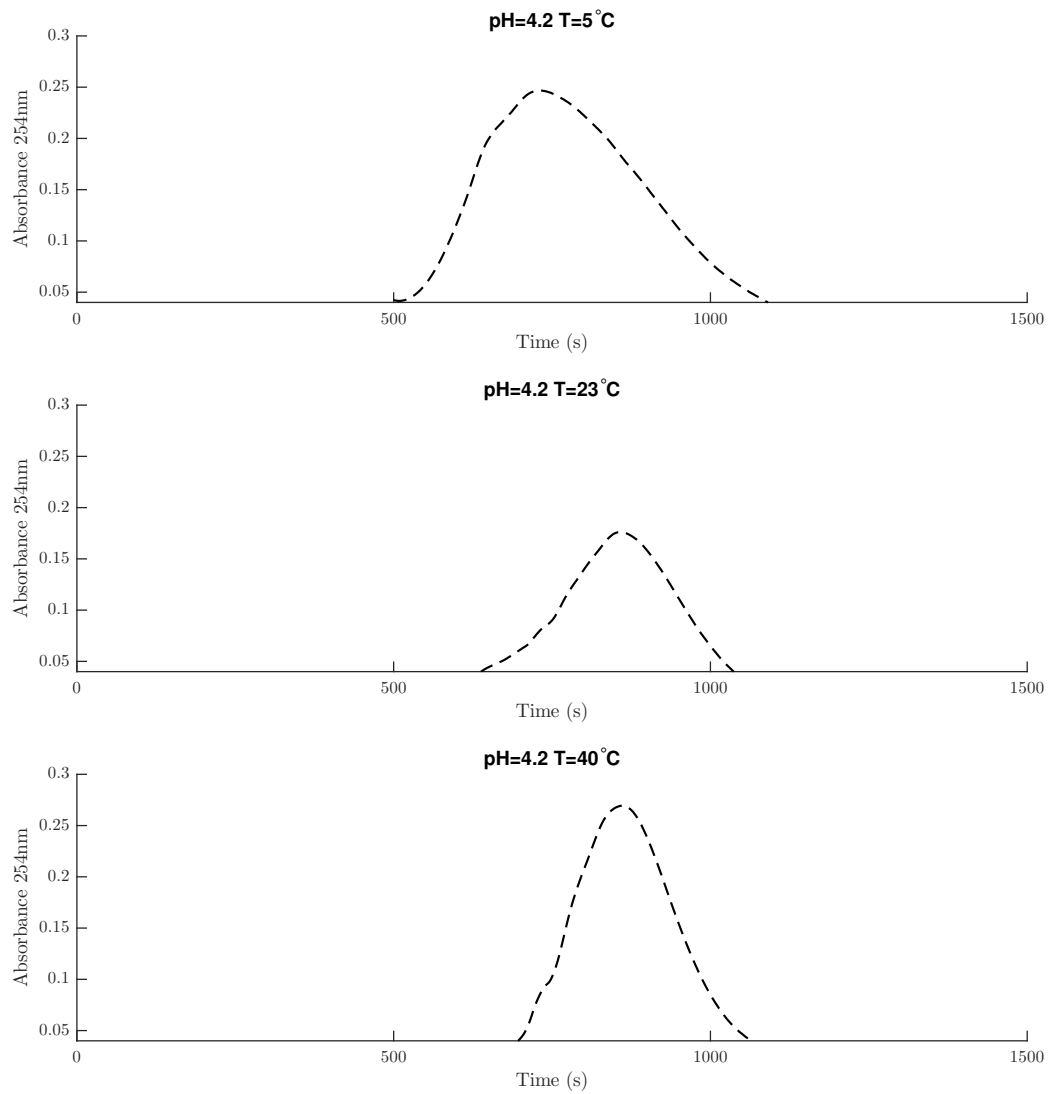


Figure 4.6: Immunoglobulin G and Lysozyme chromatograms at a pH of 4.2 at 5°C, 23°C and 40°C at a flow rate of 5ml/min. In these figures both proteins eluted as a single peak.

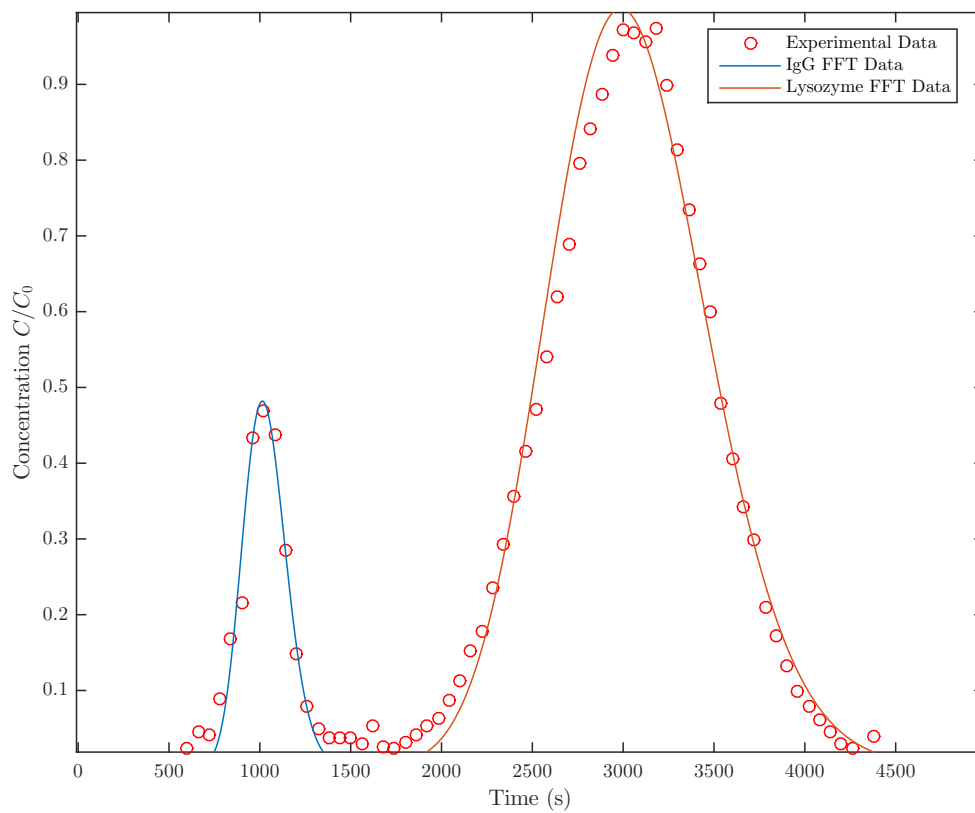


Figure 4.7: Immunoglobulin G and Lysozyme chromatogram at a pH=3.0 and temperature of 23°C with their respective FFT Simulation Data

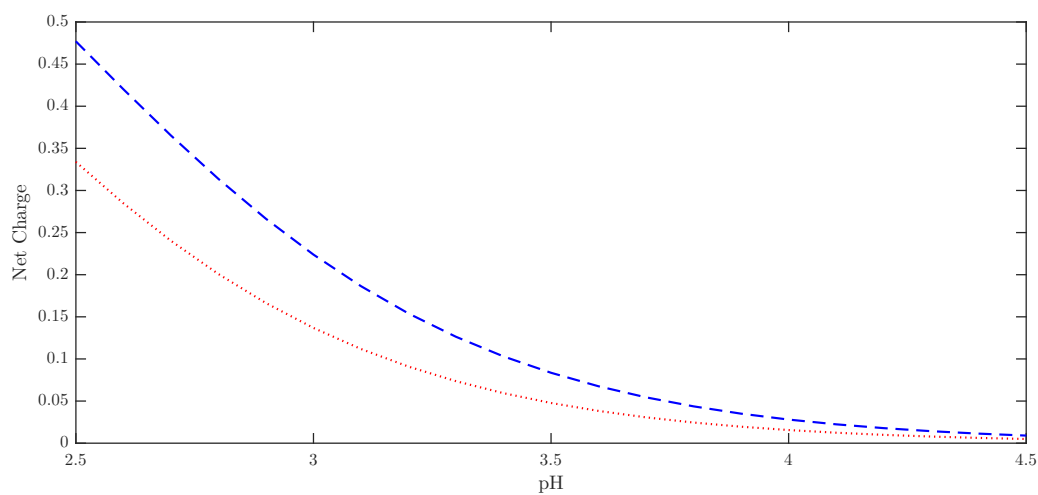
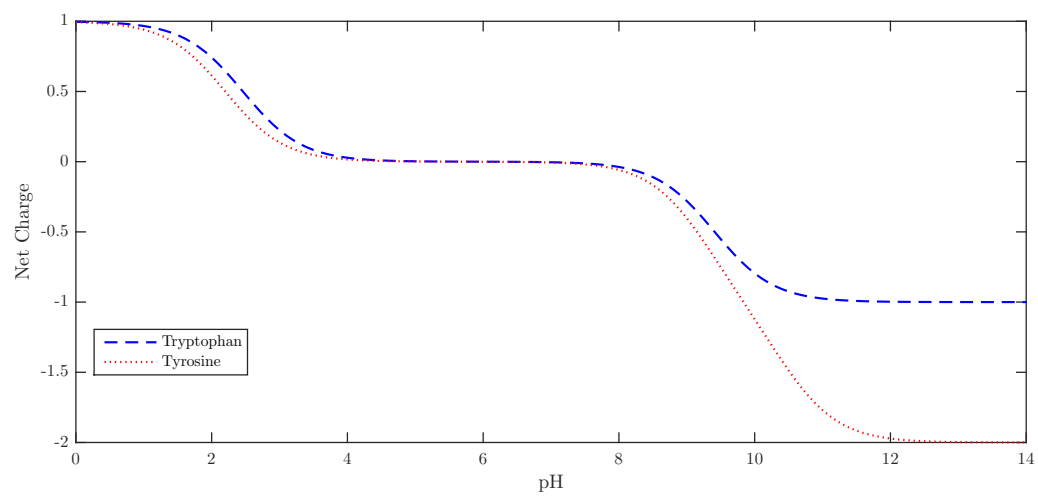


Figure 4.8: Titration curves of both tyrosine and tryptophan, including the pH range of interest

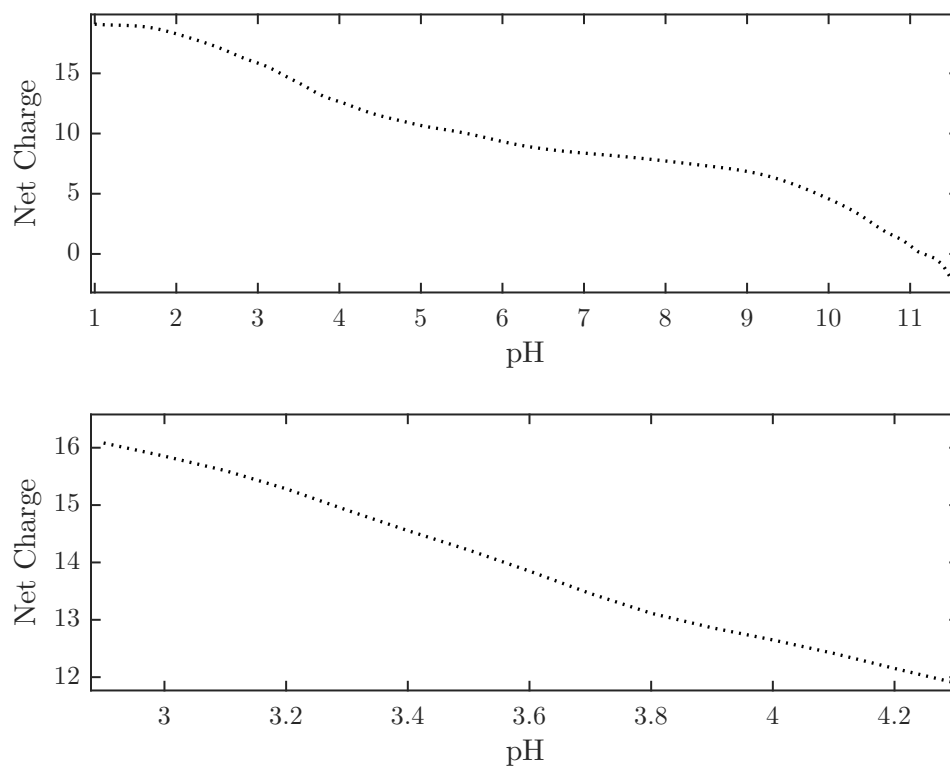


Figure 4.9: Titration curve of Lysozyme along with the pH range of interest [45]

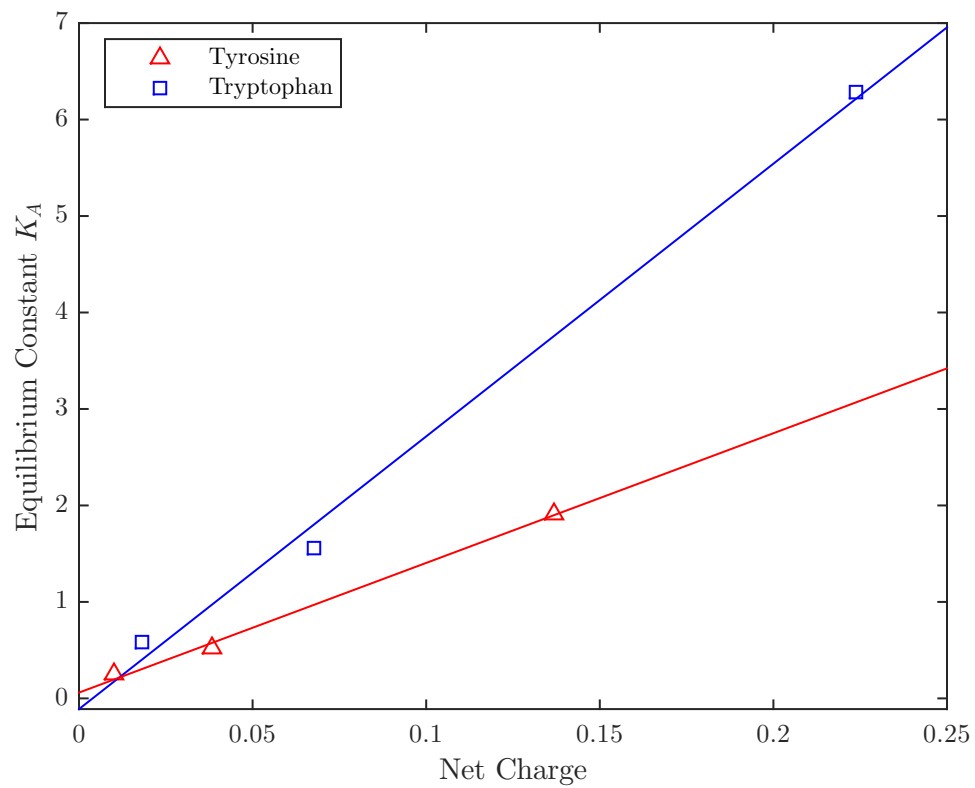


Figure 4.10: Correlation between the net charge and the equilibrium constant of tyrosine and tryptophan at 23°C

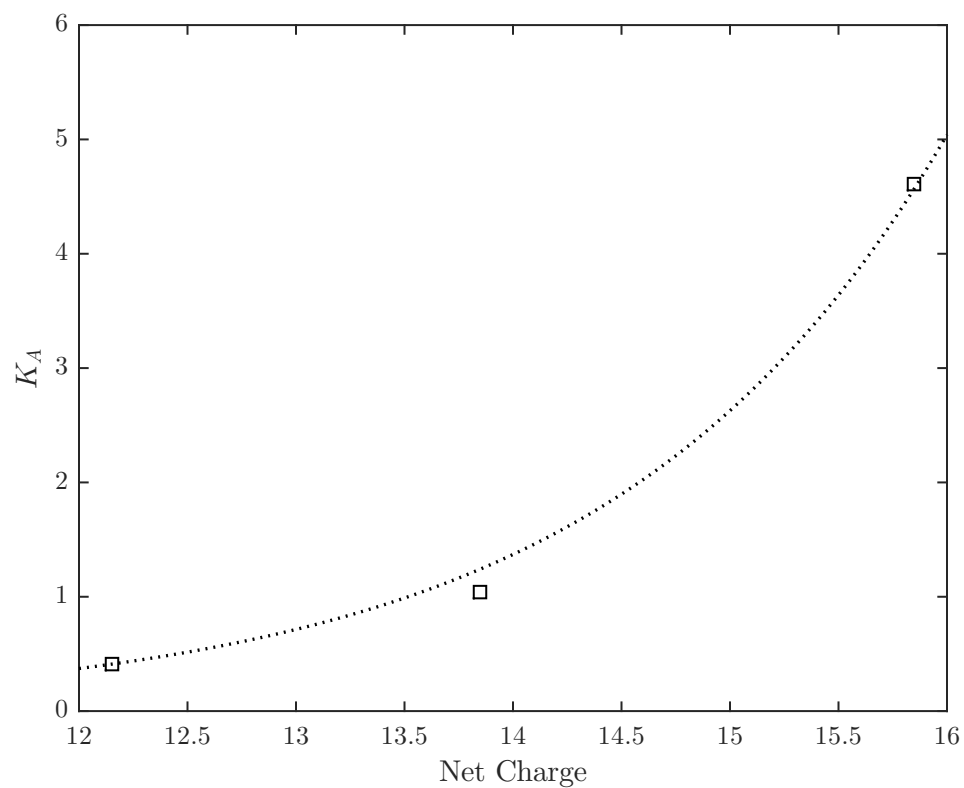


Figure 4.11: Adsorption Equilibrium constants correlated as a function of net charge of Lysozyme for 23°C

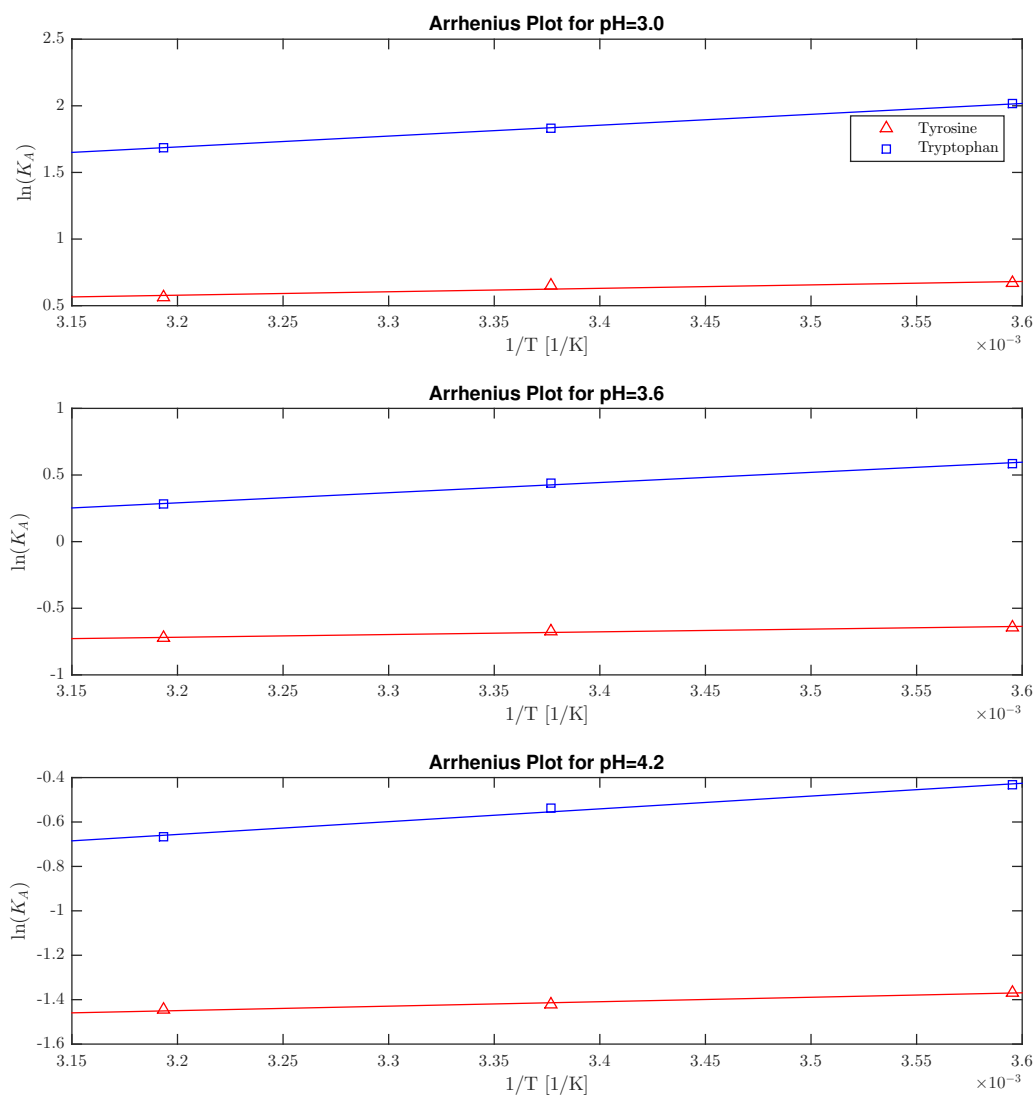


Figure 4.12: Arrhenius plots of the adsorption equilibrium constant as a function of temperature for Tyrosine and Tryptophan

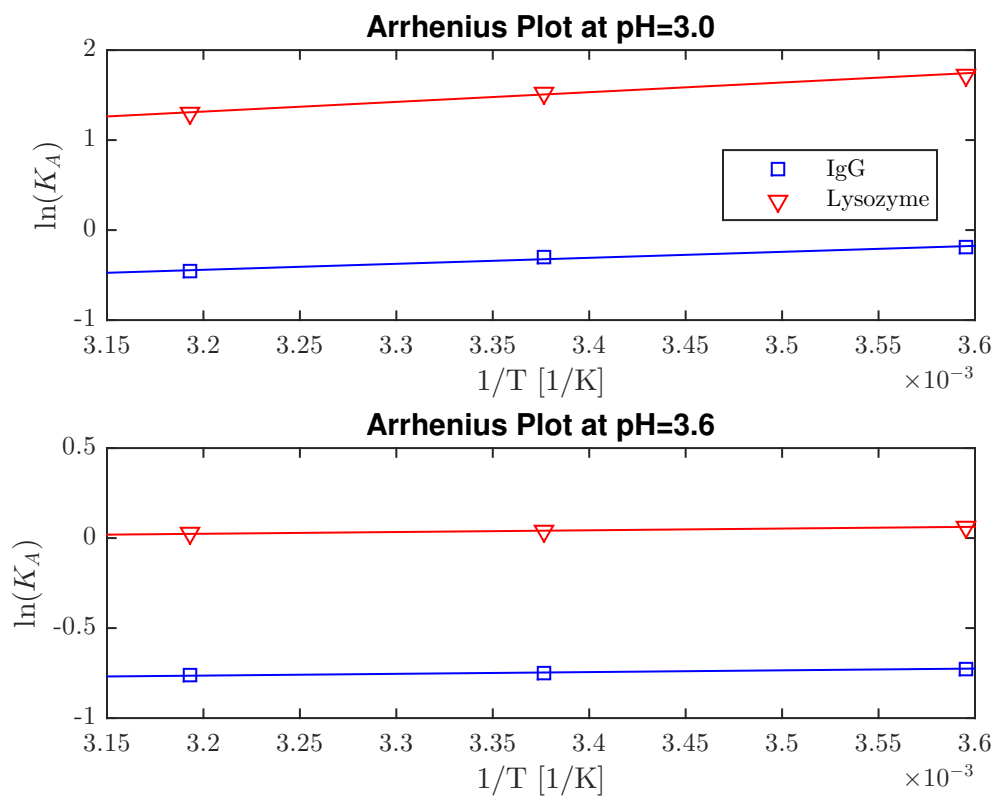


Figure 4.13: Arrhenius plots of the adsorption equilibrium constant as a function of temperature for Immunoglobulin G and lysozyme

Chapter 5

Modelling the Effect of Temperature on the Gel-Filtration

Chromatographic Protein Separation

A mechanistic model for chromatography was taken and the solution to its Laplace transfer function was obtained using the Fast Fourier Transform method. Using previously developed correlations for modelling diffusion, both in solution and intra-particle, and estimating the mass transfer coefficient, the effect of temperature in gel filtration liquid chromatography was investigated. The effect of each individual parameter on the elution curve was systematically explored allowing for reasonable estimates for the different temperature cases. In this case, a system of bovine serum albumin and phenylalanine separated by gel filtration chromatography was simulated to demonstrate how the resolution and the selectivity of the separation will change with physical parameters. Decreasing the particle size and flow rate while increasing the temperature led to higher resolution, which is consistent with experimental literature data.

5.1 Introduction

The production of biologics has actively employed the use of chromatography to separate the desired from the undesired fermentation products. Purification is one of the major costs associated with protein manufacture and its optimization is of crucial importance to the bioprocessing industry. Detailed mathematical models have been developed to characterize the behavior of the chromatographic system, however the effect of low temperature has rarely been investigated.

There is some data on the chromatographic processes that take place in higher than ambient temperatures. Varied results have been reported with different compounds, however they have not employed detailed mechanistic models to investigate the fundamental effects [15, 48] . This paper presents a model that accurately accounts for the temperature effects on physical parameters and uses it in a predictive manner to describe the column operation. Several aspects of the temperature effect were considered to understand the influence of temperature. The diffusion of the solute, both in the solvent and inside the adsorbing particles had the greatest effect on the chromatogram peak shape, retention time and resolution of the species. Other effects that play a role in chromatography are dispersion and the mass transfer coefficient, both of which vary with temperature as well as flow rate.

Several methods and correlations have been reported [9] that have used different parameters to characterize the diffusion behavior of solutes. For protein chromatography, correlations that employ the protein's molecular weight [54] were considered. Another important consideration in this system is the intraparticle diffusivity, which is estimated using the correlation by Boyer and Hsu [2] . The mass transfer coefficient was estimated using three separate correlations, one employed by Schneider and Smith [39] for a forced convection around a sphere, which is analogous to the heat transfer expression. The other method was the Wilson-Geankoplis [51] expression, and the one for protein adsorption is the one presented by Liapis [25]. For dispersion

occurring inside the bed, the Chung and Wen [5] correlation was computed. These equations give reasonable estimates of the trends of their respective parameters which are then computed in order to see the pulse response of the column.

Computing the model was accomplished by implementing the Fast Fourier Transform (FFT) technique, first introduced by Cooley and Tukey [6] for computation of the Fourier integral. The Fourier integral computation can be used in order to numerically invert Laplace transforms, as demonstrated by Hsu for chromatographic systems [20] and Hsu and Dranoff [19] for adsorption related systems. The FFT technique requires a very short computation time compared to the finite Fourier transform computation. The FFT method has been demonstrated to be computationally superior, even to the direct evaluation of the time-domain solution as in some cases the evaluation of the oscillatory integrand converges very slowly [19, 34]. Obtaining the time domain solution is very important in investigating the performance of the column when compared to the moments method introduced by Schneider and Smith [39] .

This study aims to study the effect of diffusion, dispersion and mass transfer coefficient on the chromatograms in gel filtration chromatography. After computing the elution curves, they were analyzed in order to investigate how the peaks are affected by fundamental mass transfer phenomena. These insights were taken into account to model and analyze the best way of chromatographic separation at low temperatures. Results were obtained for a model system of bovine serum albumin and phenylalanine and their subsequent resolutions at different superficial velocities, temperatures and gel particle radii.

5.2 Theory

5.2.1 Model Development

Hsu and Boyer[2] used a model for an axially dispersed liquid flow with external film diffusion and intraparticle diffusion. The model is for an isothermal chromatographic column packed with spherical particles. The protein adsorption on unsubstituted agarose matrices is negligible, so there is no adsorption accounted for in this model.

For the mobile phase

$$\frac{\partial C}{\partial t} + V \frac{\partial C}{\partial z} - D_L \frac{\partial^2 C}{\partial z^2} = -\frac{3k_f}{mR} (C - C_p|_{r=R}) \quad (5.1)$$

Intraparticle mass balance

$$\epsilon_p \frac{\partial C_p}{\partial t} = D_e \left(\frac{\partial^2 C_p}{\partial r^2} + \frac{2}{r} \frac{\partial C_p}{\partial r} \right) \quad (5.2)$$

The initial and boundary conditions

$$C(z, 0) = 0 \quad (5.3)$$

$$C(0, t) = \begin{cases} C_0, & 0 \leq t \leq t_0 \\ 0, & t_0 < t \end{cases} \quad (5.4)$$

$$C(\infty, t) = 0 \quad (5.5)$$

$$C_p(r, z, 0) = 0 \quad (5.6)$$

$$C_p(0, z, t) \neq \infty \quad (5.7)$$

$$k_f(C - C_p|_{r=R}) = D_e \left. \frac{\partial C_p}{\partial r} \right|_{r=R} \quad (5.8)$$

The variables introduced are : C - solute concentration in mobile phase, C_p - solute concentration in the pores, C_s - solute concentration on solid, C_0 - initial pulse concentration, V - mobile phase velocity, D_L - axial dispersion coefficient, $m = \epsilon/(1 - \epsilon)$, ϵ - column void fraction, ϵ_p - particle porosity, q - concentration in particles, D_e - intraparticle diffusivity, k_f - external mass transfer coefficient, t - time, z - axial position, r - intraparticle radial position, R - radius of the bead.

A solution can be obtained by inverting the equations into the Laplace domain. The result is:

$$\bar{C}(z, s) = C_0 \exp \left[\left(\frac{V}{2D_L} - \sqrt{\frac{V^2}{4D_L^2} + \frac{s}{D_L} + \frac{3k_f}{mD_LR} \alpha(s)} \right) z \right] \quad (5.9)$$

$$\alpha(s) = \frac{\sqrt{\frac{\epsilon_p s}{D_e}} \cosh \sqrt{\frac{\epsilon_p s}{D_e}} R - \frac{1}{R} \sinh \sqrt{\frac{\epsilon_p s}{D_e}} R}{\sqrt{\frac{\epsilon_p s}{D_e}} \cosh \sqrt{\frac{\epsilon_p s}{D_e}} + \left(\frac{k_f}{D_e} - \frac{1}{R} \right) \sinh \sqrt{\frac{\epsilon_p s}{D_e}} R} \quad (5.10)$$

5.2.2 Computational Method

The inversion of this transfer function was then computed using MATLAB and the built-in IFFT function. The frequency spectrum of this function is symmetrical, it was specified in the function which aids the algorithm and decreases computation time. The formula utilized by MATLAB is:

$$\bar{f}(t) = f(n \Delta T) = \frac{N}{2T} \left[\left(\frac{1}{N} \right) \sum_{k=1}^N F \left(\frac{i(k-1)\pi}{T} \right) \exp \left(i \frac{2\pi(n-1)(k-1)}{N} \right) \right] \quad (5.11)$$

$$n = 1, 2 \dots N$$

Inverting the transfer function was accomplished on a Dell Optiplex 790 with an Intel i7-2600 CPU with 8.00 GB of RAM using MATLAB version R2015a. Simulating one elution curve with the FFT method requires 0.1019 seconds with 1024 digital numbers. Other inversion methods [8] requires 21.7594 seconds. The computation performance makes the FFT method superior in obtaining rapid and precise results.

5.2.3 Adapting the model as a function of temperature

Temperature effects were investigated in a way where the physical parameters were correlated to characterize all of the physical parameters associated with the mass transfer occurring inside the column, as well as fundamental properties such as diffusion of the solute. The trends that those correlations exhibited with decreasing temperature on the chromatograms were analyzed.

The viscosity and density of water are estimated based on the physical properties for water between the range of 273K and 350K based on data taken from NIST [7]. Axial dispersion was estimated by a correlation by Chung and Wen [5].

$$D_L = \frac{2\epsilon RV}{0.2 + 0.011\text{Re}_P^{0.48}} \quad (5.12)$$

where

$$\text{Re}_P = \frac{2R\epsilon V\rho}{\mu} \quad (5.13)$$

For the protein solution diffusivity, the correlation by Young [54] was considered:

$$D_0 = 8.34 \times 10^{-10} \left(\frac{T}{\mu M_W^{\frac{1}{3}}} \right) \quad (5.14)$$

which is introduced in the Boyer and Hsu [2] correlation for intraparticle diffusivity:

$$D_e = 8.34 \times 10^{-10} \left(\frac{T}{\mu M_W^{\frac{1}{3}}} \right) \exp \left[-0.1307 \left(M_W^{\frac{1}{3}} + 12.45 \right) c_f^{\frac{1}{2}} \right] \quad (5.15)$$

The mass transfer coefficient given by Liapis [9] for protein mass transfer coefficient is:

$$\frac{2k_f R}{D_0} = 2 + 0.51 \left(\frac{E^{\frac{1}{3}} (2R)^{\frac{4}{3}} \rho}{\mu} \right)^{0.60} \text{Sc}^{\frac{1}{3}} \quad (5.16)$$

E is the energy dissipation rate

$$E = \frac{25(1 - \epsilon) \epsilon^2 C_{D0} V^3}{R} \quad (5.17)$$

C_{D0} is the drag coefficient for a particle which is given by Stokes Law as $C_{D0} = 24/\text{Re}$ and the Schmidt number as $\text{Sc} = \mu/\rho D_0$. Other variables that were not previously defined include: M_W – molecular weight, c_f – concentration of the gel, μ – viscosity, ρ – density, T – temperature. As for the intraparticle void fraction ϵ_p an estimate is made using a correlation presented in Boyer and Hsu[2], based on data given by GE Healthcare (Uppsala, Sweden) and reproduced below[42].

$$\epsilon_p = -0.1 \log(M_W) + 1.6835 \quad (5.18)$$

5.3 Parametric considerations

In the discussion that follows, the following parameters were used. $L = 100\text{cm}$, $V = 0.01\text{cm}^3/\text{s}$, $R = 0.0045\text{cm}$, $\epsilon = 0.34$, $\epsilon_p = 0.550$, $M_W = 66000\text{g/mol}$ for bovine serum albumin (BSA), $c_f = 0.06\text{g/cm}^3$ and $c_0 = 1\text{mg/cm}^3$. The effect of decreasing temperature is evident as the solute diffusivity drastically decreases in when the solute is inside the adsorbent particle. For large proteins that have low bulk diffusion, they will tend not to diffuse inside the adsorbent particle at the same rate as smaller proteins,

so larger proteins will tend to bypass the adsorbent particle and elute out faster than the smaller proteins. This retains the smaller proteins longer inside the adsorbent particle.

Dispersion also plays a role in the model. Controlling the solute dispersed into the column is important to decrease peak tailing. In Figure 5.1 the mass transfer coefficient k_f is kept constant and the dispersion is allowed to vary. The dispersion at lower temperatures leads to longer peak tailing than the higher temperature.

The mass transfer coefficient is the driving force of the solute entering the adsorbent particle. When dispersion is fixed, the peaks reach a slightly lower height at lower temperature. The peaks that demonstrate the behavior are displayed in Figure 5.2.

As is the case of gel filtration chromatography, the larger molecules elute first, and the molecules with smaller molecular weight elute last. Three model molecules were selected: blue dextran, bovine serum albumin and phenylalanine. Each have a molecular weight of 2×10^6 g/mol, 66000g/mol and 165g/mol respectively. Phenylalanine represents a small amino acid, which will completely enter the adsorbent particle pores, and albumin, which is a moderately sized protein and a common model protein which will partially enter the gel particle. Blue dextran is also added to this analysis as a void volume marker and is not expected to enter the particle due to the large size.

The adsorbent that will be used in the simulation is Sepharose CL-6B which is a 6% cross linked agarose gel. The fractionation range is 1,000-4,000,000 for globular proteins and the particle size ranges from $45\mu\text{m}$ - $165\mu\text{m}$. The intraparticle void fraction in this gel will vary relative to the molecular weight of the protein and is modeled with Equation 5.18. The normal operating temperature of the gel is 4°C to 40°C and the analysis is focused within that temperature range.

The particle size distribution of $45\mu\text{m}$ - $165\mu\text{m}$. Boyer and Hsu [2] report that the

gel has four major fractions of particle radius, ranging from $26.6\mu\text{m}$ to $70.9\mu\text{m}$, with an average particle radius of the unfractionated gel of $46.0\mu\text{m}$. In the simulation, only uniform particle radius can be entered, therefore values of $25\mu\text{m}$, $45\mu\text{m}$, and $70\mu\text{m}$ were selected to cover the possible elution outcomes.

Flow rate is also a very important factor in gel filtration. GE Healthcare [42] reports that at increasing flowrates, the resolution of the separation decreases. Flow rates of 0.1cm/s , 0.05cm/s and 0.01cm/s were taken that are within a realistic range for a liquid chromatography system. This will also allow enough residence time for the solutes to diffuse in and out of the adsorbent so that the effects of temperature can be observed from the simulation.

5.4 Data Analysis

For each of the three components used in the simulations, three different simulations for each molecule will be performed individually, and they will be plotted on the same graph to represent the chromatogram. In addition, the elution of each component at 4°C and 40°C will be directly compared on a separate graph so that the peak shape differences can be observed.

The effect of temperature on the separation was investigated using two key parameters. The first one is the resolution, which gives the degree of separation between the two protein peaks and the second one is the selectivity, which looks at the relative distance between the two peaks to determine their separation[44]. Resolution is evaluated:

$$R_s = \frac{t_{R_2} - t_{R_1}}{\frac{1}{2}(W_2 + W_1)} \quad (5.19)$$

The time difference here is between the retention times of the lagging peak t_{R_2} with the leading peak t_{R_1} . Values for W_1 and W_2 are the baseline peak width of the leading peak and the lagging peak, respectively. Selectivity is given by:

$$\beta = \frac{t_{R_2} - t_{R_0}}{t_{R_1} - t_{R_0}} \quad (5.20)$$

which is the ratio of the time difference of the lagging peak (t_{R_2}) with the tracer peak(t_{R_0}) and the difference of leading peak (t_{R_1}) with the tracer peak(t_{R_0}). The degree of separation between the two proteins can be quantified by applying the formula. The tracer peak, t_{R_0} is the blue dextran peak. The leading peak t_{R_2} in this case is the phenylalanine peak and the lagging peak t_{R_1} is bovine serum albumin (BSA).

5.5 Results

For the average particle radius of $45\mu\text{m}$, the results are displayed in Figure 5.3,5.4, and 5.5. The peaks become sharper at the elevated temperature, however the overall retention time does not change significantly. The peak shape of the dextran peak changes at different temperatures. The resolution and selectivity values are given in Table 5.1.

For the particle radius of $25\mu\text{m}$, the chromatograms are given in Figures 5.6, 5.7, and 5.8. Here, the peaks are sharper when compared to the previous results. The resolution and selectivity values are given in Table 5.2.

At the largest particle radius of $70\mu\text{m}$, the results are presented in Figure 5.9, 5.10, and 5.11. The chromatograms here had the largest width of any simulation in this study, therefore the reported values for resolution were lower than the other cases with smaller particle radius. The values resolution and selectivity are in Table 5.3.

The general trends are that the selectivity remains constant even with changing temperature, flow rate or particle radius. The resolution changes with temperature where higher resolution is observed at higher temperature and the resolution is also improved with more fine adsorbent particles. The peaks were quite sharp at the

smallest particle radius where the least peak spreading was observed. This trend is consistent with the experimental data in literature [42, 44]

5.6 Discussion

The results displayed give good insight in how temperature affects gel filtration chromatography. The model that was derived is quite comprehensive, and this analysis does not involve surface adsorption and chemical rate parameters. The diffusion, dispersion and mass transfer coefficient were varied to capture a significant amount of the physics of the process.

Looking into the resulting peaks in Figure 5.3 to 5.11, the phenylalanine and albumin were reasonably resolved. The phenylalanine, which is much smaller relative to the other solutes, has more of the intraparticle void space accessible, which increases the overall residence time within the column. Bovine serum albumin partially enters the intraparticle void space, therefore elutes faster in the column as it does not have the same amount of volume accessible as the phenylalanine. Decreasing particle size enables more volume for the retention of the smaller solutes. This becomes more favorable at higher temperature as solutes remain localized within a certain volume of the column, which is demonstrated by the minimized peak spreading and increase in resolution.

For blue dextran, which was used as a void volume marker, the residence time did not change significantly with temperature. The peak spreading was higher than the other two analytes which points at the fact that the physical phenomenon that governs the solute flow in the column is fundamentally different from either the BSA or phenylalanine. Blue dextran does not enter the adsorbent particle and bypasses the gel completely by convection, so the accessible intraparticle void volume does not play any role in its elution. Therefore the large molecules move by convection and

the smaller molecules are slowed down by as they diffuse inside the gel particles.

Even though the selectivity did not change significantly with either flow rate or particle radius, it is important to note that the accessible volume that the solute can diffuse in remained constant. That will not lead to significant changes in retention time, keeping the selectivity constant. This theoretical analysis for gel filtration proves that the selectivity will not be improved on significantly with changing physical parameters. This is due to the diffusivity and void volume that do not change to allow for a different retention of the molecule at the conditions that were considered.

Resolution is quite important in gel filtration as it is expected to decrease with increasing flow rate [42]. The data obtained from the simulation data follow that trend quite closely. Another important conclusion from the data is that at elevated temperatures there is less peak spreading, which leads to better peak resolution. In all cases investigated in this work, resolution at 40°C was higher than the one observed for 4°C. This finding is quite important as better resolution at higher flow rates by elevating the temperature may be obtained.

The fast Fourier Transform (FFT) method allowed quick computation of the elution curves to obtain a quantitative insight. FFT returns data on the chromatographic curve in the time-domain, while taking into consideration all of the parameters that are defined in the material balance based on partial differential equation model. The method of numerically inverting the Laplace transform of the model back into the time domain is a valuable analytic tool. The FFT enables a predictive solution of the elution curve by only considering the physical characteristics of the solute. The superiority of the FFT method lies in the fact that the protein chromatogram can be computed rapidly in the time domain, and figure out which conditions are most favorable for the separation. The FFT subroutine can also be applied to other systems involving adsorption as well as reactive systems[20], making for a very versatile tool for any chemical engineer.

5.7 Conclusions

A model for robust and dynamic modelling of gel filtration chromatography at different temperatures is presented. The parameters of the model that were considered ranged from implementing the density and the viscosity of the solvent, to estimating the dispersion and film mass transfer coefficient using suitable correlations. The model was solved using the Fast Fourier Transform technique which is a highly versatile and rapid way of computing a partial differential equation model.

In regards to the separation, the selectivity did not change with either temperature or flow rate, however, gains in resolution were observed at higher temperatures. The chromatograms at elevated temperatures were sharper and allowed for better resolution of the components. The best resolution is observed at the slowest flow rate with the highest temperature. A trade off can be established between the flow rate and the temperature to give good resolution between the components while minimizing elution time.

For the solute behavior inside the column, the data points to the fact that larger molecules bypass the gel packing and move by convection. The smaller molecules are slowed down by entering a defined volume of the intraparticle space and the resulting decrease in diffusivity. The amount of accessible volume is a function of the size of the molecule, which governs the retention time of the solute.

The simulations presented here exhibit all of the features commonly found in experimental data for gel filtration chromatography. The increase in resolution with decreasing flowrate is a trend that is observed both in this theoretical work and experimentally, and the long peak tailings of large molecules when injected in a gel filtration column. The model presented here can serve for accurate determination of the elution behavior for a gel filtration column and the FFT solution technique is quite important in providing rapid and useful results.

Velocity	0.01 cm/s		0.05 cm/s		0.1 cm/s	
Temperature	R_s	β	R_s	β	R_s	β
4°C	3.99	3.20	2.66	3.20	2.09	3.20
40°C	4.54	3.20	3.50	3.20	2.86	3.20

Table 5.1: Resolution and Selectivity values for the data at particle radius of $45\mu\text{m}$ at different superficial velocities for component 1 BSA and component 2 phenylalanine

Velocity	0.01 cm/s		0.05 cm/s		0.1 cm/s	
Temperature	R_s	β	R_s	β	R_s	β
4°C	5.83	3.20	4.29	3.20	3.47	3.20
40°C	6.40	3.20	5.29	3.20	4.58	3.20

Table 5.2: Resolution and Selectivity values for the data at particle radius of $25\mu\text{m}$ at different superficial velocities for component 1 BSA and component 2 phenylalanine

Velocity	0.01 cm/s		0.05 cm/s		0.1 cm/s	
Temperature	R_s	β	R_s	β	R_s	β
4°C	2.91	3.20	1.84	3.20	1.41	3.20
40°C	3.46	3.20	2.48	3.20	2.00	3.20

Table 5.3: Resolution and Selectivity values for the data at particle radius of $70\mu\text{m}$ at different superficial velocities for component 1 BSA and component 2 phenylalanine

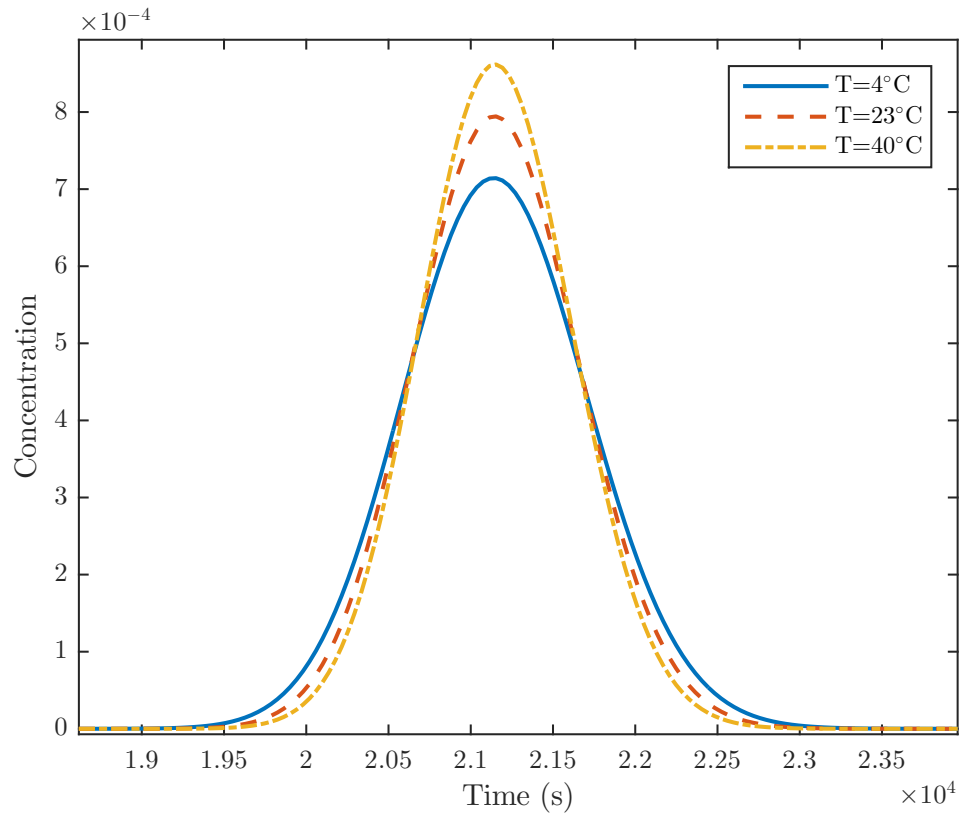


Figure 5.1: Elution curves for Bovine Serum Albumin at a fixed mass transfer coefficient ($k_f = 0.0015\text{cm/sec}$) and varying dispersion caused by temperature changes. Notice that the peak tailing increases as the temperature decreases.

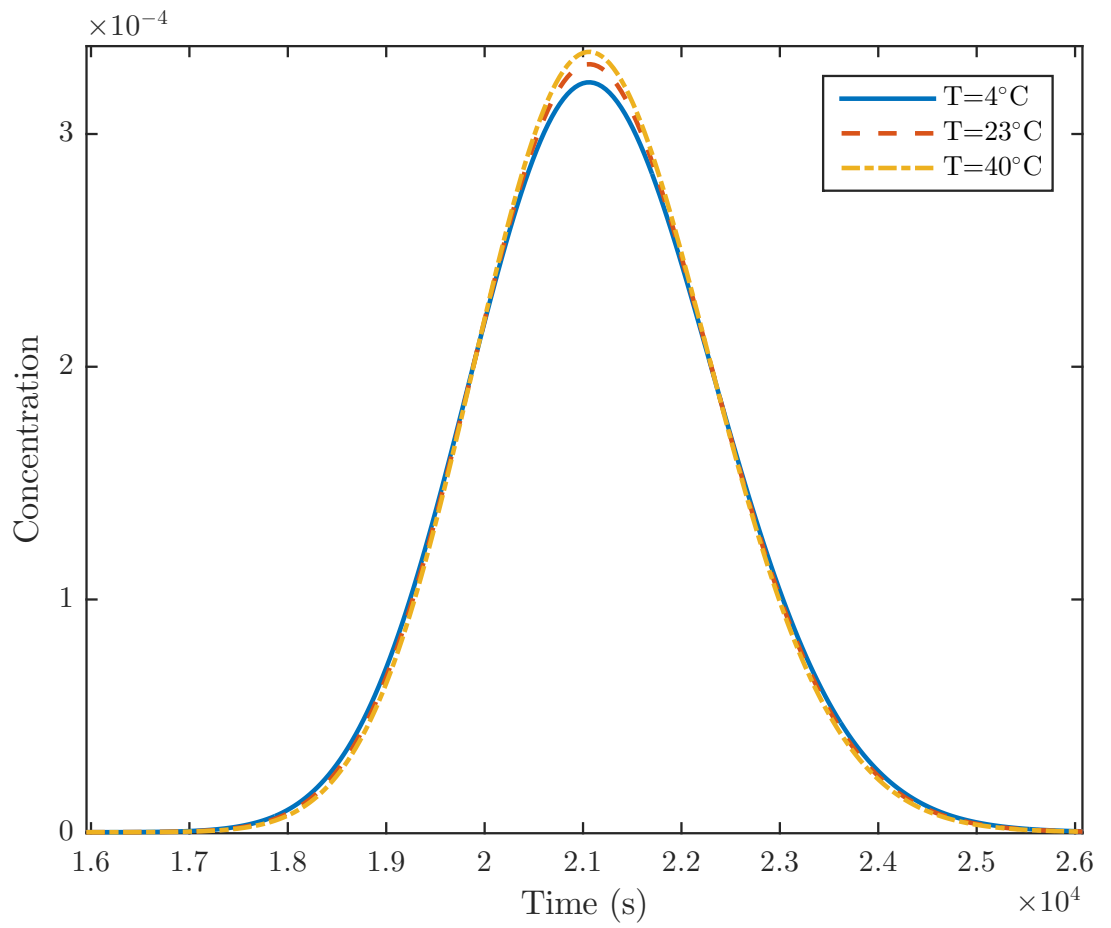


Figure 5.2: Effect of the mass transfer coefficient at different temperatures at fixed dispersion ($D_L = 0.0015\text{cm}^2/\text{sec}$). The peak height decreases slightly at lower temperatures.

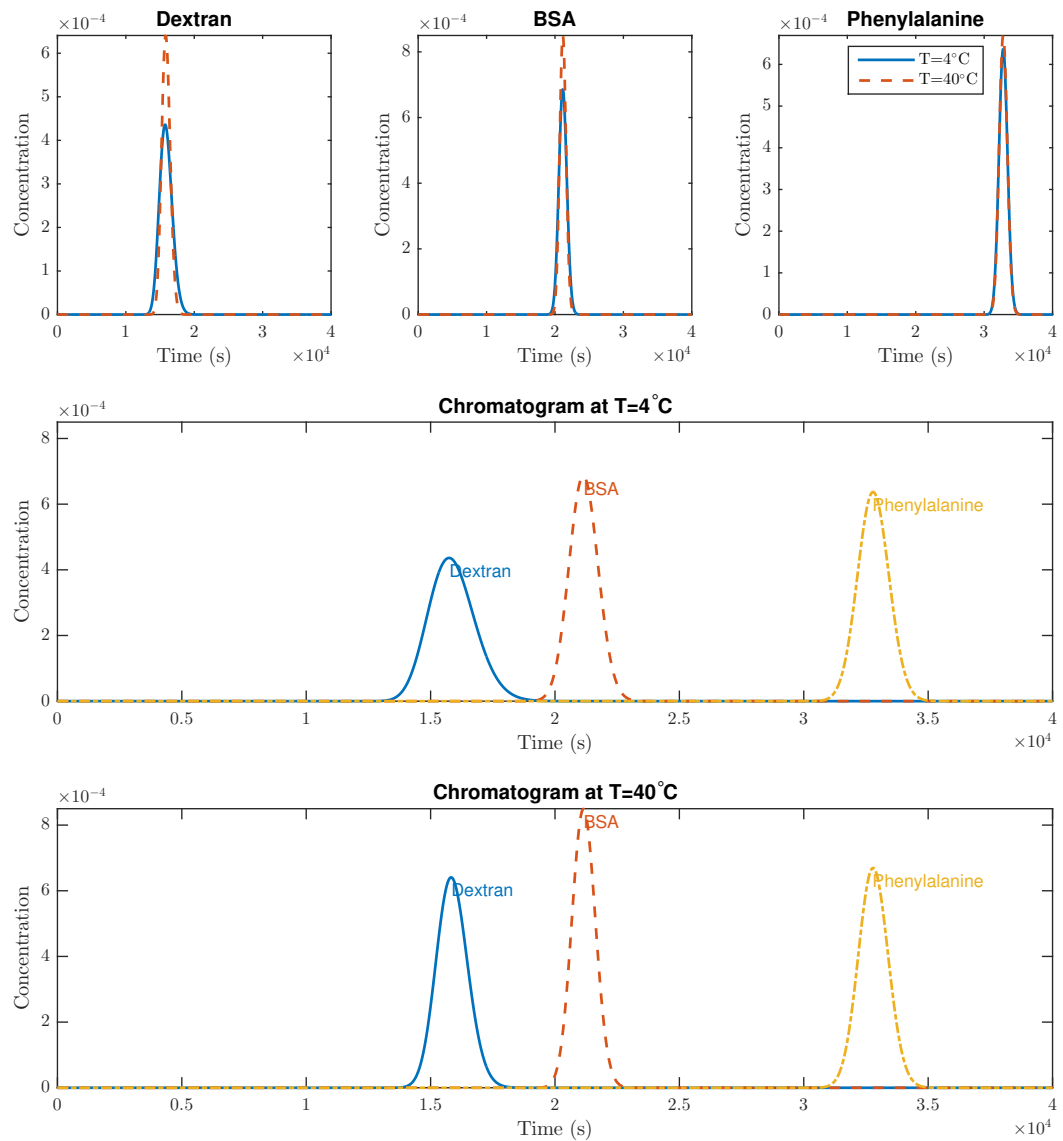


Figure 5.3: Chromatograms at a superficial velocity of $0.01\text{cm}/\text{s}$ and particle radius of $45\mu\text{m}$

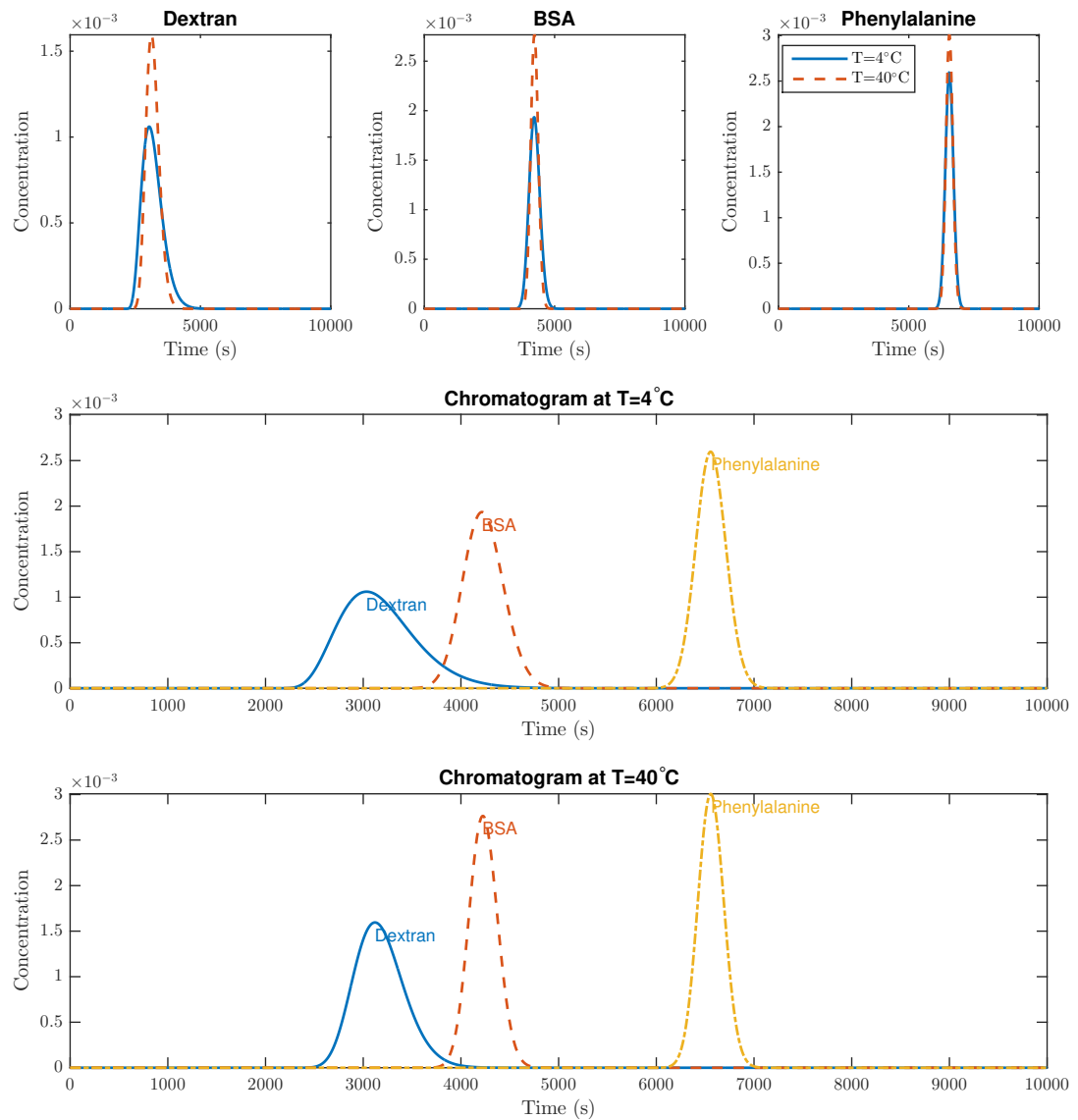


Figure 5.4: Chromatograms at a superficial velocity of 0.05cm/s and particle radius of $45\mu\text{m}$

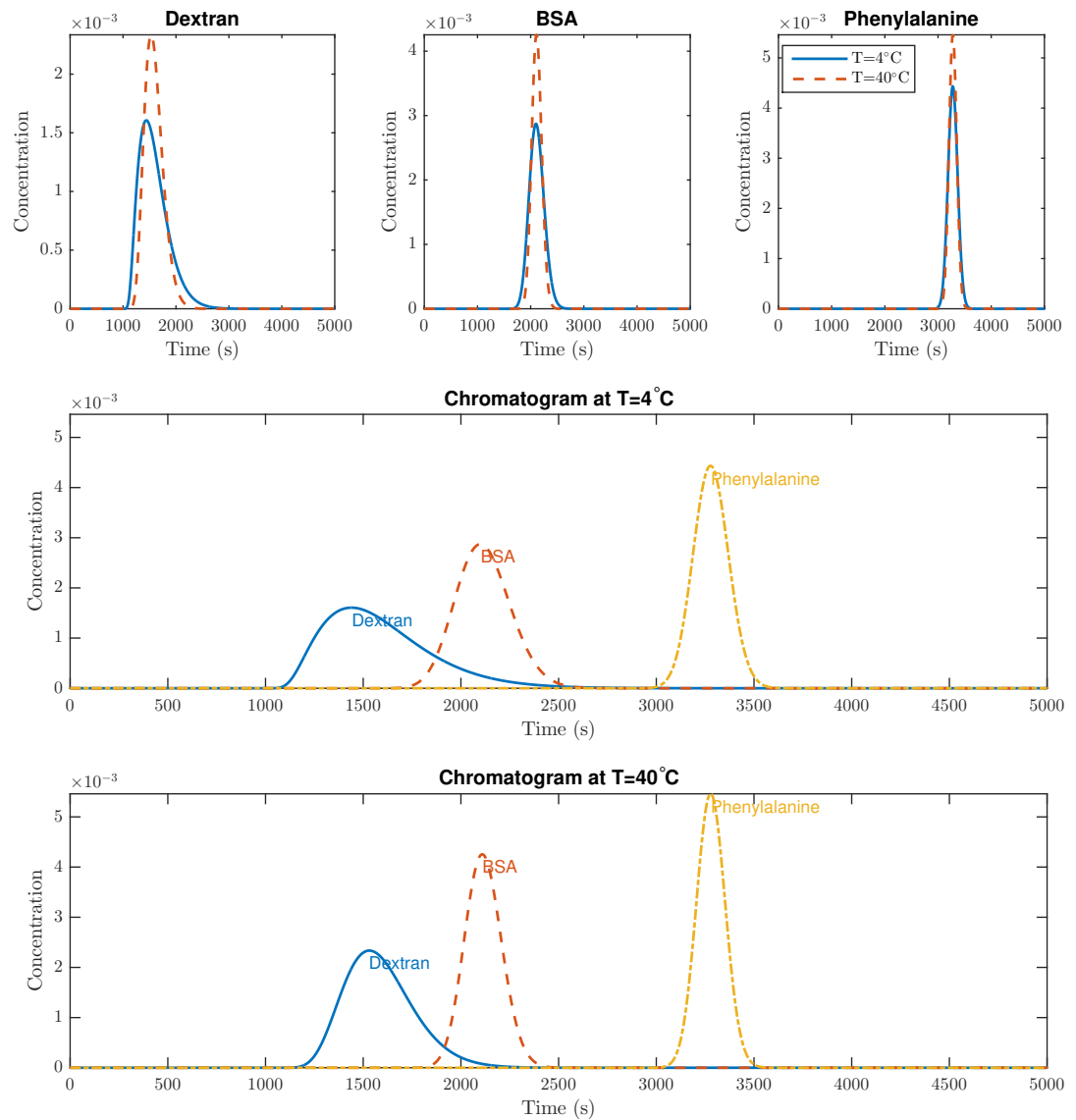


Figure 5.5: Chromatograms at a superficial velocity of 0.1cm/s and particle radius of $45\mu\text{m}$

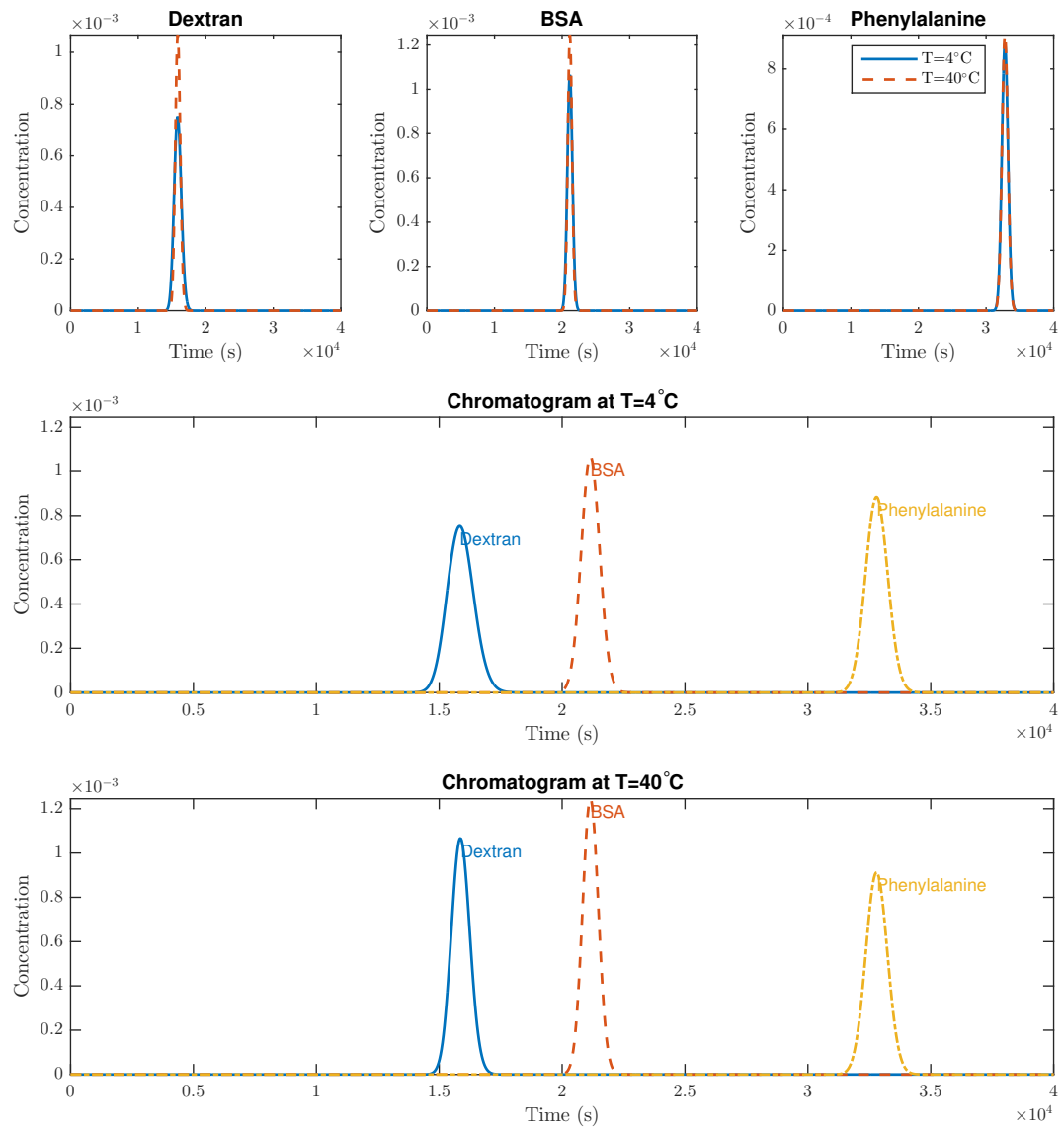


Figure 5.6: Chromatograms at a superficial velocity of 0.01cm/s and particle radius of $25\mu\text{m}$

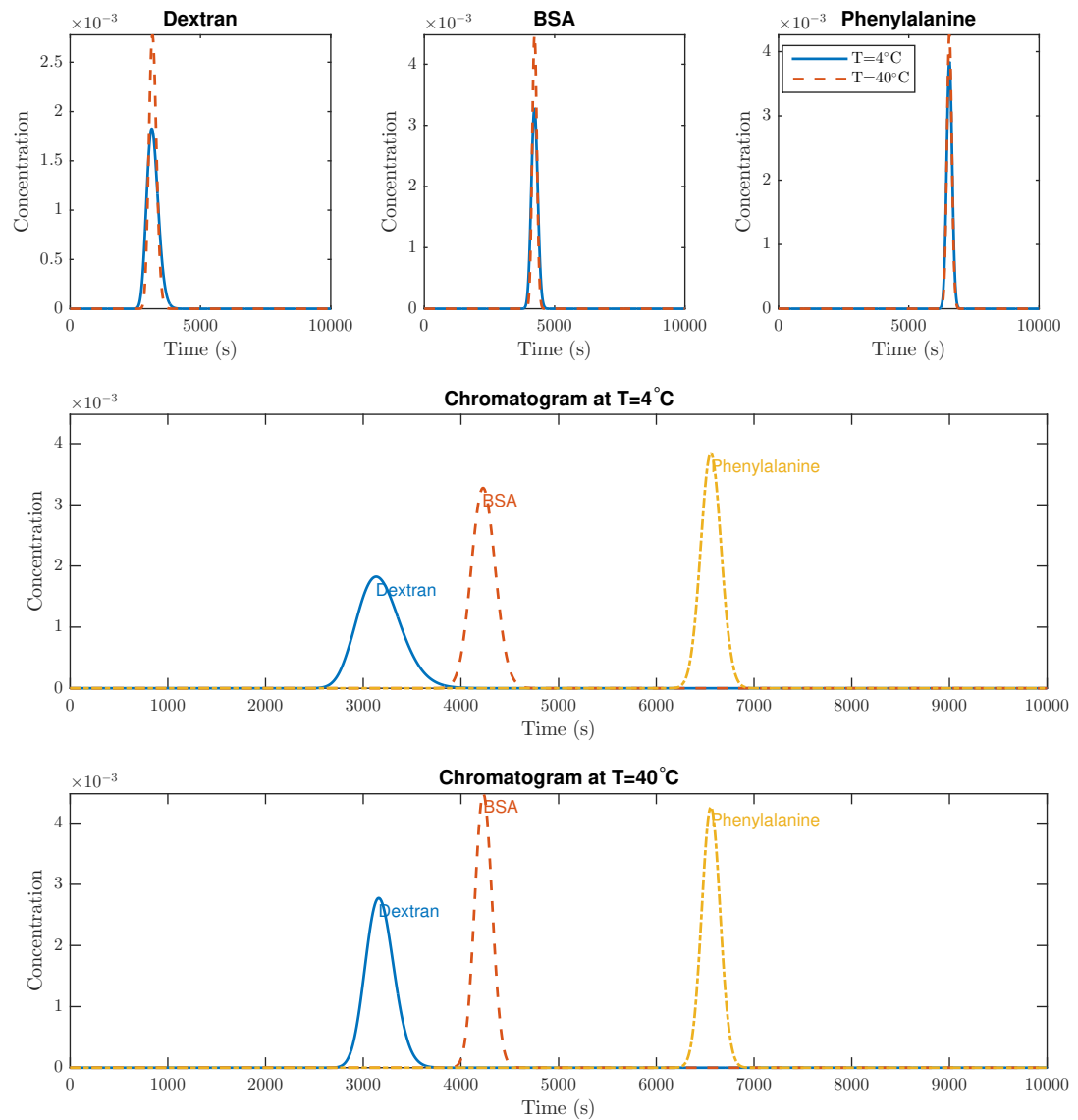


Figure 5.7: Chromatograms at a superficial velocity of 0.05cm/s and particle radius of $25\mu\text{m}$

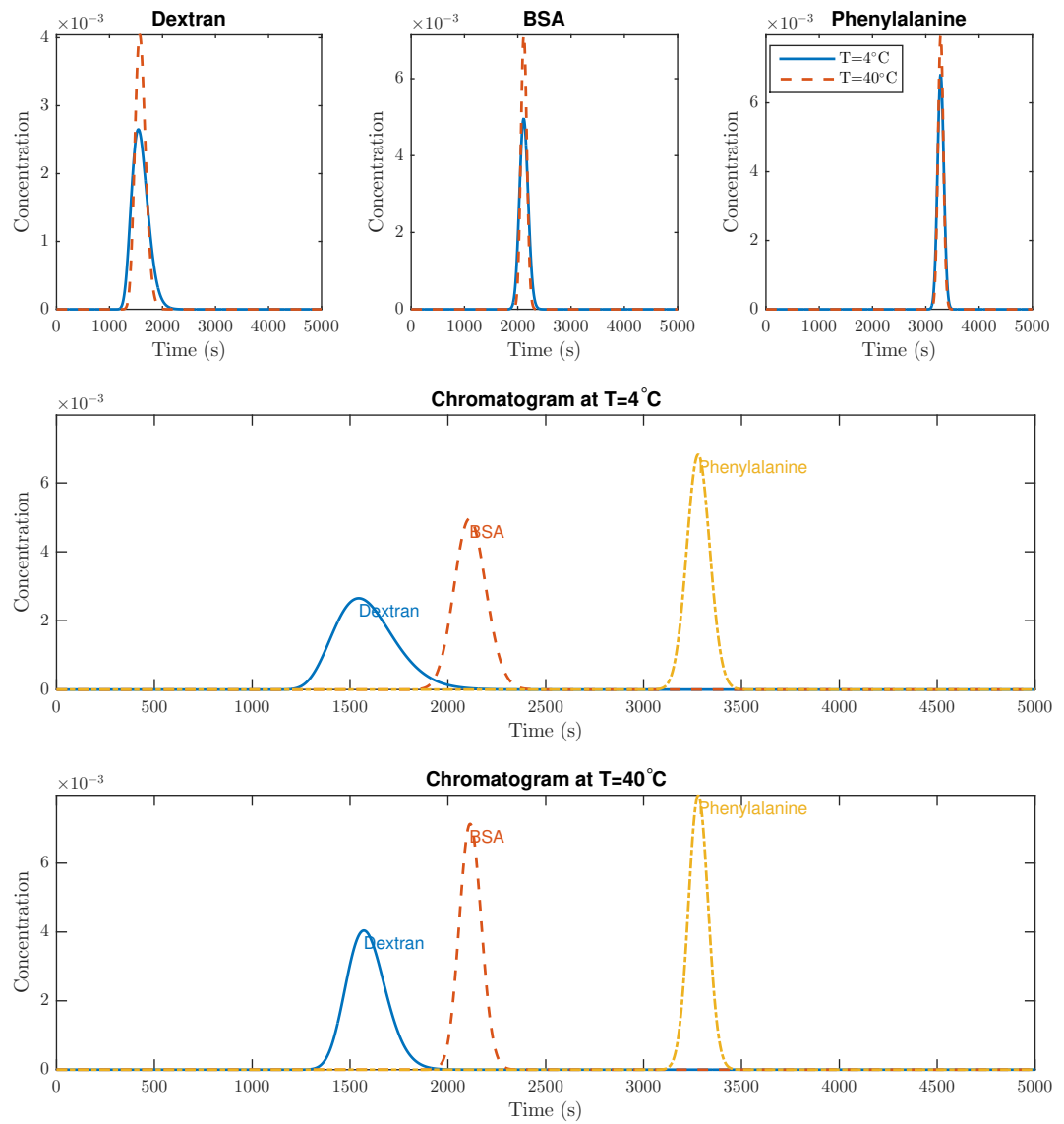


Figure 5.8: Chromatograms at a superficial velocity of 0.1cm/s and particle radius of $25\mu\text{m}$

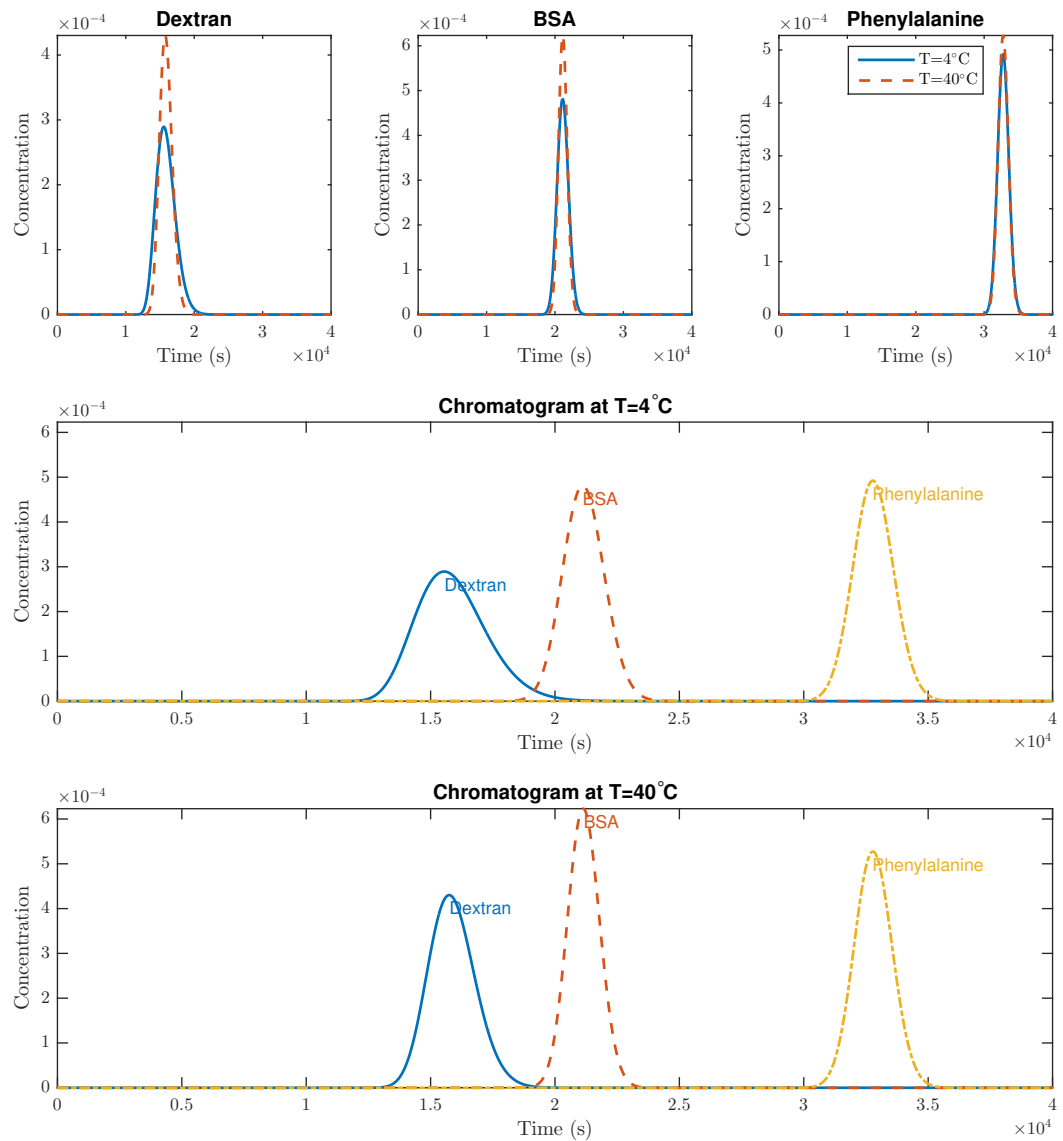


Figure 5.9: Chromatograms at a superficial velocity of 0.01cm/s and particle radius of $70\mu\text{m}$

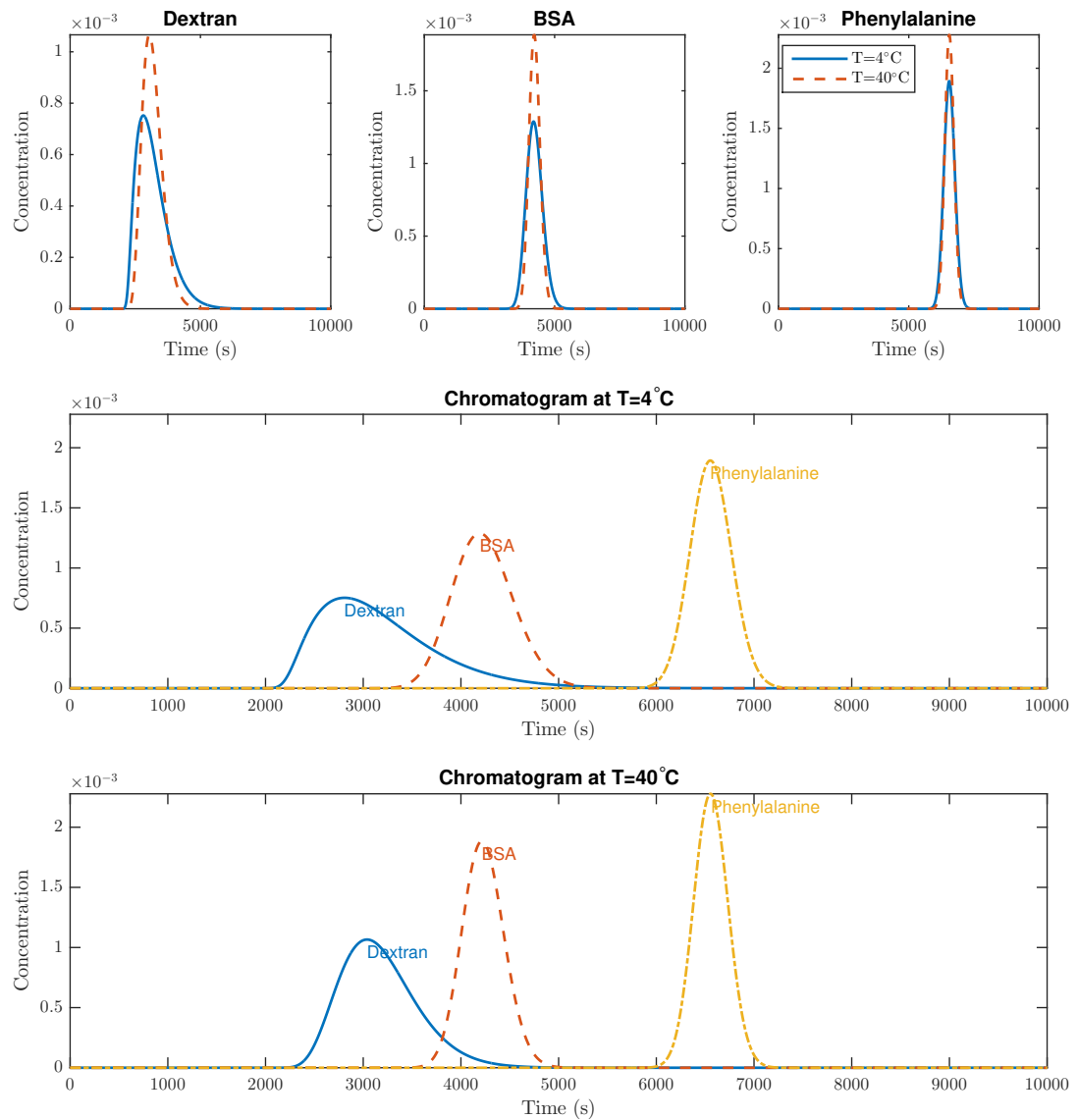


Figure 5.10: Chromatograms at a superficial velocity of 0.05cm/s and particle radius of $70\mu\text{m}$

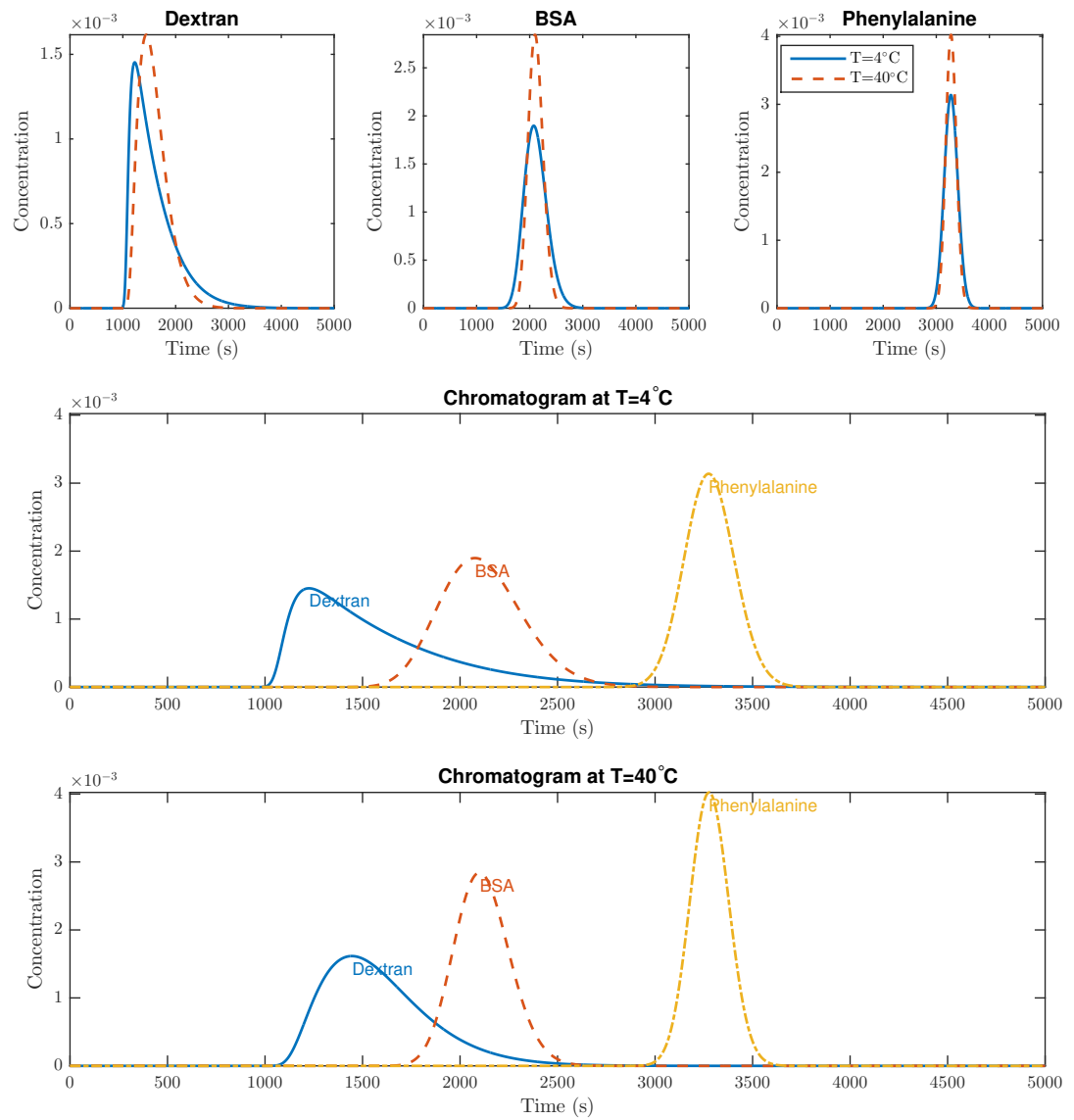


Figure 5.11: Chromatograms at a superficial velocity of $0.1\text{cm}/\text{s}$ and particle radius of $70\mu\text{m}$

Chapter 6

Numerical Study of the Effect of pH and Temperature of Protein Separation in Anion and Cation Exchange Chromatography

In this chapter, a numerical study based on the experimental findings and the generalized rate model is presented. A model for chromatography was taken, and the solution to its Laplace transfer function was obtained using the Fast Fourier Transform method. Using the previously developed correlations for modelling physical variables such as diffusion, both in solution and intraparticle, and the mass transfer coefficient, the effect of temperature in ion-exchange liquid chromatography was investigated. The shape of the chromatogram was systematically analyzed to understand the efficiency of the separation. In this study, a system of bovine serum albumin introduced to an anion-exchange column and lysozyme introduced to a cation-exchange column was used. Experimental data was taken to understand how the height-equivalent theoretical plate (HETP) measure will change at different pH and temperature con-

ditions. The model predicted the experimental results quite well and was able to provide insightful information about which pH and temperature values will result in better efficiency of the column.

6.1 Introduction

Ion-exchange chromatography is a workhorse of the chemical and pharmaceutical processing industry. Therefore, an accurate and robust model for predicting its operation at different process parameters is very important. Several researchers in the past, such as Schneider and Smith [39] and Horvath and Lin [17] have presented mechanistic models that accounts for all the physical and chemical processes that occur inside of the chromatography column. This allows us to predict the operation of the chromatography unit under different conditions, without the need to run a lot of experiments, and can be used for column scale up and troubleshooting.

In previous work [32] the adsorption equilibrium constant K_A and adsorption rate constant k_{ads} for anion exchange chromatography were presented. In that work, bovine serum albumin (BSA) was a model protein used to determine how the pH and temperature influence the retention of the molecule inside the column. Another data that is also presented here is lysozyme data for cation exchange chromatography. This data is used in a predictive manner to determine how the retention will be affected by different pH and temperature conditions. Using the work of Schneider and Smith [39], and Hsu and Chen [18] how the separation will be affected at different conditions and it can be used to optimize the separation conditions.

Using the mechanistic model developed by Schneider and Smith [39], various correlations are employed in this work in order to accurately model the physical parameters such as the mass transfer rate [25] and the dispersion coefficient[5]. For the chemical parameters, such as the adsorption equilibrium constant K_A and adsorption rate con-

stant k_{ads} , empirical correlations were used. This is due to the fact that the nature of the interaction can be most accurately represented using a set of experimental data, which are parametrized in such a way that the model can reasonably predict the elution. When the adsorption equilibrium constant K_A and adsorption rate constant k_{ads} are determined, the same model can be readily used for separation.

Summarizing, the goal of this work is to present chromatograms derived from known physical variables about the proteins, which can be used as inputs to the model and used to predict the elution at different conditions. Specifically, at a given pH and temperature, the protein charge can be determined, converted to the adsorption equilibrium constant by an empirical correlation, and use that data for the entire pH and temperature range for the analysis. This work provides a robust and fast model to compute the elution curves for the ranges of pH and temperature that can be used to optimize and scale up the ion-exchange chromatography process.

6.2 Theory

6.2.1 Model Development

Hsu and Chen [18] used a model derived by Horvath and Lin [17] to do a theoretical analysis for chromatographic separations. They described an isothermal chromatographic column packed with spherical particles, including transport processes such as external film diffusion, intraparticle diffusion and adsorption on the particle surface. The flow pattern was assumed axial-dispersed plug flow with a linear adsorption equilibrium.

For the mobile phase material balance

$$\frac{\partial C}{\partial t} + V \frac{\partial C}{\partial z} - D_L \frac{\partial^2 C}{\partial z^2} = -\frac{1}{m} \frac{\partial q}{\partial t} \quad (6.1)$$

Intraparticle material balance

$$\epsilon_p \frac{\partial C_p}{\partial t} + \frac{\partial C_s}{\partial t} = \epsilon_p D_p \left(\frac{\partial^2 C_p}{\partial r^2} + \frac{2}{r} \frac{\partial C_p}{\partial r} \right) \quad (6.2)$$

Adsorption term on the particle surface

$$\frac{\partial C_s}{\partial t} = k_{ads} \left(C_p - \frac{C_s}{K_A} \right) \quad (6.3)$$

The initial and boundary conditions

$$C = C_p = C_s = 0 \text{ at } z > 0, t = 0 \quad (6.4)$$

$$C = C_0 \delta(t) \text{ at } z = 0 \quad (6.5)$$

$$C = 0 \text{ at } z = \infty \quad (6.6)$$

The last boundary condition leads to a simpler solution using $\frac{\partial C}{\partial z} = 0$ at $z = L$ however this will only affect the solution if the axial Peclet number and column length are both small.

The other boundary conditions are:

$$\frac{\partial C_p}{\partial r} = 0 \text{ at } r = 0 \quad (6.7)$$

$$\frac{\partial q}{\partial t} = \frac{3k_f}{b}(C - C_p) = \frac{3}{b}\epsilon_p D_p \frac{\partial C_p}{\partial r} = 0 \text{ at } r = b \quad (6.8)$$

The variables introduced are: C - solute concentration in mobile phase, C_p - solute concentration in the pores, C_s - solute concentration on solid, C_0 - initial pulse concentration, V - mobile phase velocity, D_L - axial dispersion coefficient, $m = \epsilon/(1 -$

ϵ), ϵ - column void fraction, ϵ_p - particle porosity, q - concentration in particles, D_p - intraparticle diffusivity, k_{ads} - adsorption rate constant, K_A - adsorption equilibrium constant, k_f - external mass transfer coefficient, t - time, z - axial position, r - intraparticle radial position, b - radius of the bead.

A solution can be obtained by taking the Laplace transform:

$$\bar{C}(z, s) = C_0 \exp \left[\left(\frac{V}{2D_L} - \sqrt{\frac{V^2}{4D_L^2} + \frac{s}{D_L} + \frac{3k_f\varphi_2}{bmD_L}} \right) z \right] \quad (6.9)$$

$$\varphi_2(s) = \frac{\epsilon_p D_p \varphi_1 b \cosh \varphi_1 b - \sinh \varphi_1 b}{\epsilon_p D_p \varphi_1 b \cosh \varphi_1 b - \epsilon_p D_p \sinh \varphi_1 b + k_f b \sinh \varphi_1 b} \quad (6.10)$$

$$\varphi_1(s) = \left[\frac{1}{\epsilon_p D_p} \left(\epsilon_p s + \frac{k_{ads} s}{s + \frac{k_{ads}}{K_A}} \right) \right]^{1/2} \quad (6.11)$$

where s is the Laplace domain.

6.2.2 Computational Method

The inversion of this transfer function was then computed using MATLAB and the built-in IFFT function. As the frequency spectrum of this function is symmetrical, it was specified in the function which aids the algorithm and decreases computation time. The formula utilized by MATLAB is as follows:

$$\bar{f}(t) = f(n \Delta T) = \frac{N}{2T} \left[\left(\frac{1}{N} \right) \sum_{k=1}^N F \left(\frac{i(k-1)\pi}{T} \right) \exp \left(i \frac{2\pi(n-1)(k-1)}{N} \right) \right] \quad (6.12)$$

$$n = 1, 2, \dots, N$$

Inverting the transfer function presented above was accomplished on a Dell Optiplex 790 with an Intel i7-2600 CPU with 8.00 GB of RAM using MATLAB version

R2015a. Simulating one elution curve with the FFT (Fast Fourier Transform) method required 0.1019 seconds with 1024 digital numbers. Other inversion methods [8] required 21.7594 seconds. The computation performance makes the FFT method quite useful in obtaining rapid and precise results.

6.2.3 Adapting the model as a function of temperature

Temperature effects were investigated in a way where the physical parameters were correlated to characterize all of the physical parameters associated with the mass transfer occurring inside the column, as well as fundamental properties such as diffusion of the solute. The trends that those correlations exhibited with decreasing temperature on the chromatograms were analyzed.

The viscosity and density of water are estimated based on the physical properties for water between the range of 273K and 350K based on data taken from NIST [7]. Axial dispersion was estimated by a correlation by Chung and Wen [5]:

$$D_L = \frac{2\epsilon RV}{0.2 + 0.011\text{Re}_P^{0.48}} \quad (6.13)$$

where

$$\text{Re}_P = \frac{2R\epsilon V\rho}{\mu} \quad (6.14)$$

For the protein solution diffusivity, the correlation by Young [54] was considered:

$$D_0 = 8.34 \times 10^{-10} \left(\frac{T}{\mu M_W^{\frac{1}{3}}} \right) \quad (6.15)$$

which is introduced in the Boyer and Hsu [2] correlation for intraparticle diffusivity:

$$D_e = 8.34 \times 10^{-10} \left(\frac{T}{\mu M_W^{\frac{1}{3}}} \right) \exp \left[-0.1307 \left(M_W^{\frac{1}{3}} + 12.45 \right) c_f^{\frac{1}{2}} \right] \quad (6.16)$$

The mass transfer coefficient given by Liapis [9] for protein mass transfer coefficient is:

$$\frac{2k_f R}{D_0} = 2 + 0.51 \left(\frac{E^{\frac{1}{3}} (2R)^{\frac{4}{3}} \rho}{\mu} \right)^{0.60} \text{Sc}^{\frac{1}{3}} \quad (6.17)$$

E is the energy dissipation rate

$$E = \frac{25(1 - \epsilon) \epsilon^2 C_{D0} V^3}{R} \quad (6.18)$$

C_{D0} is the drag coefficient for a particle which is given by Stokes Law as $C_{D0} = 24/\text{Re}$ and the Schmidt number as $\text{Sc} = \mu/\rho D_0$. Other variables that were not previously defined include: M_W – molecular weight, c_f – concentration of the gel, μ – viscosity, ρ – density, T – temperature. As for the intraparticle void fraction ϵ_p an estimate is made using a correlation presented in Boyer and Hsu[2], based on data given by GE Healthcare (Uppsala, Sweden) and reproduced in Equation 6.19[42].

$$\epsilon_p = -0.1 \log(M_W) + 1.6835 \quad (6.19)$$

6.2.4 Solution Algorithm

Literature data for the titration curve of BSA was taken in this work to correlate the pH to the net charge of the protein[38]. A correlated pH range between 7.5 and 10 for BSA is presented in Figure 6.1. For the lysozyme titration data [45], a correlation between the pH of 2.5 and 4.5 is presented in Figure 6.2. This allowed to evaluate the protein charge at any pH within the experimental domain. The values obtained from the interpolation were used to develop a function for the adsorption equilibrium constant, K_A as a function of the protein net charge. In Figure 6.3 and 6.4, linear correlations for K_A as a function of net charge are presented, each corresponding to the temperature at which the experiment was conducted. The adsorbents used in those studies were Q Sepharose for the BSA case and SP Sepharose for the lysozyme

case. These approximations will allow to not only predict the elution for the entire pH range at the selected temperature conditions.

The adsorption rate constant k_{ads} can be predicted using the same independent variable, net charge, as the surface charges govern the adsorption rate. In the same fashion as for K_A , the k_{ads} values were correlated for each net charge. In Figure 6.5, the correlations for BSA are using an exponential fit of the type $y = A \exp(Bx)$. For lysozyme the k_{ads} values were averaged as all values were all within the same range. As the adsorptive forces are weaker in cation exchange, representing the variation of the k_{ads} values was not of great importance and a single value was used for each temperature condition. The values used for k_{ads} were $1.22 \text{ mL/g} \cdot \text{sec}$ for 5°C , $0.051 \text{ mL/g} \cdot \text{sec}$ for 23°C , and $0.026 \text{ mL/g} \cdot \text{sec}$ for 40°C ,

Similar correlations can be derived for varying the temperature at a fixed pH conditions. In this case, both the K_A and the k_{ads} can be plotted on an Arrhenius plot to accurately account for the trends. The plots are presented in Figure 6.6, 6.7, 6.8 and 6.9. These equations approximate the trends quite well so they can be utilized to predict how the components will elute within the usable range of the adsorbent material.

Using the correlations outlined in this section, elution curves can be computed for the entire pH range and for each temperature condition. Afterwards, the chromatograms can be analyzed to determine the efficiency of the separation.

6.3 Results

All of the correlations presented are within the pH ranges between 7.5 and 10 for anion exchange chromatography and pH range between 2.5 and 4.5 for cation exchange chromatography. The reasoning behind this range is that the proteins may denature in basic conditions of pH above 10 or acidic conditions of pH below 2.5. The calculations

were run for the three experimental temperatures of 5°C, 23°C and 40°C.

6.3.1 pH Effect

The results are displayed on a mesh plot in Figure 6.10 for BSA and Figure 6.11 for lysozyme. For the case of BSA, the immediate observation from the BSA peaks is that the retention increases with increasing pH as observed in anion exchange chromatography[32]. These findings validate the model for use in a predictive manner. Note that the mesh plots are not presented on the same timescales, whereby at the highest temperature of 40°C the retention is much more significant than the one observed in 5°C.

For the lysozyme case, the effects are less prominent, especially in the cases of 23°C and 40°C. The adsorption becomes much weaker with increasing temperature, so at 23°C the retention does not change very significantly, and at 40°C, the adsorption is slightly improved at higher pH. The data that follows the experimental trends very well is the 5°C mesh which can be used in a predictive manner.

For a more direct comparison of the elution curves in anion exchange, the results for pH values of 8.0, 9.0, and 10.0 were compared on a single plot. They are taken from the same curves as given in Figure 6.10 and presented in Figure 6.14. All chromatograms are presented on the same timescale to allow for a more direct comparison. The temperature effect that the adsorption increases with increasing temperature is very prominent, however the expense in performance is that the peak spreads over a long elution time. There is an important tradeoff between the peak spreading versus the retention time, which will be analyzed in detail in the next section.

For the cation exchange case, the direct comparison of the elution curves is given in Figure 6.15. As in the anion exchange case, the elution curves here are presented on the same timescale where the 5°C results show the highest retention, where the trend follows the experimentally observed trends. Here, the highest retention is observed at

the lowest pH value as it provides the highest positive net charge of the sorbate. For the 23°C and 40°C cases, the peaks almost overlap one another since there is weaker adsorption of lysozyme at those conditions as demonstrated by the experimental data.

6.3.2 Temperature Effect

The mesh plots for anion exchange with varying temperature are presented in Figure 6.12 for BSA. Here, the peaks get more retained as temperature increases, similar to the experimental results. For the cation exchange case with Lysozyme the results are presented in Figure 6.13, where the peaks get more retained as the temperature decreases. In these figures, the pH values that were fixed were 7.8, 8.4 and 8.8 in the anion exchange case and pH of 3.0, 3.6 and 4.2 for cation exchange. The reasoning behind these values is because the retention data that was used[32] reported the chromatograms at those pH values for the temperature range of the adsorbent. The temperatures that were inputted were between 5°C and 40°C to cover all possible elution temperatures for the Q Sepharose and SP Sepharose adsorbents.

As the elution curves are not compared on the same timescales on the mesh plots, individual chromatograms at 5°C, 20°C and 40°C are presented at the three pH values for both anion and cation exchange chromatography in Figures 6.16 and 6.17. The temperature effect becomes quite prominent in anion-exchange, where the retention shifts quite significantly as both pH and temperature are increased. In cation exchange the effect is less prominent due to weaker adsorption, however it is significant enough to show increased retention at lower temperatures.

6.4 Discussion

The results that were computed follow the experimentally observed chromatograms, making the model valid for use in a predictive manner to optimize and improve the

separation conditions. A key parameter that can be determined about the separation conditions that can be determined from the wealth of chromatograms presented previously is the height-equivalent-theoretical plates (HETP). With small HETP, the peaks are narrower, and with a higher HETP the peaks are wider. As HETP is a good measure of the column efficiency and peak distribution throughout the column, HETP can help to understand how the peak will behave under different temperature and pH conditions. To compute the HETP, Equation 6.20 is used[2]:

$$h = \frac{\mu_2 L}{\mu_1'^2} \quad (6.20)$$

which can be calculated by the first and second moment μ_1' and μ_2 of the peak. The moments can be computed:

The n th absolute moment of $c(z, t)$ is defined as:

$$\mu_n' = \frac{m_n}{m_0} \quad (6.21)$$

where

$$m_n = \int_0^\infty t^n c(z, t) dt \quad (6.22)$$

The n th central moment is defined as:

$$\mu_n = \left(\frac{1}{m_0}\right) \int_0^\infty (t - \mu_1')^n c(z, t) dt \quad (6.23)$$

The results for varying pH in the anion-exchange are presented in Figure 6.18 and the results for cation-exchange are in Figure 6.19. From the BSA case, the lowest HETP is achieved at the highest temperature of 40°C between the pH range of 8.2 to 9.8. The elution that will be achieved at these conditions will be significantly better when compared to the other two temperatures at the same pH, as it retains the molecule better, even with the peak spreading that is observed. Interestingly, within the pH

range of 8.2 to 8.8, the HETP of 5°C and 23°C is similar in value. This would not result in improved conditions for separation as predicted by the simulation data.

For the Lysozyme case, the results do not form the same trends in all temperature conditions. For the 40°C case, the HETP increases with increasing pH, which is opposite than the one observed in the other two temperatures. This is due to the weak adsorption that has demonstrated higher retention at higher pH at 40°C, which is a reflection of using the experimental data that does not have enough variance to give a clear retention trend. For the 5°C and 23°C the trends are quite clear, where at lower pH, especially between 2.5 to 3.0 the HETP is similar, since the peak spreading outweighs the benefits provided by the higher retention. On the other hand, at pH values between 3.5 and 4.5 the 5°C retention data proves better as it provides better HETP, despite having a higher peak spreading.

For the varying temperature, the results for anion-exchange are given in Figure 6.20 and for cation-exchange they are presented in Figure 6.21. In the BSA case, there is a clear optimum value at a temperature of 295K and a pH of 7.8, where the peak spreading is minimized when scaled to the retention. However, this is not an indication of how the separation performance will be affected, as HETP is not a measure of selectivity or resolution. Another result from this graph is that even though higher retention is observed at pH of 8.8, at the same temperature, the column might be more efficiently used at a lower pH.

In the lysozyme case, the temperature variance presented a very clear optimum at a pH of 3.0 around 290K. Even though HETP continues to decrease with increasing temperature in the case of pH values of 3.6 and 4.2, the retention might not be very good as observed in the chromatograms. The HETP plots can provide a useful guideline of the tradeoff between peak spreading and retention to determine the column efficiency, however they should not be used as an indication of the separation performance.

These plots would help a practicing engineer or researcher to establish a broad range of possible operating variables and test them to identify efficient conditions. To determine the best separation conditions, these models can be run in a predictive manner using binding data for the biomolecules that need to be separated. Using the FFT method, the chromatograms can then be directly compared to determine their resolution and selectivity. This has been performed for gel-filtration chromatography [31] and can be used along with the method presented in this work to completely characterize separation performance. Note that this analysis was done by using a very limited set of data, which was correlated to the physical parameters such as the net charge of the sorbate that drive the adsorption. This chromatography model can be a very important analytical tool which provides rapid results due to the use of the FFT algorithm and experimental data to connect the theory with the experimental findings to use it in a predictive way for a range of sorbates.

6.5 Conclusion

A solution method was implemented that used experimentally derived variables to predict the elution behavior of ion-exchange chromatography columns. To compute the mechanistic model in this work, the Fast Fourier Transform (FFT) method was used. To account for the charges on the protein, bovine serum albumin (BSA) and lysozyme were used as a model proteins. The mechanistic model accurately predicted the trends with varying pH and temperature by utilizing experimental correlations. It handled a range of pH values and computed each elution curve for the desired condition. The HETP method was used to determine the efficiency for the column for the given pH and temperature values. To compare with the other biomolecules elution curves, the separation of both biomolecules can be obtained. This solution method can be used to find the optimal separation conditions quickly and use real

experimental data to drive the computational analysis.

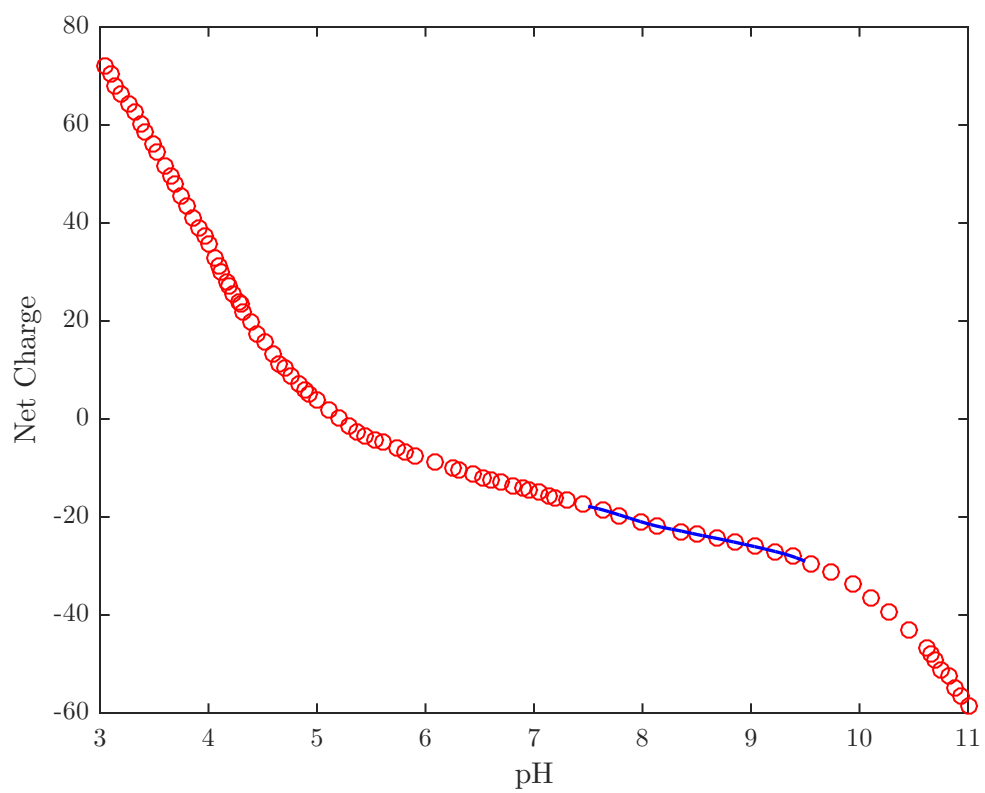


Figure 6.1: Interpolated values of the net charge of BSA as a function of pH

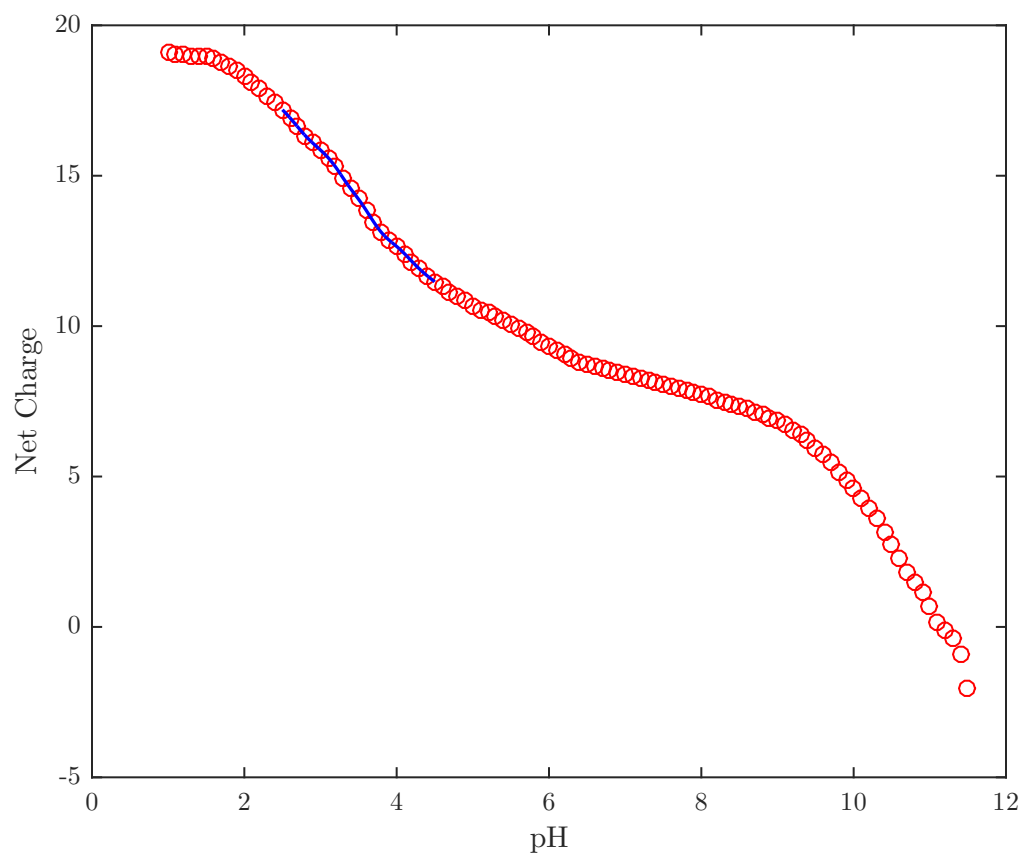


Figure 6.2: Interpolated values of the net charge of Lysozyme as a function of pH

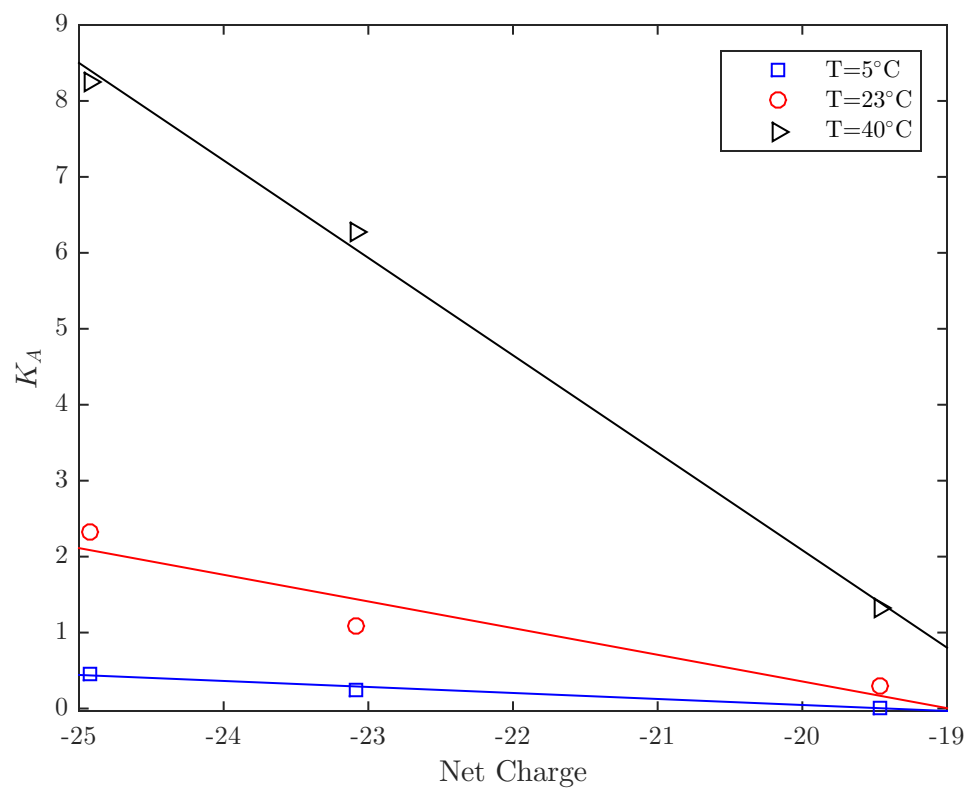


Figure 6.3: Correlations of the adsorption equilibrium constant as a function of net charge at different experimental temperatures for BSA

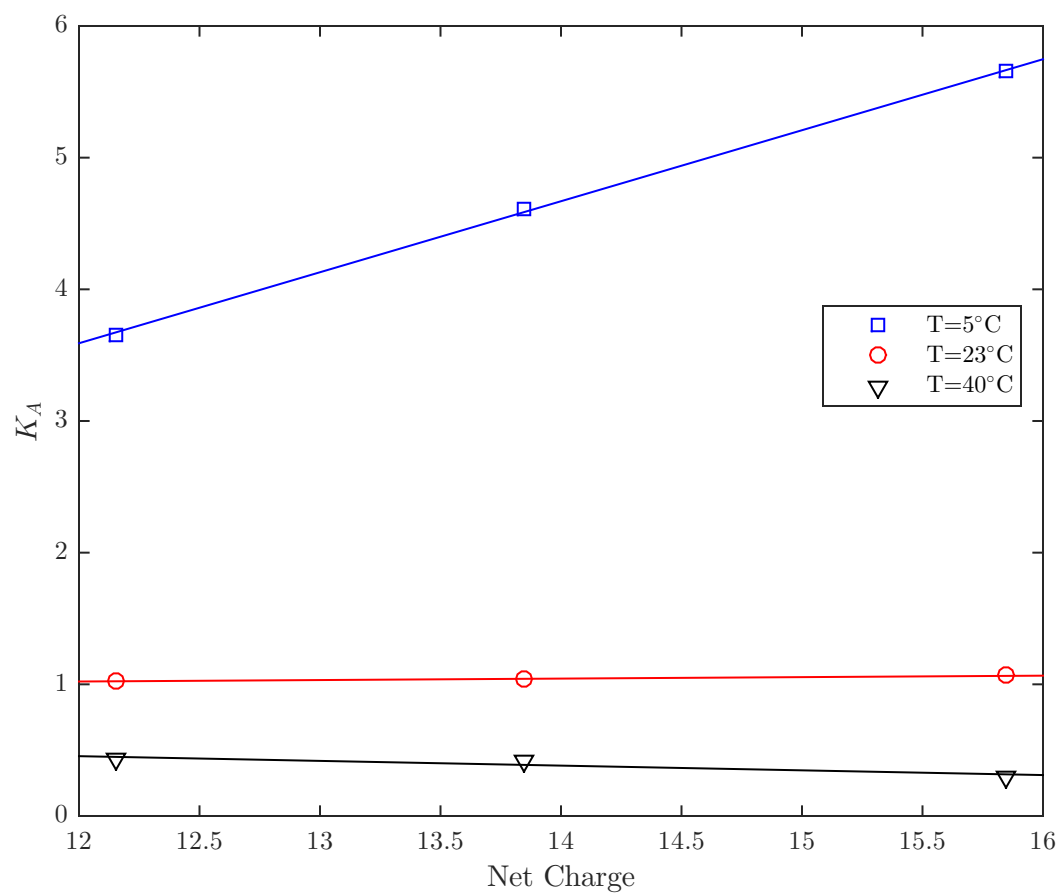


Figure 6.4: Correlations of the adsorption equilibrium constant as a function of net charge at different experimental temperatures for Lysozyme

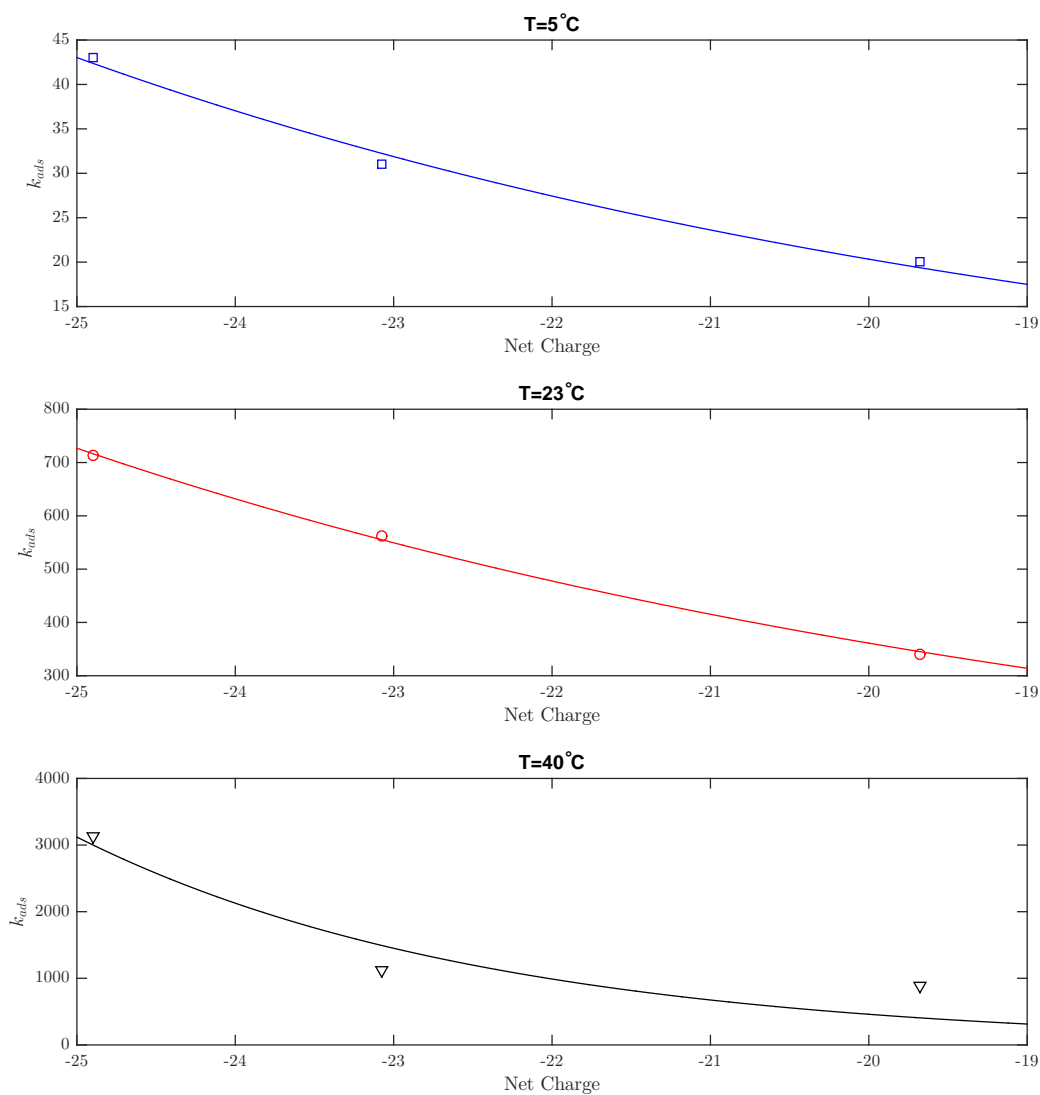


Figure 6.5: Correlations of the adsorption rate constant as a function of net charge at different experimental temperatures for BSA using the regression model $y = A \exp(Bx)$

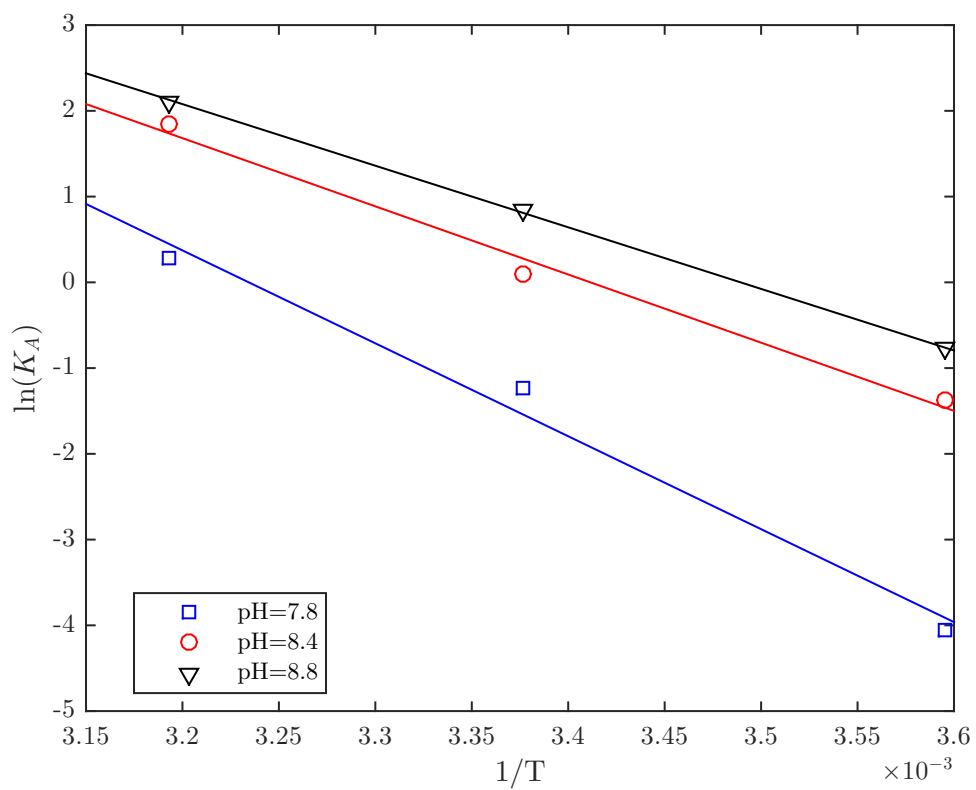


Figure 6.6: Arrhenius plot of the adsorption equilibrium constant as a function of temperature at different experimental pH values for BSA

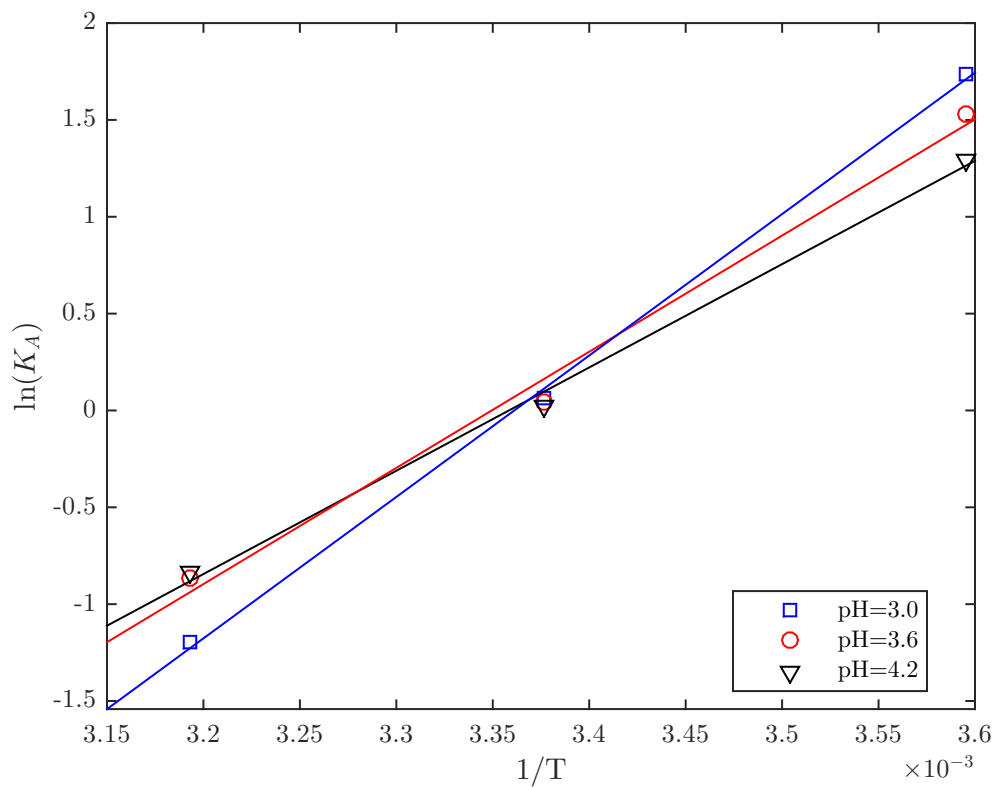


Figure 6.7: Arrhenius plot of the adsorption equilibrium constant as a function of temperature at different experimental pH values for Lysozyme

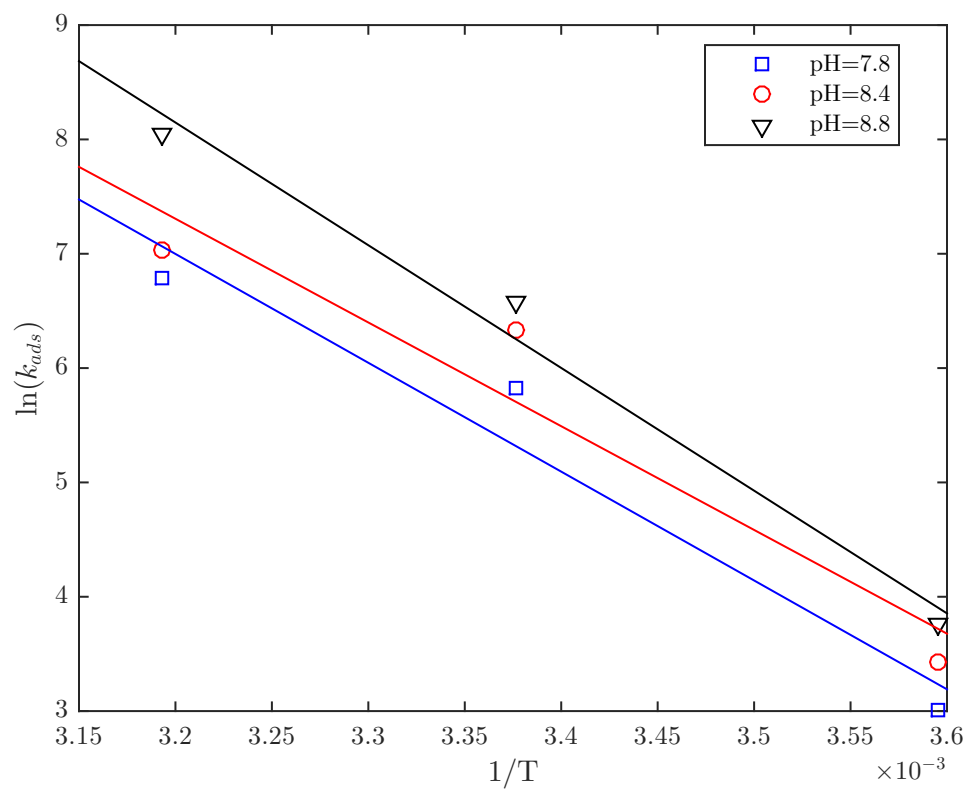


Figure 6.8: Arrhenius plot of the adsorption rate constant as a function of temperature at different experimental pH values for BSA

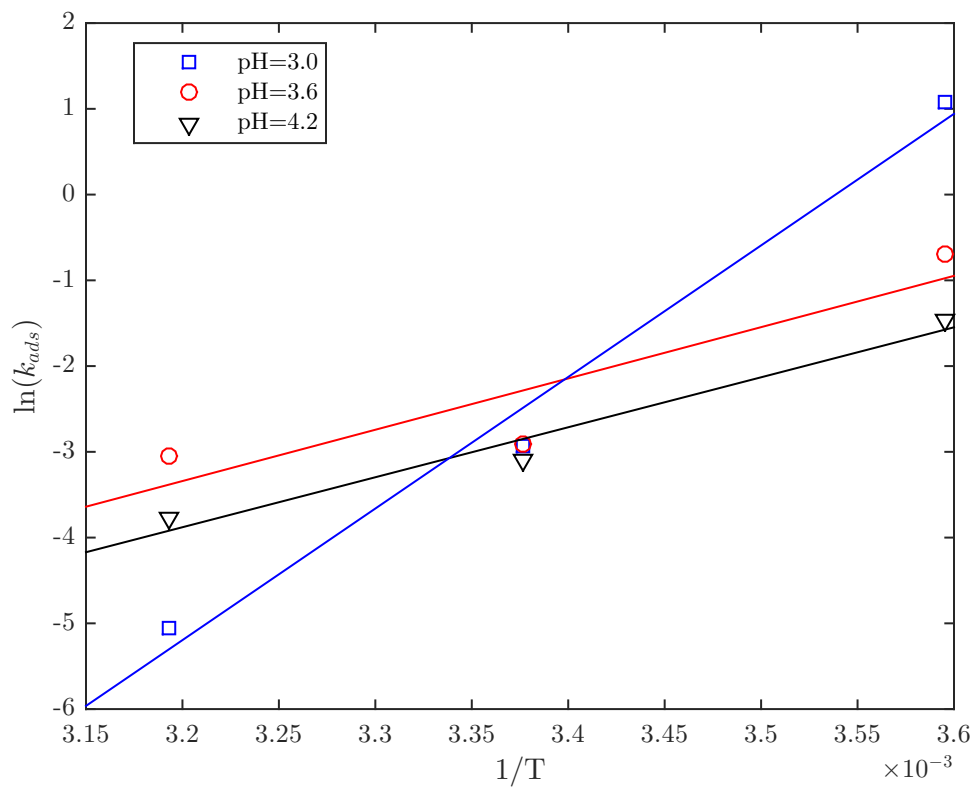


Figure 6.9: Arrhenius plot of the adsorption rate constant as a function of temperature at different experimental pH values for LYS

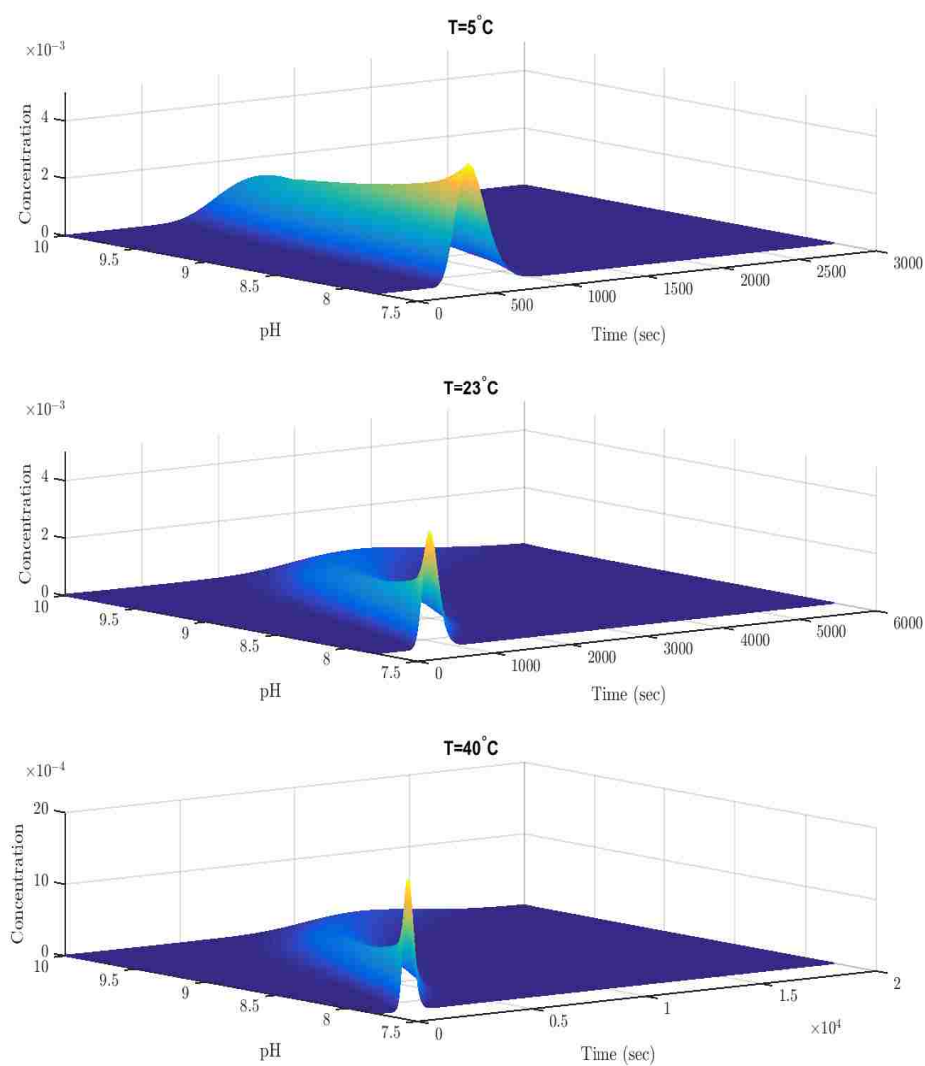


Figure 6.10: Mesh plots of BSA chromatograms at a flow rate of 0.1cm/s within the pH range of 7.8 and 10 in anion-exchange chromatography

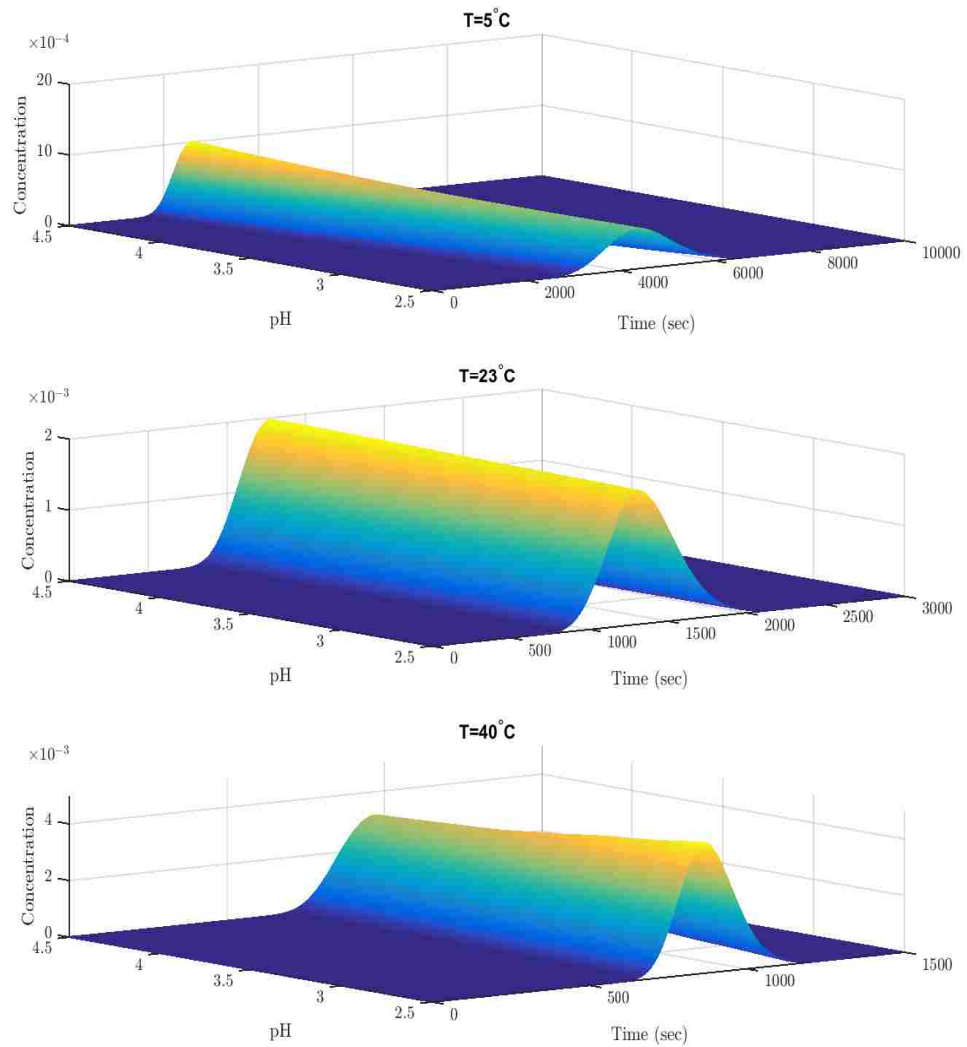


Figure 6.11: Mesh plots of Lysozyme chromatograms at a flow rate of 0.1cm/s within the pH range of 2.5 and 4.5 in cation-exchange chromatography

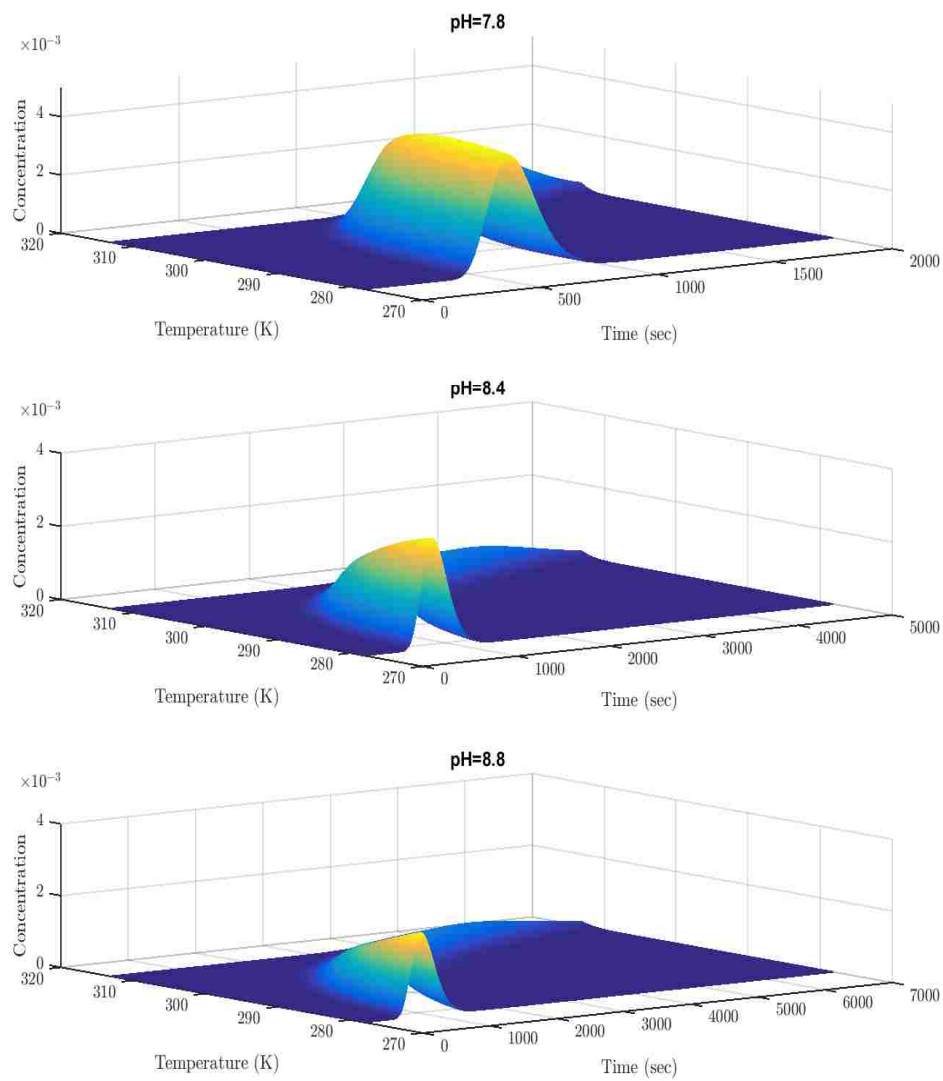


Figure 6.12: Mesh plots of BSA chromatograms at a flow rate of 0.1cm/s within the temperature range of 273K to 315K in anion-exchange chromatography

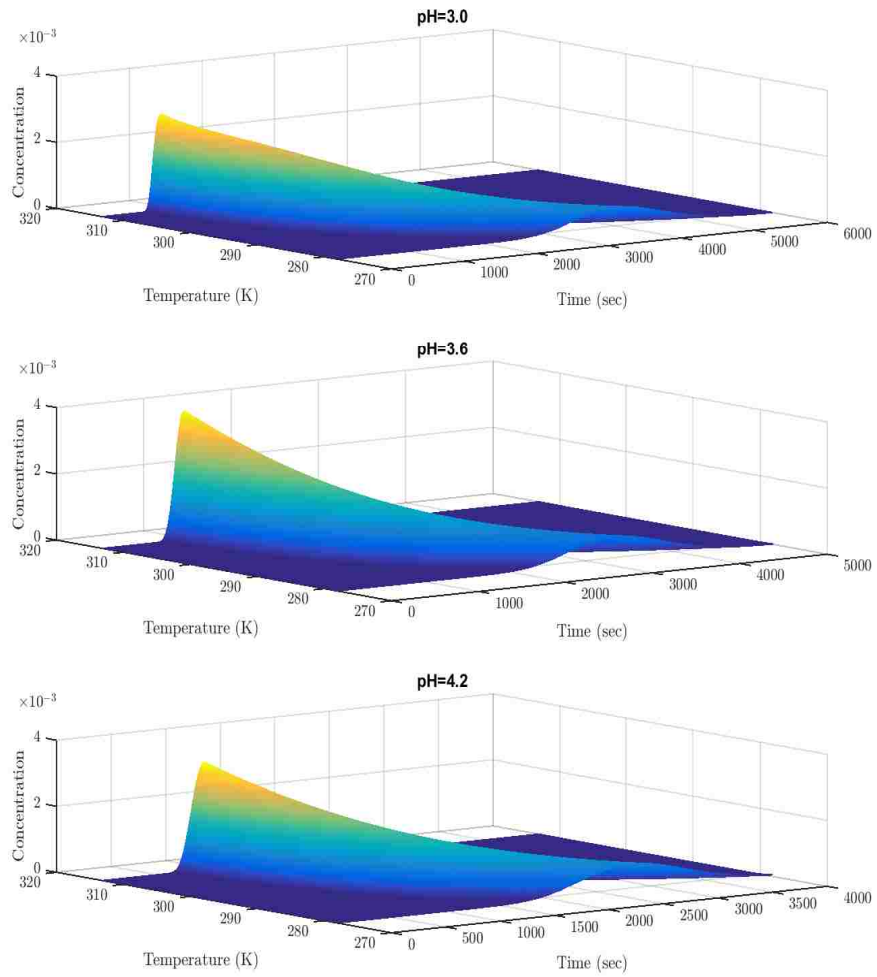


Figure 6.13: Mesh plots of Lysozyme chromatograms at a flow rate of 0.1 cm/s within the temperature range of 273K to 315K in cation-exchange chromatography

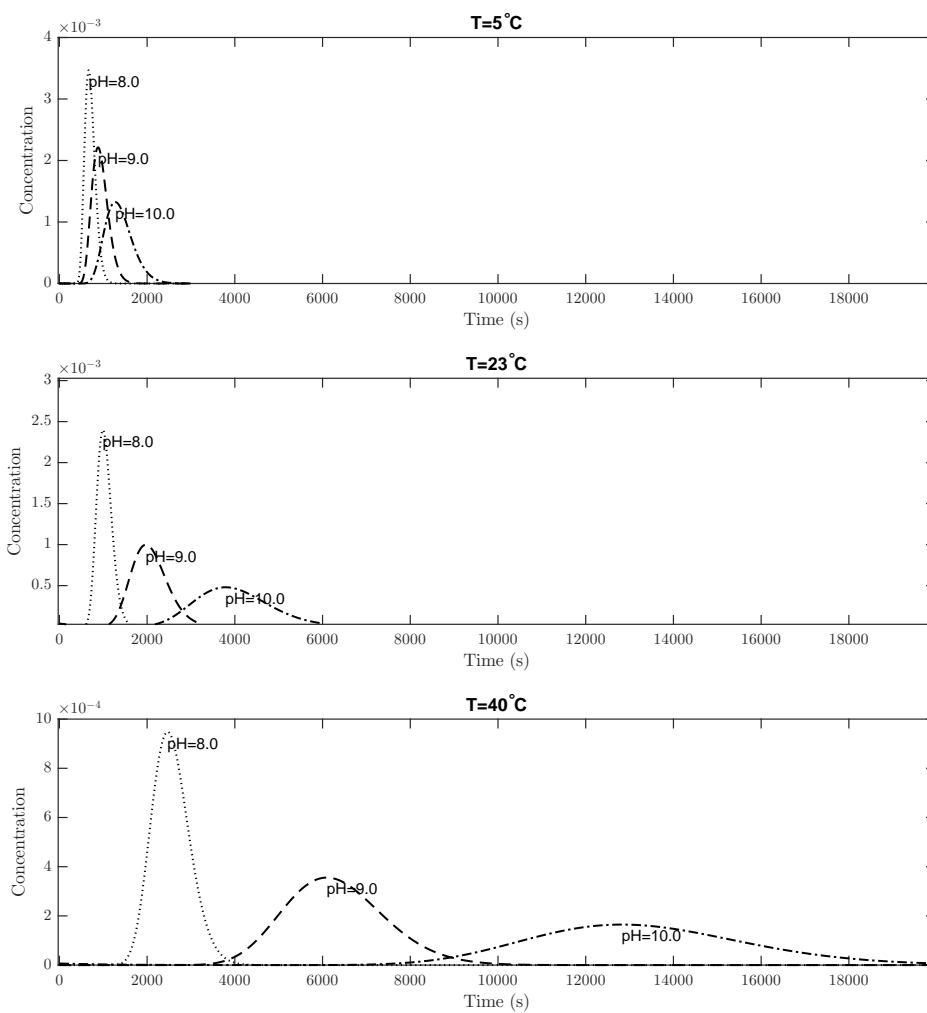


Figure 6.14: Elution curves for BSA at pH values of 8.0, 9.0 and 10.0 for three different temperatures in anion-exchange chromatography

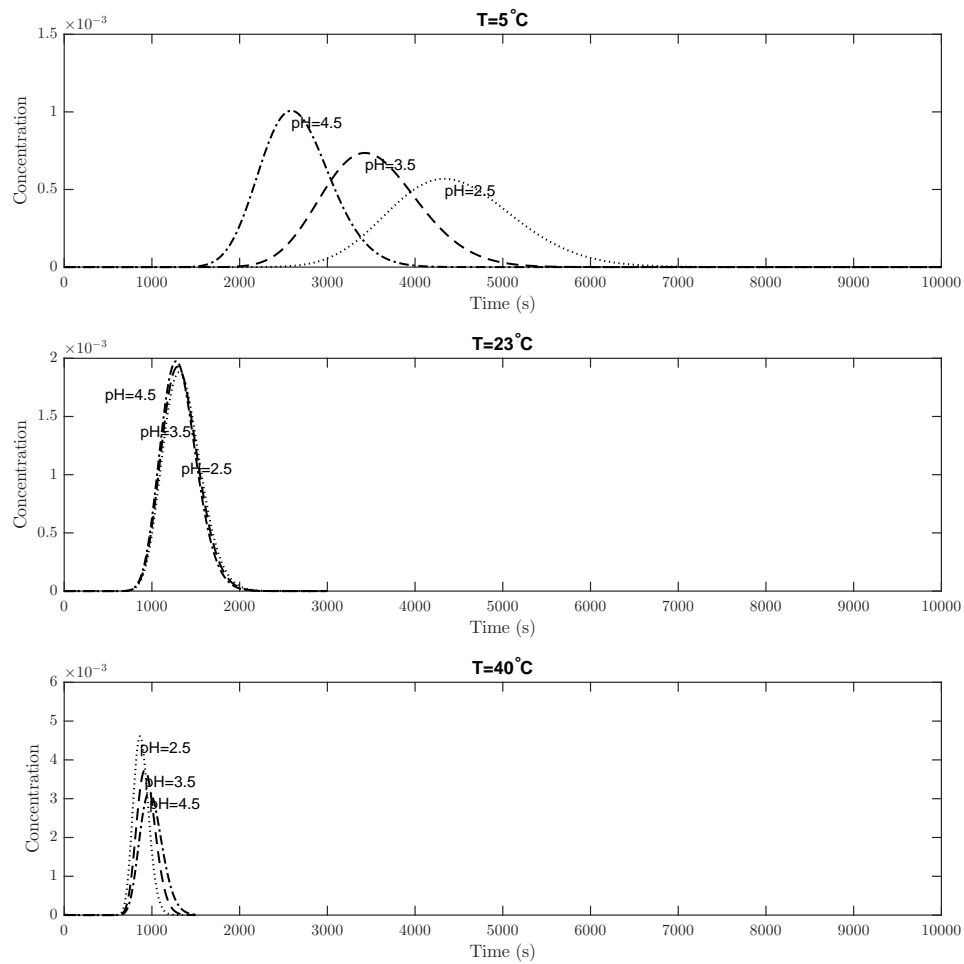


Figure 6.15: Elution curves for Lysozyme at pH values of 2.5, 3.5 and 4.5 for three different temperatures in cation-exchange chromatography

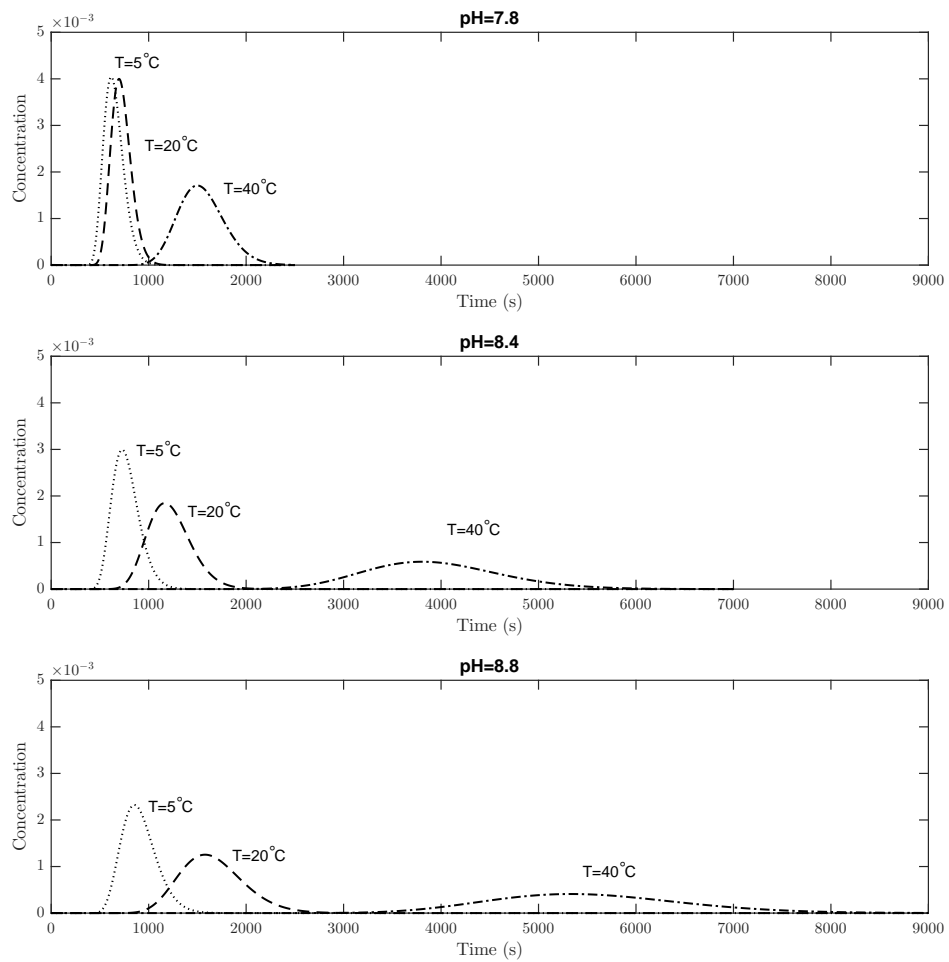


Figure 6.16: Elution curves for BSA at temperature values of 5°C , 20°C and 40°C for three different pH values in anion-exchange chromatography

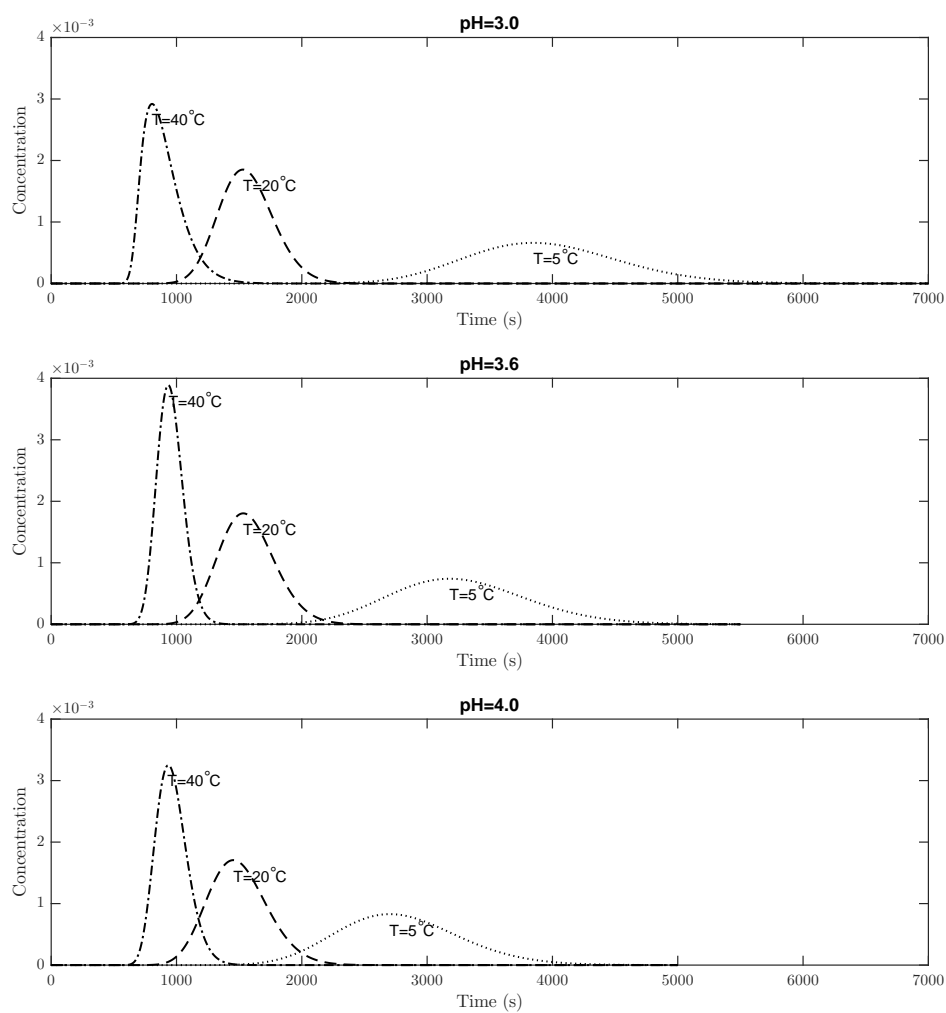


Figure 6.17: Elution curves for Lysozyme at 5°C, 20°C and 40°C for three different pH values in cation-exchange chromatography

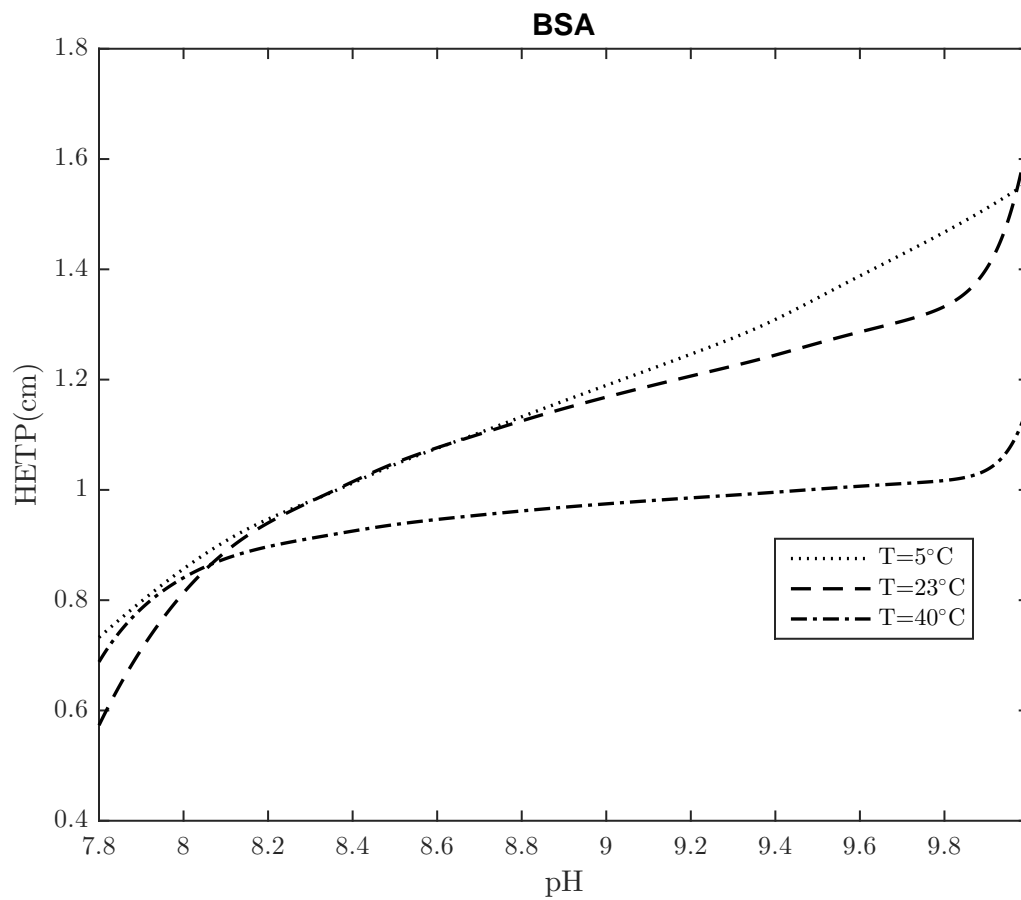


Figure 6.18: HETP for BSA as a function of pH for three different temperatures in anion-exchange chromatography

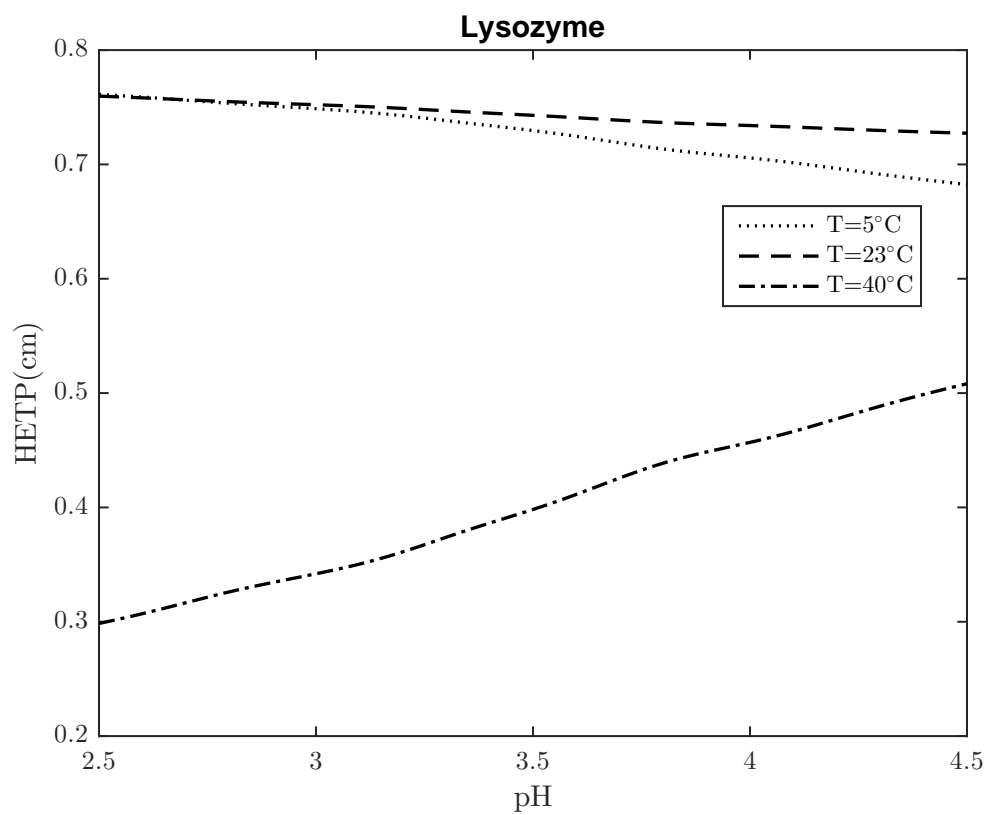


Figure 6.19: HETP for Lysozyme as a function of pH for three different temperatures in cation-exchange chromatography

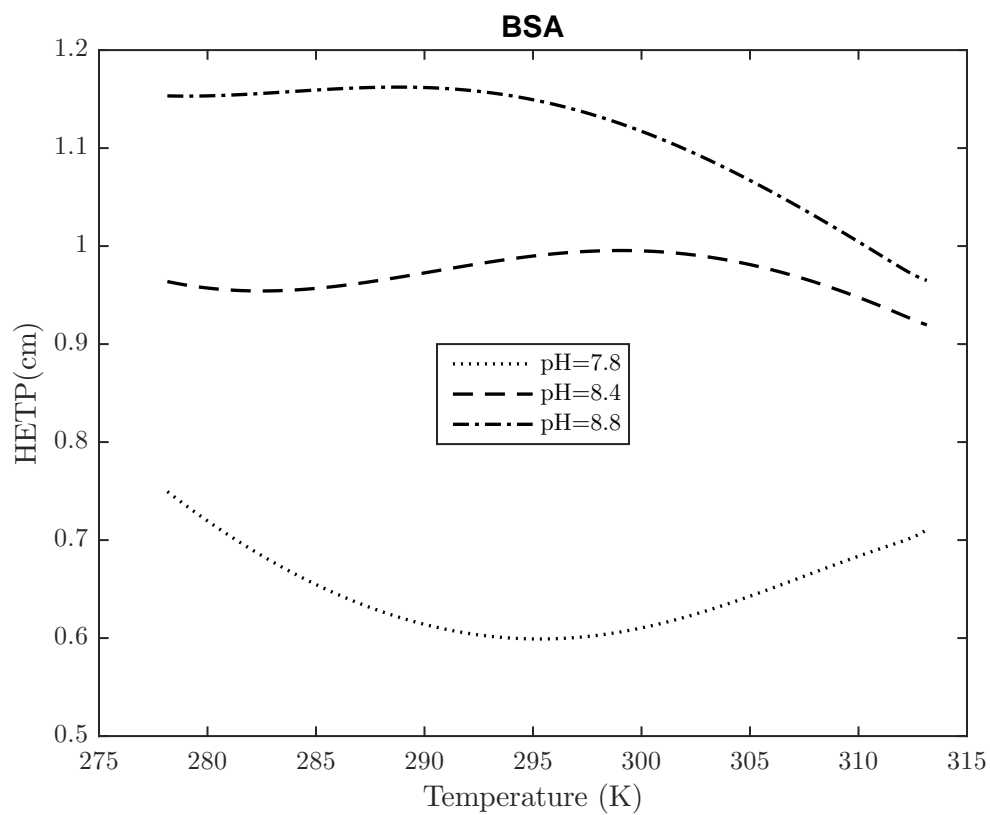


Figure 6.20: HETP for BSA as a function of temperature for three different pH values in anion-exchange chromatography

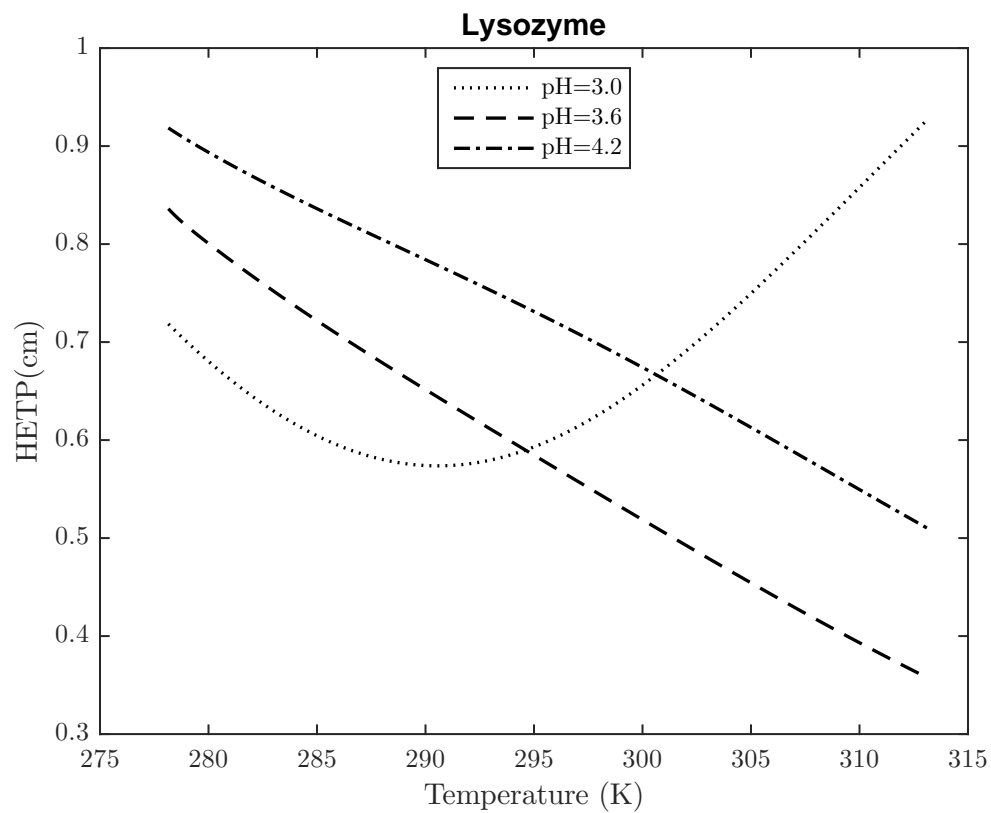


Figure 6.21: HETP for Lysozyme as a function of temperature for three different pH values in cation-exchange chromatography

Chapter 7

Summary of Conclusions and Future Work

7.1 Conclusions

The major findings about the *Effect of pH, Temperature and Protein Tertiary Structure on Biomolecular Separation Engineering in Ion-Exchange Chromatography* are summarized as follows:

7.1.1 pH Effect

- In *anion-exchange chromatography*, more basic pH leads to higher retention.
- In *cation-exchange chromatography*, more acidic pH leads to higher retention.
- In both cases, the buffer pH should be away from the pI value of the sorbate to allow a higher net charge of the molecule.

7.1.2 Temperature Effect

- In *anion-exchange chromatography*, higher temperature leads to higher retention. This may be due to the chemisorptive nature of the adsorption which may involve electron transfer. The activation energies presented in this work are positive values.
- In *cation-exchange chromatography*, lower temperature leads to higher retention. This may be due to the induced dipole forces that drive the physisorption to adsorb the solute. The activation energies presented in this work are negative values.
- The effect of temperature on the physical parameters: diffusion, mass transfer rate coefficient, dispersion is quite limited. In *gel-filtration chromatography* it can improve the separation at higher temperatures.

7.1.3 Tertiary Structure Effect

- In chromatographic adsorbent beds large molecules move mainly by convection whereas smaller molecules move by diffusion.
- Charged amino acid residues on the surface of the biomolecule can lead to increased retention in *ion-exchange chromatography*. Even one surface charge difference between biomolecules can create a large improvement in the separation performance.

7.1.4 Theoretical Studies

- The Fast Fourier Transform (FFT) algorithm for inversion of the Laplace transform into the time domain proved to be a rapid and precise simulation tool.

- In *ion-exchange chromatography*, the generalized rate model (GRM) was successfully implemented using real data for use in a predictive manner to identify operating conditions.

7.2 Future Work

This work can be extended in a variety of different ways, some of which are listed here:

1. *Determination of the adsorption energy in ion-exchange processes*: By using a highly sensitive calorimeter, such as an isothermal titration calorimeter, known amounts of adsorbent can be titrated with a known concentration of sorbate. The heat released can then be used to compute the enthalpy and entropy of the adsorption kinetics, as well as determine the capacity of the adsorbent for the solute. Preliminary results were obtained however due to equipment issues, the study was unable to continue.
2. *Extension of the methodology to other chromatographic methods*: Using data from other chromatographic processes, such as hydrophobic interaction or affinity chromatography, extract important parameters such as the equilibrium constant K_A or adsorption rate constant k_{ads} so that they can be used for scale-up.
3. *Generating a binding library from tertiary structure information*: By knowing the tertiary structure of a protein and the binding kinetics of each amino acid residue, based on the surface charges of the biomolecule the strength and nature of the binding can be calculated. This data can then be validated using chromatogram results and used in a predictive manner to aid biomolecular separation engineering.

Bibliography

- [1] H. M. Berman. The Protein Data Bank. *Nucleic Acids Research*, 28(1):235–242, Jan 2000.
- [2] Philip M. Boyer and James T. Hsu. Experimental studies of restricted protein diffusion in an agarose matrix. *AIChE Journal*, 38(2):259–272, feb 1992.
- [3] Philip M Boyer and James T Hsu. Protein purification by dye-ligand chromatography. In *Chromatography*, pages 1–44. Springer, 1993.
- [4] Stephen Brunauer, Lola S. Deming, W. Edwards Deming, and Edward Teller. On a Theory of the van der Waals Adsorption of Gases. *Journal of the American Chemical Society*, 62(7):1723–1732, Jul 1940.
- [5] S. F. Chung and C. Y. Wen. Longitudinal dispersion of liquid flowing through fixed and fluidized beds. *AIChE Journal*, 14(6):857–866, nov 1968.
- [6] James W. Cooley and John W. Tukey. An algorithm for the machine calculation of complex fourier series. *Mathematics of Computation*, 19(90):297–297, May 1965.
- [7] JR Cooper and RB Dooley. Release of the IAPWS formulation 2008 for the viscosity of ordinary water substance, 2008.
- [8] Kenny S. Crump. Numerical Inversion of Laplace Transforms using a Fourier Series approximation. *Journal of the ACM*, 23(1):89–96, Jan 1976.

- [9] E. L. Cussler. *Diffusion*. Cambridge University Press (CUP), 2009.
- [10] Aptum Biologics EpiQuest. Incharge epiquest 2015 v2.0.1.8, 2015.
- [11] Gilbert F. Froment, Kenneth B. Bischoff, and Juray De Wilde. *Chemical Reactor Analysis and Design*. Wiley, 2010.
- [12] Tyge Greibrokk and Thomas Andersen. High-temperature liquid chromatography. *Journal of Chromatography A*, 1000(1):743–755, 2003.
- [13] Georges Guiochon, Sadroddin Golshan. Shirazi, and Anita M. Katti. *Fundamentals of preparative and nonlinear chromatography*. Academic Press, 1994.
- [14] Roger G. Harrison, Paul W. Todd, Scott R. Rudge, and Demetri Petrides. *Bioseparations Science and Engineering (Topics in Chemical Engineering)*. Oxford University Press, 2002.
- [15] Sabine Heinisch and Jean-Louis Rocca. Sense and nonsense of high-temperature liquid chromatography. *Journal of Chromatography A*, 1216(4):642–658, jan 2009.
- [16] Friedrich Helfferich. *Ion Exchange (Dover Science Books)*. Dover Publications, 1995.
- [17] Csaba Horvath and Hung-Jye Lin. Band spreading in liquid chromatography. *Journal of Chromatography A*, 149:43–70, Feb 1978.
- [18] James T. Hsu and Teh-Liang Chen. Theoretical analysis of the asymmetry in chromatographic peaks. *Journal of Chromatography A*, 404:1–9, Jan 1987.
- [19] James T. Hsu and Joshua S. Dranoff. Numerical inversion of certain Laplace transforms by the direct application of Fast Fourier Transform (FFT) algorithm. *Computers & Chemical Engineering*, 11(2):101–110, Jan 1987.

- [20] Tsai-An Hsu. *Computer Automation of Cascade Chromatography and the Application of fast Fourier transform to distributed parameter models*. PhD thesis, , Northwestern University, Evanston, Ill., 1979.
- [21] Vijesh Kumar, Samuel Leweke, Eric von Lieres, and Anurag S Rathore. Mechanistic modeling of ion-exchange process chromatography of charge variants of monoclonal antibody products. *Journal of Chromatography A*, 1426:140–153, 2015.
- [22] K. Kurpiewska and A. Biela. Bovine β -lactoglobulin complex with dodecane, ambient pressure, Mar 2016.
- [23] Irving Langmuir. The adsorption of gases on plane surfaces of glass, mica and platinum. *Journal of the American Chemical society*, 40(9):1361–1403, 1918.
- [24] Leon Lapidus and Neal R Amundson. Mathematics of adsorption in beds. VI. The effect of longitudinal diffusion in ion exchange and chromatographic columns. *The Journal of Physical Chemistry*, 56(8):984–988, 1952.
- [25] A. I. Liapis, B. Anspach, M. E. Findley, J. Davies, M. T. W. Hearn, and K. K. Unger. Biospecific adsorption of lysozyme onto monoclonal antibody ligand immobilized on nonporous silica particles. *Biotechnol. Bioeng.*, 34(4):467–477, aug 1989.
- [26] J.I. Loch, M. Kopec, and K. Lewinski. Bovine lactoglobulin complex with decanol, Nov 2016.
- [27] SR Logan. The origin and status of the Arrhenius equation. *Journal of Chemical Education*, 59(4):279, 1982.
- [28] Robert G Luo and James T Hsu. Rate parameters and gradient correlations for gradient-elution chromatography. *AIChE journal*, 43(2):464–474, 1997.

- [29] AJP Martin and RL Mo Syngé. A new form of chromatogram employing two liquid phases: A theory of chromatography. 2. Application to the micro-determination of the higher monoamino-acids in proteins. *Biochemical Journal*, 35(12):1358, 1941.
- [30] A. D. Mcnaught and A. Wilkinson. IUPAC. Compendium of Chemical Terminology, 2nd ed. (the "gold book"). In *IUPAC Compendium of Chemical Terminology*. International Union of Pure and Applied Chemistry (IUPAC), August 1997.
- [31] Gorgi Pavlov and James T. Hsu. Modelling the effect of Temperature on the Gel-filtration chromatographic protein separation. *Computers & Chemical Engineering*, 112:304 – 315, 2018.
- [32] Gorgi Pavlov and James T. Hsu. The pH, temperature, and protein structure effect on β -lactoglobulin A and B separation in anion-exchange chromatography. *AIChE Journal*, jan 2018.
- [33] Shamsul Qamar, Javeria N. Abbasi, Shumaila Javeed, Munawar Shah, Farman U. Khan, and Andreas Seidel-Morgenstern. Analytical solutions and moment analysis of chromatographic models for rectangular pulse injections. *Journal of Chromatography A*, 1315:92 – 106, 2013.
- [34] Anders Rasmuson. Exact solution of a model for diffusion in particles and longitudinal dispersion in packed beds: Numerical evaluation. *AIChE Journal*, 31(3):518–519, Mar 1985.
- [35] Pier Giorgio Righetti and Tiziana Caravaggio. Isoelectric points and molecular weights of proteins: A table. *Journal of Chromatography A*, 127(1):1–28, 1976.
- [36] Philip D Ross and S Subramanian. Thermodynamics of protein association reactions: forces contributing to stability. *Biochemistry*, 20(11):3096–3102, 1981.

- [37] Douglas M. Ruthven. *Principles of Adsorption and Adsorption Processes*. Wiley, 1984.
- [38] Andrea Salis, Mathias Boström, Luca Medda, Francesca Cugia, Brajesh Barse, Drew F Parsons, Barry W Ninham, and Maura Monduzzi. Measurements and theoretical interpretation of points of zero charge/potential of BSA protein. *Langmuir*, 27(18):11597–11604, 2011.
- [39] Peter Schneider and JM Smith. Adsorption rate constants from chromatography. *AIChE Journal*, 14(5):762–771, 1968.
- [40] GE Healthcare Life Sciences. Instructions for AF Q Sepharose Fast Flow, 2014.
- [41] GE Healthcare Life Sciences. Ion Exchange Chromatography: Principles and Methods, 2014.
- [42] GE Healthcare Life Sciences. Size Exclusion Chromatography: Principles and Methods, 2014.
- [43] Sigma-Aldrich. *Trizma Buffers Product Specification*, 1996. T494109.
- [44] Lloyd R. Snyder, Joseph J. Kirkland, and John W. Dolan. *Introduction to Modern Liquid Chromatography*. Wiley, 2010.
- [45] Charles Tanford and Robert Roxby. Interpretation of protein titration curves. Application to lysozyme. *Biochemistry*, 11(11):2192–2198, 1972. PMID: 5027621.
- [46] JJ Van Deemter, FJ Zuiderweg, and A van Klinkenberg. Longitudinal diffusion and resistance to mass transfer as causes of nonideality in chromatography. *Chemical Engineering Science*, 5(6):271–289, 1956.
- [47] van Der Laan. Letters to the editors. *Chemical Engineering Science*, 7(3):187 – 191, 1958.

- [48] Gerd Vanhoenacker and Pat Sandra. Elevated temperature and temperature programming in conventional liquid chromatography – fundamentals and applications. *J. Sep. Sci.*, 29(12):1822–1835, aug 2006.
- [49] Donald Voet and Judith G. Voet. *Biochemistry*. Wiley, 2003.
- [50] LR Wetter and HFr Deutsch. Immunological studies on egg white proteins IV. Immunochemical and physical studies of lysozyme. *Journal of Biological Chemistry*, 192(1):237–242, 1951.
- [51] E. J. Wilson and C. J. Geankoplis. Liquid Mass Transfer at Very Low Reynolds Numbers in Packed Beds. *Ind. Eng. Chem. Fund.*, 5(1):9–14, feb 1966.
- [52] EJ Wood. Data for biochemical research by RMC Dawson, DC Elliott, WH Elliott and KM Jones, pp 580. Oxford Science Publications, OUP, Oxford, 1986. isbn 0-19-855358-7. *Biochemical Education*, 15(2):97–97, 1987.
- [53] Xing-Zheng Wu, Tiemin Huang, Wayne M Mullett, Jupiter M Yeung, and Janusz Pawliszyn. Determination of isoelectric point and investigation of immunoreaction in peanut allergenic proteins–rabbit IgG antibody system by whole-column imaged capillary isoelectric focusing. *Journal of Microcolumn Separations*, 13(8):322–326, 2001.
- [54] M. E. Young, P. A. Carroad, and R. L. Bell. Estimation of diffusion coefficients of proteins. *Biotechnol. Bioeng.*, 22(5):947–955, May 1980.

Appendix A

Curriculum Vitae

A.1 Publications

1. Gorgi Pavlov and James T. Hsu. Modelling the Effect of Temperature on the Gel-Filtration Chromatographic Protein Separation. *Computers & Chemical Engineering*, 112:304 - 315, 2018
2. Gorgi Pavlov and James T. Hsu. The pH, Temperature, and Protein Structure Effect on β -lactoglobulin A and B Separation in Anion-exchange Chromatography. *AIChE Journal*, 2018
3. Gorgi Pavlov and James T. Hsu. Comparison of Anion-Exchange Chromatography and Cation-Exchange Chromatography for Biomolecular Separation. *In preparation*
4. Gorgi Pavlov and James T. Hsu. Numerical Study of the Effect of pH and Temperature of Protein Separation in Anion and Cation Exchange Chromatography. *In preparation*

A.2 Presentations

1. Engineering Studies of the Effect of pH and Temperature on the Adsorbent Surface Interaction for the Anion-Exchange Chromatographic Separation, *AICHE Annual Meeting, Minneapolis, MN, October 2017*
2. Effect of physical variables on Biomolecular Separation Engineering in Ion-Exchange chromatography, *Lehigh University Department of Chemical and Biomolecular Engineering Graduate Student Symposium, Bethlehem, PA, September 2017*

A.3 Poster Presentations

1. Fundamental Studies of Liquid Chromatography under Cryogenic Conditions, *Preparative and Process Chromatography (PREP) Symposium, July 2015*
2. Thermodynamic Analysis of Multiple Components Resolution in Chromatography at Various Temperatures, *Preparative and Process Chromatography (PREP) Symposium, July 2016*
3. Fundamental Studies of the Effect of pH and Temperature on the Adsorbent Surface Interaction for the Anion-exchange Chromatographic Separation, *Preparative and Process Chromatography (PREP) Symposium, July 2017*
4. The Effect of pH and Temperature on Protein Separation in Anion-exchange Chromatography, *Preparative and Process Chromatography (PREP) Symposium, July 2017*
5. Engineering Studies of the Effect of pH, Temperature and Protein Tertiary Structure on β -Lactoglobulin A and B Separation in Anion-Exchange Chromatography, *AICHE Annual Meeting, Minneapolis, MN, October 2017*

Biography

Gorgi Pavlov was born on April 14, 1992 in Gevgelija, Republic of Macedonia as a first child to Jasmina Karakabakova Pavlova and Mitko Pavlov. Gorgi grew up in Gevgelija where he attended primary school. Gorgi then attended Private Yahya Kemal College high school in Skopje, Macedonia, graduating in 2010, where he received three international awards for his work in IT and Turkish language.

Gorgi decided to attend Lehigh University in Bethlehem, PA in the fall of 2010, entering initially in the Bioengineering program, however during his sophomore year opting to study Chemical Engineering. As an undergraduate at Lehigh, Gorgi was quite active in the student community, serving as a President of the Association of International Students and also as a Founding Father and Vice President of the Phi Delta Theta Fraternity. Gorgi spent a summer semester studying in Bogazici University in Istanbul, Turkey, as well as doing an international internship with 3M in Shanghai, P.R. China. Gorgi graduated from Lehigh University in 2014 with a B.S. degree with honors in Chemical Engineering and a technical minor in Biotechnology. Gorgi entered graduate school immediately after receiving his B.S. degree, working with Professor James T. Hsu. While in graduate school, Gorgi was fortunate to publish his work in several journals and was also given the opportunity to present his work at international conferences in Philadelphia, PA and Minneapolis, MN. During this time, Gorgi served as the Vice President of the Chemical Engineering Graduate Association (ChEGA) and as President of the Graduate Student Senate. Gorgi also

served on a search committee to select the new Vice Provost for Student Affairs. For his work, Gorgi has received the Graduate Student Senate Champion Award, as well as the Graduate Student Merit Award presented by the Lehigh University Alumni Association. Outside of his research responsibilities, Gorgi served as a teaching assistant for the majority of his time in graduate school, being the primary teaching assistant for the Integrated Biotechnology Laboratory. He has also served as a teaching assistant for the Unit Operations lab, as well as the Senior Design Course. For his teaching assistant work, Gorgi has received the Teaching Assistant Award. He is selected to deliver the Graduate Student Address at the 150th Commencement Exercises.

In his personal time, Gorgi enjoys skiing, even after breaking his leg during a skiing accident. He also enjoys swimming and going to the gym, as well as travelling. Over the last few years, Gorgi has visited several countries and continents in addition to learning several languages. Gorgi can speak Macedonian, English, Turkish, Serbian, Croatian, Bulgarian, and has a basic knowledge of German, French and Italian. Gorgi's other interests include reading, listening to music and aviation. Upon completing his doctorate, Gorgi will be joining Evonik Corporation as a process engineer working within the Process Technology and Engineering with a primary focus in microbial fermentation and downstream operations in Tippecanoe Labs in Lafayette, IN.